



VTEM™ Plus

REPORT ON A HELICOPTER-BORNE VERSATILE TIME DOMAIN
ELECTROMAGNETIC (VTEM™ Plus) AND HORIZONTAL MAGNETIC
GRADIOMETER GEOPHYSICAL SURVEY

PROJECT: KUDZ ZE KAYAH, PELLY AND WOLF
LOCATION: WOLVERINE LAKE, YUKON
FOR: BMC MINERALS (NO. 1) LTD
SURVEY FLOWN: APRIL - JULY 2016
PROJECT: GL160037

Geotech Ltd.
245 Industrial Parkway North
Aurora, ON Canada L4G 4C4

Tel: +1 905 841 5004
Web: www.geotech.ca
Email: info@geotech.ca



TABLE OF CONTENTS

EXECUTIVE SUMMARY.....	III
1. INTRODUCTION.....	1
1.1 General Considerations.....	1
1.2 Survey and System Specifications.....	2
1.3 Topographic Relief and Cultural Features.....	3
2. DATA ACQUISITION.....	6
2.1 Survey Area.....	6
2.2 Survey Operations.....	6
2.3 Flight Specifications.....	8
2.4 Aircraft and Equipment.....	8
2.4.1 Survey Aircraft.....	8
2.4.2 Electromagnetic System.....	8
2.4.3 Full waveform vtem™ sensor calibration.....	12
2.4.4 Horizontal Magnetic Gradiometer.....	12
2.4.5 Radar Altimeter.....	12
2.4.6 GPS Navigation System.....	12
2.4.7 Digital Acquisition System.....	12
2.5 Base Station.....	13
3. PERSONNEL.....	14
4. DATA PROCESSING AND PRESENTATION.....	15
4.1 Flight Path.....	15
4.2 Electromagnetic Data.....	15
4.3 Horizontal Magnetic Gradiometer Data.....	17
5. DELIVERABLES.....	18
5.1 Survey Report.....	18
5.2 Maps.....	18
5.3 Digital Data.....	19
6. CONCLUSIONS AND RECOMMENDATIONS.....	23

LIST OF FIGURES

Figure 1: Survey location.....	1
Figure 2: Survey area location on Google Earth.....	2
Figure 3: Flight path of Kudz Ze Kayah over a Google Earth Image.....	3
Figure 4: Flight path of Pelly over a Google Earth Image.....	4
Figure 5: Flight path of Wolf over a Google Earth Image.....	5
Figure 6: VTEM™ Transmitter Current Waveform.....	8
Figure 7: VTEM™Plus System Configuration.....	11
Figure 8: Z, X and Fraser filtered X (FFx) components for "thin" target.....	16

LIST OF TABLES

Table 1: Survey Specifications.....	6
Table 2: Survey schedule.....	6
Table 3: Off-Time Decay Sampling Scheme.....	9
Table 4: Acquisition Sampling Rates.....	12
Table 5: Geosoft GDB Data Format.....	19
Table 6: Geosoft Resistivity Depth Image GDB Data Format.....	22
Table 7: Geosoft database for the VTEM waveform.....	22

APPENDICES

A.	Survey location maps
B.	Survey Survey area Coordinates
C.	Geophysical Maps
D.	Generalized Modelling Results of the VTEM System.....
E.	TAU Analysis
F.	TEM Resistivity Depth Imaging (RDI)
G.	Resistivity Depth Images (RDI).....

EXECUTIVE SUMMARY

KUDZ ZE KAYAH, PELLY AND WOLF - WOLVERINE LAKE, YUKON

During April 23rd to July 31st 2016 Geotech Ltd. carried out a helicopter-borne geophysical survey over Kudz Ze Kayah, Pelly and Wolf situated near Wolverine Lake, Yukon.

Principal geophysical sensors included a versatile time domain electromagnetic (VTEMplus) system and horizontal magnetic gradiometer with two caesium sensors. Ancillary equipment included a GPS navigation system and a radar altimeter. A total of 1589 line-kilometres of geophysical data were acquired during the survey.

In-field data quality assurance and preliminary processing were carried out on a daily basis during the acquisition phase. Preliminary and final data processing, including generation of final digital data and map products were undertaken from the office of Geotech Ltd. in Aurora, Ontario.

The processed survey results are presented as the following maps:

- Electromagnetic stacked profiles of the B-field Z Component,
- Electromagnetic stacked profiles of dB/dt Z Component,
- B-Field Z Component Channel grids,
- dB/dt X Component Fraser Filtered Channel grid,
- Total Magnetic Intensity (TMI),
- Magnetic Total Horizontal Gradient,
- Magnetic Tilt-Angle Derivative of TMI,
- Calculated Time Constant (Tau) with Calculated Vertical Derivative contours and
- Resistivity Depth Images (RDI) sections are presented.

Digital data includes all electromagnetic and magnetic products, plus ancillary data including the waveform.

The survey report describes the procedures for data acquisition, processing, final image presentation and the specifications for the digital data set.

1. INTRODUCTION

1.1 GENERAL CONSIDERATIONS

Geotech Ltd. performed a helicopter-borne geophysical survey over Kudz Ze Kayah, Pelly and Wolf situated near Wolverine Lake, Yukon (Figure 1 & Figure 2).

Robin Black represented BMC Minerals (No. 1) Ltd during the data acquisition and data processing phases of this project.

The geophysical surveys consisted of helicopter borne EM using the versatile time-domain electromagnetic (VTEMplus) system with Full-Waveform processing. Measurements consisted of Vertical (Z), In-line Horizontal (X) and Cross-line Horizontal (Y) components of the EM fields using induction coils and the aeromagnetic total field using a magnetic gradiometer. A total of 1589 line-km of geophysical data were acquired during the survey.

The crew was based out of Watson Lake (Figure 2) in Yukon for the acquisition phase of the survey. Survey flying started on April 23rd and was completed on July 31st, 2016.

Data quality control and quality assurance, and preliminary data processing were carried out on a daily basis during the acquisition phase of the project. Final data processing followed immediately after the end of the survey. Final reporting, data presentation and archiving were completed from the Aurora office of Geotech Ltd. in October, 2016.

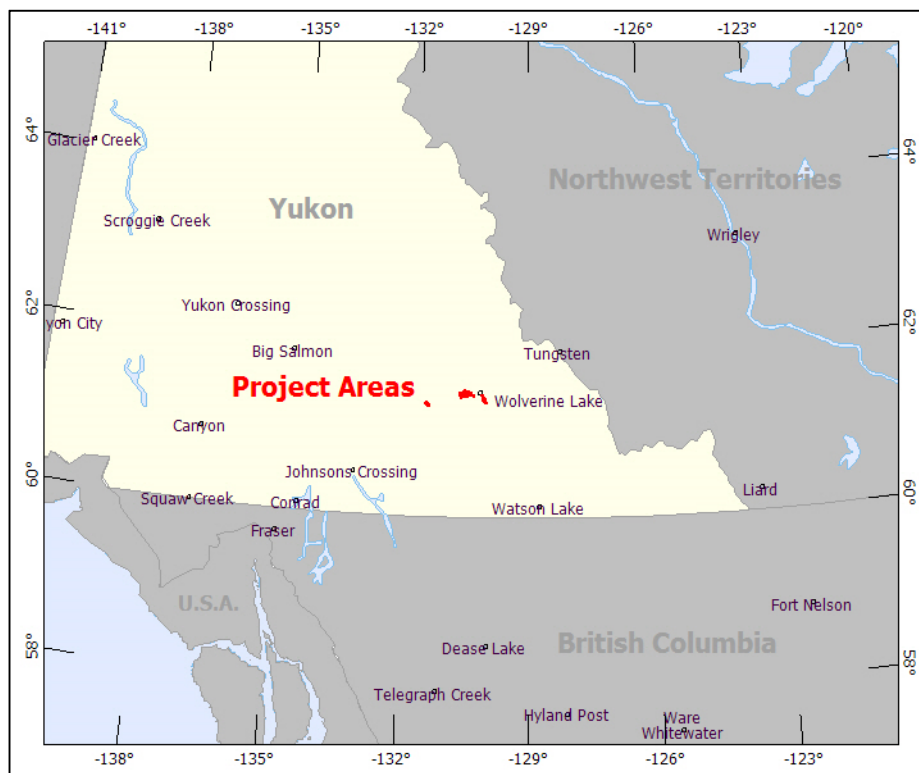


Figure 1: Survey location

1.2 SURVEY AND SYSTEM SPECIFICATIONS

The survey areas, Kudz Ze Kayah, Pelly and Wolf are located approximately 8 kilometres west, 2 kilometres east and 71 kilometres southwest of Wolverine Lake, Yukon respectively (Figure 2).

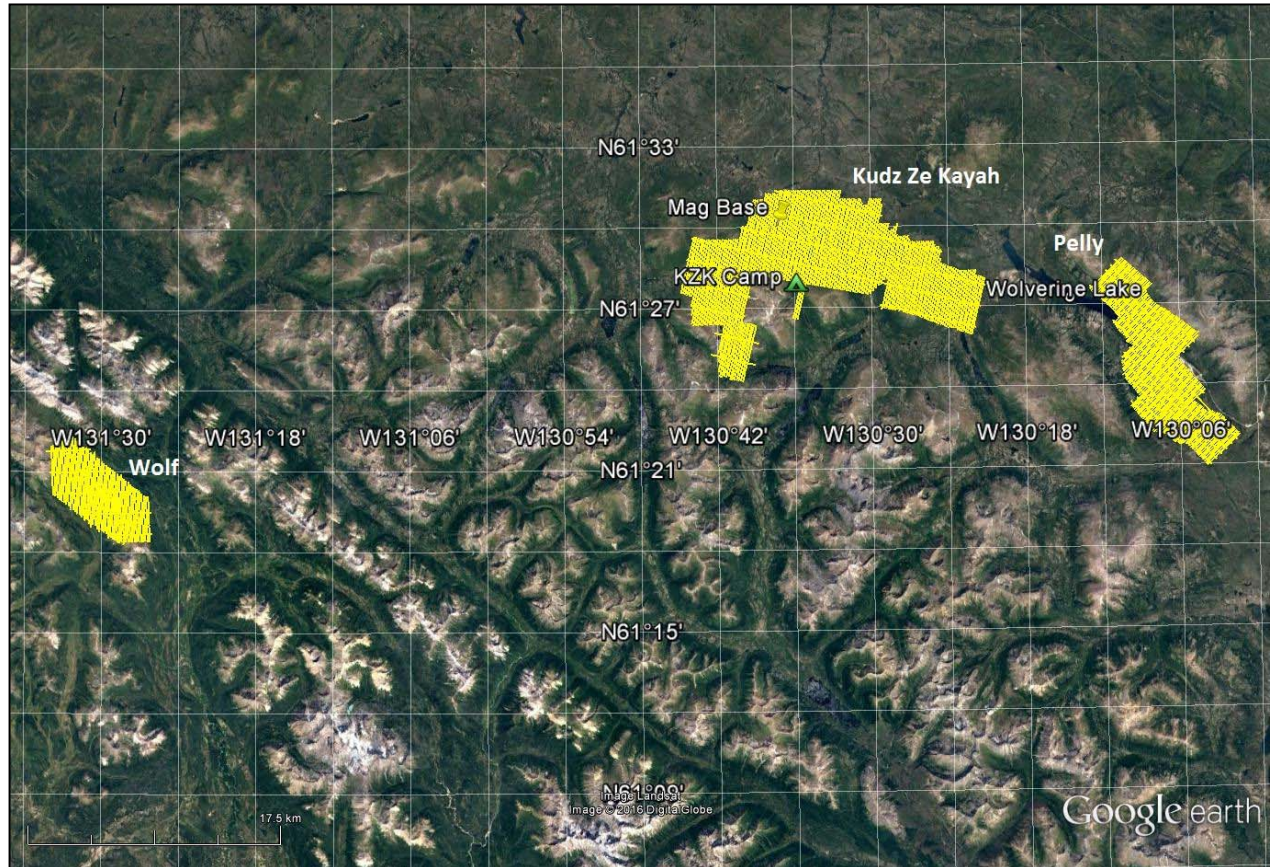


Figure 2: Survey area location on Google Earth.

The block, Kudz Ze Kayah was flown in a northeast to southwest (N 15° E azimuth) direction; Pelly was flown in a southwest to northeast (N48° E azimuth) direction and Wolf was flown in a north to south (N0° E azimuth) direction with traverse line spacing of 150 metres as depicted in Figure 3 to 4. Tie lines were flown perpendicular to the traverse lines at a spacing of 1500 metres respectively. For more detailed information on the flight spacing and direction see Table 1.

1.3 TOPOGRAPHIC RELIEF AND CULTURAL FEATURES

Topographically, the survey areas exhibits an extremely rugged relief with an elevation ranging from 1104 to 2079 metres above mean sea level over an area of 241 square kilometres (Figure 3 to 5).

There are various rivers and streams running through the survey areas which connect various lakes. There are no visible signs of culture such as roads, transmission lines, mining areas and settlements located in the survey areas (Figure 3 to 5).

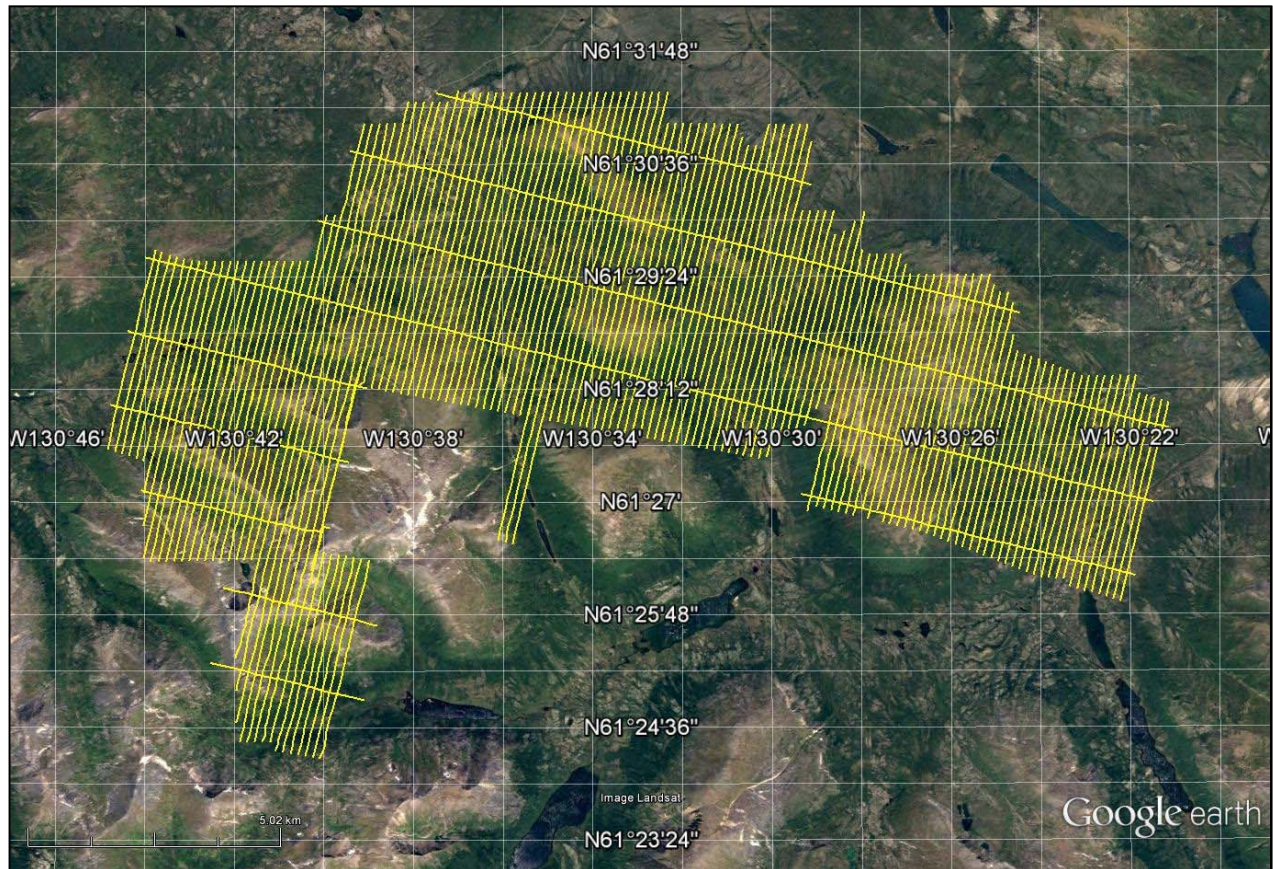


Figure 3: Flight path of Kudz Ze Kayah over a Google Earth Image.

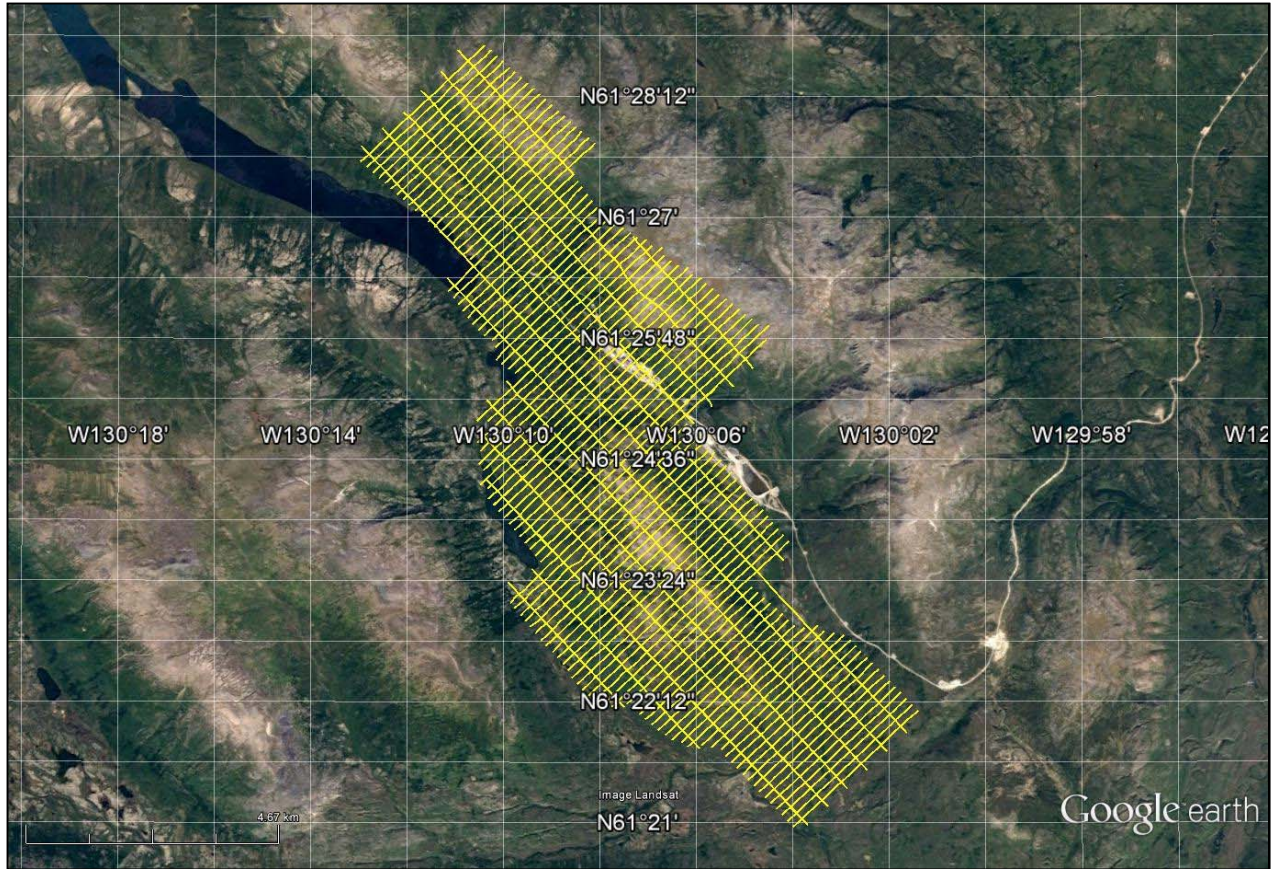


Figure 4: Flight path of Pelly over a Google Earth Image.

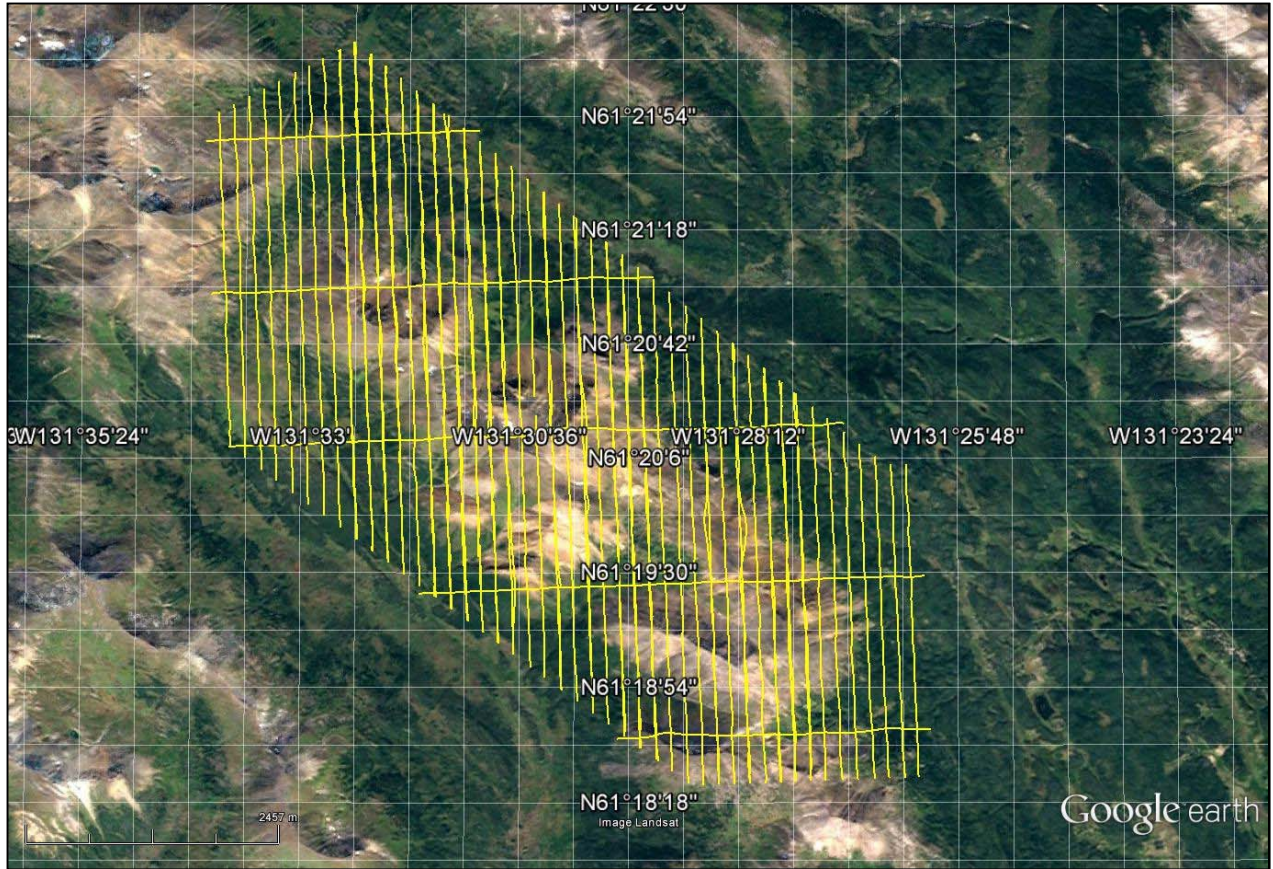


Figure 5: Flight path of Wolf over a Google Earth Image.

2. DATA ACQUISITION

2.1 SURVEY AREA

The survey areas (see Figure 3, Figure 4, Figure 5 and Appendix A) and general flight specifications are as follows:

Table 1: Survey Specifications

Survey block	Line spacing (m)	Area (Km ²)	Planned ¹ Line-km	Actual Line-km	Flight direction	Line numbers
Kudz Ze Kayah	Traverse: 150	121	902	851.8	N 15° E / N 195° E	L3000 - L4350 L1305 - L1555
	Tie: 1500			86.5	N 105° E / N 285° E	T5000 - T5080
Pelly	Traverse: 150	91	473	370.1	N 48° E / N 228° E	L4000 - L4960
	Tie: 1500			111.5	N 138° E / N 318° E	T5000 - T5040
Wolf	Traverse: 150	29	214	295.5	N 0° E / N 180° E	L6000 - L6440
	Tie: 1500			21.1	N 90° E / N 270° E	T7000 - T7040
TOTAL		241	1589	1736.5		

Survey area boundaries co-ordinates are provided in Appendix B.

2.2 SURVEY OPERATIONS

Survey operations were based out of Watson Lake and Kudz Ze Kayah Camp in Yukon from April 11th until July 31st 2016. The following table shows the timing of the flying.

Table 2: Survey schedule

Date	Flight #	Flown km	Block	Crew location	Comments
11-Apr-2016				Watson Lake, Yukon	Crew arrived
12-Apr-2016				Watson Lake, Yukon	System assembly limited due to weather
13-Apr-2016				Watson Lake, Yukon	System assembly
14-Apr-2016				Watson Lake, Yukon	Testing
15-Apr-2016				Watson Lake, Yukon	No production due to technical issues
16-Apr-2016				Watson Lake, Yukon	No production due to technical issues
17-Apr-2016				Watson Lake, Yukon	No production due to technical issues & recon flight
18-Apr-2016				Watson Lake, Yukon	No production due to technical issues
19-Apr-2016				Watson Lake, Yukon	No production due to technical issues
20-Apr-2016				Watson Lake, Yukon	No production due to technical issues & test flight
21-Apr-2016				Watson Lake, Yukon	Mobilized to camp
22-Apr-2016				KZK CAMP, Yukon	Set up & testing – no production

¹ Note: Actual Line kilometres represent the total line kilometres in the final database. These line-km normally exceed the Planned Line-km, as indicated in the survey NAV files. However, flying was stopped early as requested by the client.

Date	Flight #	Flown km	Block	Crew location	Comments
					due to weather
23-Apr-2016	1,2,3	280	KZK	KZK CAMP, Yukon	280km flown
24-Apr-2016	4,5	188	KZK	KZK CAMP, Yukon	188km flown
25-Apr-2016	6	25	KZK	KZK CAMP, Yukon	25km flown limited due to weather
26-Apr-2016	7,8,9	247	KZK	KZK CAMP, Yukon	247km flown
27-Apr-2016				KZK CAMP, Yukon	No production due to weather
28-Apr-2016	10,11	149	KZK	KZK CAMP, Yukon	149km flown
29-Apr-2016				KZK CAMP, Yukon	No production due to weather
30-Apr-2016				KZK CAMP, Yukon	No production due to weather
1-May-2016	12	6	Pelly	KZK CAMP, Yukon	6km flown limited due to weather
2-May-2016				KZK CAMP, Yukon	No production due to weather
3-May-2016	13,14	155	KZK	KZK CAMP, Yukon	155km flown – Stopped until July
5-Jul-2016				KZK CAMP, Yukon	Crew arrived
6-Jul-2016				KZK CAMP, Yukon	System set & recon flight
7-Jul-2016	15	56	wolf	KZK CAMP, Yukon	56km flown limited due to technical issues
8-Jul-2016	16,17	106	wolf	KZK CAMP, Yukon	160km flown
9-Jul-2016	18,19,20	52	wolf	KZK CAMP, Yukon	52km flown
10-Jul-2016	21	49	Pelly	KZK CAMP, Yukon	49km flown limited due to weather
11-Jul-2016	22,23,24	123	Pelly	KZK CAMP, Yukon	123km flown
12-Jul-2016	25,26	106	Pelly	KZK CAMP, Yukon	106km flown
13-Jul-2016	27,28,29	110	Pelly	KZK CAMP, Yukon	110km flown
14-Jul-2016	30	35	Pelly	KZK CAMP, Yukon	30km flown & waiting for reflight confirmation
15-Jul-2016			Pelly	KZK CAMP, Yukon	Waiting for reflight confirmation
16-Jul-2016	31,32	77	Pelly	KZK CAMP, Yukon	77km flown
17-Jul-2016	33	50	Pelly	KZK CAMP, Yukon	Remaining kms were flown – flying completed
18-Jul-2016				KZK CAMP, Yukon	Waiting on re-flights
19-Jul-2016				KZK CAMP, Yukon	Waiting on re-flights
20-Jul-2016			wolf	KZK CAMP, Yukon	No production due to weather
21-Jul-2016	34	24	wolf	KZK CAMP, Yukon	24km flown limited due to technical issues
22-Jul-2016				KZK CAMP, Yukon	No production due to weather
23-Jul-2016				KZK CAMP, Yukon	No production due to weather
24-Jul-2016				KZK CAMP, Yukon	No production due to weather
25-Jul-2016				KZK CAMP, Yukon	Flight aborted due to weather
26-Jul-2016				KZK CAMP, Yukon	Flight aborted due to weather
27-Jul-2016				KZK CAMP, Yukon	No production due to weather
28-Jul-2016				KZK CAMP, Yukon	No production due to weather
29-Jul-2016				KZK CAMP, Yukon	No production due to weather
30-Jul-2016		20	wolf	KZK CAMP, Yukon	20km flown
31-Jul-2016		103	wolf	KZK CAMP, Yukon	Remaining kms were flown – flying complete

2.3 FLIGHT SPECIFICATIONS

During the survey the helicopter was maintained at a mean altitude of 101 metres above the ground with an average survey speed of 80 km/hour. This allowed for an actual average Transmitter-receiver loop terrain clearance of 70 metres and a magnetic sensor clearance of 80 metres.

The on board operator was responsible for monitoring the system integrity. He also maintained a detailed flight log during the survey, tracking the times of the flight as well as any unusual geophysical or topographic features.

On return of the aircrew to the base camp the survey data was transferred from a compact flash card (PCMCIA) to the data processing computer. The data were then uploaded via ftp to the Geotech office in Aurora for daily quality assurance and quality control by qualified personnel.

2.4 AIRCRAFT AND EQUIPMENT

2.4.1 SURVEY AIRCRAFT

The survey was flown using a Eurocopter Aerospatiale (Astar) 350 B3 helicopter, registration C-GTNI and C-FVTM. The helicopter is owned and operated by Trans North Helicopters. Installation of the geophysical and ancillary equipment was carried out by a Geotech Ltd crew.

2.4.2 ELECTROMAGNETIC SYSTEM

The electromagnetic system was a Geotech Time Domain EM (VTEM™Plus) full receiver-waveform streamed data recorded system. The “full waveform VTEM system” uses the streamed half-cycle recording of transmitter and receiver waveforms to obtain a complete system response calibration throughout the entire survey flight. The VTEM™ transmitter current waveform is shown diagrammatically in Figure 6. VTEM with the Serial number 17 and 31 had been used for the survey.

The VTEM™ Receiver and transmitter coils were in concentric-coplanar and Z-direction oriented configuration. The receiver system for the project also included a coincident-coaxial X-direction coil to measure the in-line dB/dt and calculate B-Field responses. The Transmitter-receiver loop was towed at a mean distance of 31 metres below the aircraft as shown in Figure 7.

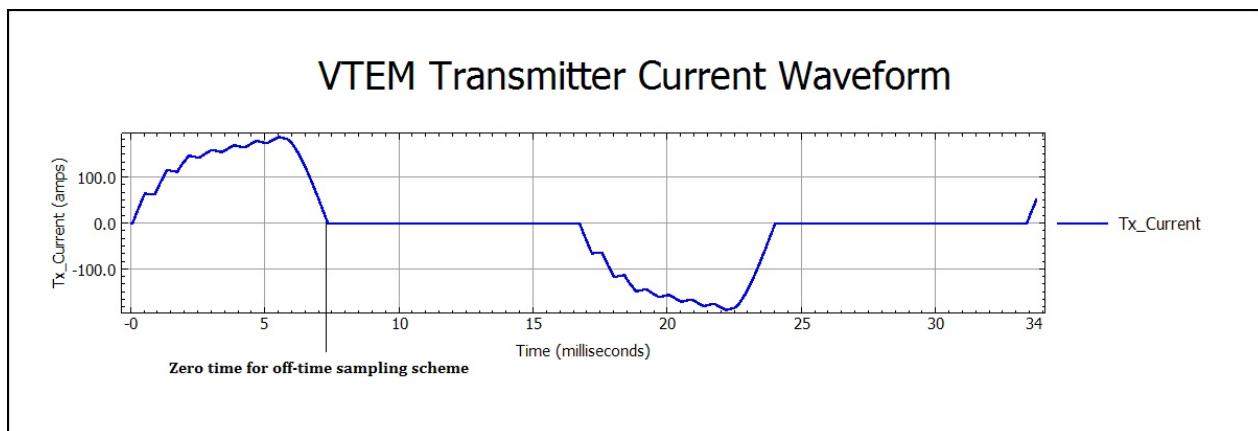


Figure 6: VTEM™ Transmitter Current Waveform

The VTEM™ decay sampling scheme is shown in Table 3 below. Forty-three time measurement gates were used for the final data processing in the range from 0.021 to 8.083 msec. Zero time for the off-time sampling scheme is equal to the current pulse width and is defined as the time near the end of the turn-off ramp where the dI/dt waveform falls to 1/2 of its peak value.

Table 3: Off-Time Decay Sampling Scheme

VTEM™ Decay Sampling Scheme				
Index	Start	End	Middle	Width
Milliseconds				
4	0.018	0.023	0.021	0.005
5	0.023	0.029	0.026	0.005
6	0.029	0.034	0.031	0.005
7	0.034	0.039	0.036	0.005
8	0.039	0.045	0.042	0.006
9	0.045	0.051	0.048	0.007
10	0.051	0.059	0.055	0.008
11	0.059	0.068	0.063	0.009
12	0.068	0.078	0.073	0.010
13	0.078	0.090	0.083	0.012
14	0.090	0.103	0.096	0.013
15	0.103	0.118	0.110	0.015
16	0.118	0.136	0.126	0.018
17	0.136	0.156	0.145	0.020
18	0.156	0.179	0.167	0.023
19	0.179	0.206	0.192	0.027
20	0.206	0.236	0.220	0.030
21	0.236	0.271	0.253	0.035
22	0.271	0.312	0.290	0.040
23	0.312	0.358	0.333	0.046
24	0.358	0.411	0.383	0.053
25	0.411	0.472	0.440	0.061
26	0.472	0.543	0.505	0.070
27	0.543	0.623	0.580	0.081
28	0.623	0.716	0.667	0.093
29	0.716	0.823	0.766	0.107
30	0.823	0.945	0.880	0.122
31	0.945	1.086	1.010	0.141
32	1.086	1.247	1.161	0.161
33	1.247	1.432	1.333	0.185
34	1.432	1.646	1.531	0.214
35	1.646	1.891	1.760	0.245
36	1.891	2.172	2.021	0.281
37	2.172	2.495	2.323	0.323
38	2.495	2.865	2.667	0.370

VTEM™ Decay Sampling Scheme				
Index	Start	End	Middle	Width
Milliseconds				
39	2.865	3.292	3.063	0.427
40	3.292	3.781	3.521	0.490
41	3.781	4.341	4.042	0.560
42	4.341	4.987	4.641	0.646
43	4.987	5.729	5.333	0.742
44	5.729	6.581	6.125	0.852
45	6.581	7.560	7.036	0.979
46	7.560	8.685	8.083	1.125

Z Component: 4 - 46 time gates
X Component: 20 - 46 time gates
Y Component: 20 - 46 time gates

VTEM™ system specifications:

Transmitter	Receiver
<ul style="list-style-type: none"> • Transmitter loop diameter: 26 m • Number of turns: 4 • Effective Transmitter loop area: 2123.7 m² • Transmitter base frequency: 30 Hz • Peak current: 189 A • Pulse width: 7.34 ms • Waveform shape: Bi-polar trapezoid • Peak dipole moment: 401,382 nIA • Actual average Transmitter-receiver loop terrain clearance: 70 metres above the ground 	<ul style="list-style-type: none"> • X Coil diameter: 0.32 m • Number of turns: 245 • Effective coil area: 19.69 m² • Z-Coil and Y-coil diameter: 1.2 m • Number of turns: 100 • Effective coil area: 113.04 m²

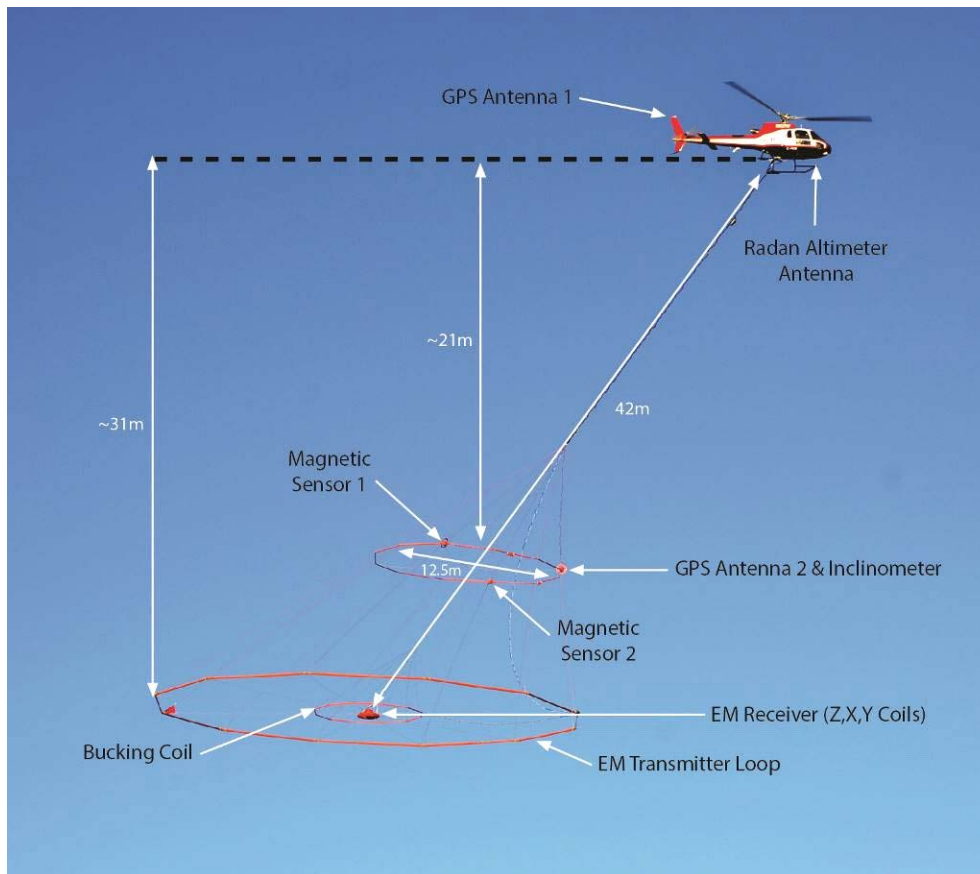


Figure 7: VTEM™ Plus System Configuration.

2.4.3 FULL WAVEFORM VTEM™ SENSOR CALIBRATION

The calibration is performed on the complete VTEM™ system installed in and connected to the helicopter, using special calibration equipment.

The procedure takes half-cycle files acquired and calculates a calibration file consisting of a single stacked half-cycle waveform. The purpose of the stacking is to attenuate natural and man-made magnetic signals, leaving only the response to the calibration signal.

2.4.4 HORIZONTAL MAGNETIC GRADIOMETER

The horizontal magnetic gradiometer consists of two Geometrics split-beam field magnetic sensors with a sampling interval of 0.1 seconds. These sensors are mounted 12.5 metres apart on a separate loop, 10 metres above the Transmitter-receiver loop. A GPS antenna and Gyro Inclinometer is installed on the separate loop to accurately record the tilt and position of the magnetic gradiometer.

2.4.5 RADAR ALTIMETER

A Terra TRA 3000/TRI 40 radar altimeter was used to record terrain clearance. The antenna was mounted beneath the bubble of the helicopter cockpit (Figure 7).

2.4.6 GPS NAVIGATION SYSTEM

The navigation system used was a Geotech PC104 based navigation system utilizing a NovAtel's WAAS (Wide Area Augmentation System) enabled GPS receiver, Geotech navigate software, a full screen display with controls in front of the pilot to direct the flight and a NovAtel GPS antenna mounted on the helicopter tail (Figure 7). As many as 11 GPS and two WAAS satellites may be monitored at any one time. The positional accuracy or circular error probability (CEP) is 1.8 m, with WAAS active, it is 1.0 m. The co-ordinates of the survey area were set-up prior to the survey and the information was fed into the airborne navigation system. The second GPS antenna is installed on the additional magnetic loop together with Gyro Inclinometer.

2.4.7 DIGITAL ACQUISITION SYSTEM

A Geotech data acquisition system recorded the digital survey data on an internal compact flash card. Data is displayed on an LCD screen as traces to allow the operator to monitor the integrity of the system. The data type and sampling interval as provided in Table 4.

Table 4: Acquisition Sampling Rates

Data Type	Sampling
TDEM	0.1 sec
Magnetometer	0.1 sec
GPS Position	0.2 sec
Radar Altimeter	0.2 sec
Inclinometer	0.1 sec

2.5 BASE STATION

A combined magnetometer/GPS base station was utilized on this project. A Geometrics Caesium vapour magnetometer was used as a magnetic sensor with a sensitivity of 0.001 nT. The base station was recording the magnetic field together with the GPS time at 1 Hz on a base station computer.

The base station magnetometer sensor was installed at the tree line; back of the camp (61°30.0666'N, 130°37.3108'W); away from electric transmission lines and moving ferrous objects such as motor vehicles. The base station data were backed-up to the data processing computer at the end of each survey day.

3. PERSONNEL

The following Geotech Ltd. personnel were involved in the project.

FIELD:

Project Manager:	Darren Tuck (Office)
Data QC:	Nick Venter (Office)
Crew chief:	Jan Dabrowski
Operator:	Jan Dabrowski Roger Leblanc

The survey pilot and the mechanical engineer were employed directly by the helicopter operator – Trans North Helicopters

Pilot:	Doug Hladun Pierre Forand
Mechanical Engineer:	Clayton Whitney

OFFICE:

Preliminary Data Processing:	Nick Venter
Final Data Processing:	Gaurav Nailwal
Final Data QA/QC:	Geoffrey Plastow
Reporting/Mapping:	Liz Mathew

Data acquisition phase was carried out under the supervision of Andrei Bagrianski, P. Geo, and Chief Operating Officer. Processing phase was carried out under the supervision of Geoffrey Plastow, P. Geo, Data Processing Manager. The customer relations were looked after by David Hitz.

4. DATA PROCESSING AND PRESENTATION

Data compilation and processing were carried out by the application of Geosoft OASIS Montaj and programs proprietary to Geotech Ltd.

4.1 FLIGHT PATH

The flight path, recorded by the acquisition program as WGS 84 latitude/longitude, was converted into the NAD83 Datum, UTM Zone 9 North coordinate system in Oasis Montaj.

The flight path was drawn using linear interpolation between x, y positions from the navigation system. Positions are updated every second and expressed as UTM easting's (x) and UTM northing's (y).

4.2 ELECTROMAGNETIC DATA

The Full Waveform EM specific data processing operations included:

- Half cycle stacking (performed at time of acquisition);
- System response correction;
- Parasitic and drift removal by deconvolution.

A three stage digital filtering process was used to reject major spheric events and to reduce noise levels. Local spheric activity can produce sharp, large amplitude events that cannot be removed by conventional filtering procedures. Smoothing or stacking will reduce their amplitude but leave a broader residual response that can be confused with geological phenomena. To avoid this possibility, a computer algorithm searches out and rejects the major spheric events.

The signal to noise ratio was further improved by the application of a low pass linear digital filter. This filter has zero phase shift which prevents any lag or peak displacement from occurring, and it suppresses only variations with a wavelength less than about 1 second or 15 metres. This filter is a symmetrical 1 sec linear filter.

The results are presented as stacked profiles of EM voltages for the time gates, in linear - logarithmic scale for the B-field Z component and dB/dt responses in the Z and X components. B-field Z component time channel recorded at 2.021 milliseconds after the termination of the impulse is also presented as a colour image. Calculated Time Constant (TAU) with Calculated Vertical Derivative contours is presented in Appendix C and E. Resistivity Depth Image (RDI) is also presented in Appendix F and G.

VTEM has three receiver coil orientations. Z-axis coil is oriented parallel to the transmitter coil axis and both are horizontal to the ground. The X-axis and Y-axis coil is oriented parallel to the ground and along the line-of-flight. This combined three coil configuration provides information on the position, depth, dip and thickness of a conductor. Generalized modeling results of VTEM max data are shown in Appendix D.

In general X-component data produce cross-over type anomalies: from “+ to -” in flight direction of flight for “thin” sub vertical targets and from “- to +” in direction of flight for “thick” targets. Z component data produce double peak type anomalies for “thin” sub vertical targets and single peak for “thick” targets.

The limits and change-over of “thin-thick” depends on dimensions of a TEM system (Appendix D, Figure D-16).

Because of X component polarity is under line-of-flight, convolution Fraser Filter (Figure 8) is applied to X component data to represent axes of conductors in the form of grid map. In this case positive FF anomalies always correspond to “plus-to-minus” X data crossovers independent of the flight direction.

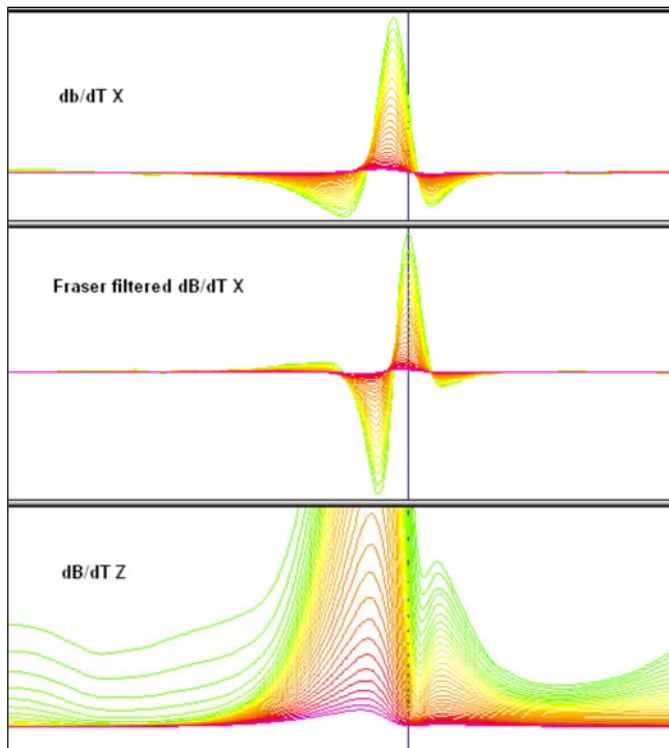


Figure 8: Z, X and Fraser filtered X (FFx) components for “thin” target.

4.3 HORIZONTAL MAGNETIC GRADIOMETER DATA

The horizontal gradients data from the VTEM™Plus are measured by two magnetometers 12.5 m apart on an independent bird mounted 10m above the VTEM™ loop. A GPS and a Gyro Inclinometer help to determine the positions and orientations of the magnetometers. The data from the two magnetometers are corrected for position and orientation variations, as well as for the diurnal variations using the base station data.

The position of the centre of the horizontal magnetic gradiometer bird is calculated from the GPS utilizing in-house processing tool in Geosoft. Following that total magnetic intensity is calculated at the center of the bird by calculating the mean values from both sensors. In addition to the total intensity advanced processing is done to calculate the in-line and cross-line (or lateral) horizontal gradient which enhance the understanding of magnetic targets. The in-line (longitudinal) horizontal gradient is calculated from the difference of two consecutive total magnetic field readings divided by the distance along the flight line direction, while the cross-line (lateral) horizontal magnetic gradient is calculated from the difference in the magnetic readings from both magnetic sensors divided by their horizontal separation.

Two advanced magnetic derivative products, the total horizontal derivative (THDR), and tilt angle derivative and are also created. The total horizontal derivative or gradient is defined as:

$THDR = \sqrt{H_x^2 + H_y^2}$, where H_x and H_y are cross-line and in-line horizontal gradients.

The tilt angle derivative (TDR) is defined as:

$TDR = \arctan(V_z/THDR)$, where THDR is the total horizontal derivative, and V_z is the vertical derivative.

Measured cross-line gradients can help to enhance cross-line linear features during gridding.

5. DELIVERABLES

5.1 SURVEY REPORT

The survey report describes the data acquisition, processing, and final presentation of the survey results. The survey report is provided in two paper copies and digitally in PDF format.

5.2 MAPS

Final maps were produced at scale of 1:20,000 (Kudz Ze Kayah and Pelly) and 1:10,000 (Wolf) for best representation of the survey size and line spacing. The coordinate/projection system used was NAD83 Datum, UTM Zone 9 North. All maps show the flight path trace and topographic data; latitude and longitude are also noted on maps.

The preliminary and final results of the survey are presented as EM profiles, a late-time gate gridded EM channel, and a colour magnetic TMI contour map.

- Maps at 1:20,000 (Kudz Ze Kayah and Pelly) and 1:10,000 (Wolf) in Geosoft MAP format, as follows:

GL160037_scalek_bb_dBdtz: dB/dt profiles Z Component, Time Gates 0.220 – 7.036 ms in linear – logarithmic scale.

GL160037_scalek_bb_Bfieldz: B-field profiles Z Component, Time Gates 0.220 – 7.036 ms in linear – logarithmic scale.

GL160037_scalek_bb_BFz36: B-field Z Component Channel 36, Time Gate 2.021 ms colour image.

GL160037_scalek_bb_SFxFF20: dBdt X Component Fraser Filtered Channel 20, Time Gate 0.220 ms colour image.

GL160037_scalek_bb_TMI: Total magnetic intensity (TMI) colour image and contours.

GL160037_scalek_bb_TauSF: dB/dt Calculated Time Constant (Tau) with Calculated Vertical Derivative contours

GL160037_scalek_bb_TotHGrad: Magnetic Total Horizontal Gradient colour image.

GL160037_scalek_bb_TiltDrv: Magnetic Tilt-Angle Derivative colour image.

where *scale* represents the scale of the map

bb represents the block name

- Maps are also presented in PDF format.
- The topographic data base was derived from 1:50,000 NRC (Natural Resources Canada) NTDB data, www.geogratis.ca.
- A Google Earth file *GL160037_FP.kml* showing the flight path of the block is included. Free versions of Google Earth software from: <http://earth.google.com/download-earth.html>

5.3 DIGITAL DATA

Two copies of the data and maps on DVD were prepared to accompany the report. Each DVD contains a digital file of the line data in GDB Geosoft Montaj format as well as the maps in Geosoft Montaj Map and PDF format.

- DVD structure.

Data contains databases, grids and maps, as described below.
Report contains a copy of the report and appendices in PDF format.

Databases in Geosoft GDB format, containing the channels listed in Table 5.

Table 5: Geosoft GDB Data Format

Channel name	Units	Description
X:	metres	UTM Easting NAD83 Zone 9 North
Y:	metres	UTM Northing NAD83 Zone 9 North
Longitude:	Decimal Degrees	WGS 84 Longitude data
Latitude:	Decimal Degrees	WGS 84 Latitude data
Z:	metres	GPS antenna elevation (above Geoid)
Zb:	metres	EM bird elevation (above Geoid)
Radar:	metres	helicopter terrain clearance from radar altimeter
Radarb:	metres	Calculated EM transmitter-receiver loop terrain clearance from radar altimeter
DEM:	metres	Digital Elevation Model
Gtime:	Seconds of the day	GPS time
Mag1L:	nT	Measured Total Magnetic field data (left sensor)
Mag1R:	nT	Measured Total Magnetic field data (right sensor)
Basemag:	nT	Magnetic diurnal variation data
Mag2LZ:	nT	Z corrected (w.r.t. loop center) and diurnal corrected magnetic field left mag
Mag2RZ:	nT	Z corrected (w.r.t. loop center) and diurnal corrected magnetic field right mag
TMI2:	nT	Calculated from diurnal corrected total magnetic field intensity of the centre of the loop
TMI3:	nT	Microleveled total magnetic field intensity of the centre of the loop
Hginline:		Calculated in-line gradient
Hgcxline:		measured cross-line gradient
CVG:	nT/m	Calculated Magnetic Vertical Gradient
SFz[4]:	pV/(A*m ⁴)	Z dB/dt 0.021 millisecond time channel
SFz[5]:	pV/(A*m ⁴)	Z dB/dt 0.026 millisecond time channel
SFz[6]:	pV/(A*m ⁴)	Z dB/dt 0.031 millisecond time channel
SFz[7]:	pV/(A*m ⁴)	Z dB/dt 0.036 millisecond time channel
SFz[8]:	pV/(A*m ⁴)	Z dB/dt 0.042 millisecond time channel
SFz[9]:	pV/(A*m ⁴)	Z dB/dt 0.048 millisecond time channel
SFz[10]:	pV/(A*m ⁴)	Z dB/dt 0.055 millisecond time channel
SFz[11]:	pV/(A*m ⁴)	Z dB/dt 0.063 millisecond time channel
SFz[12]:	pV/(A*m ⁴)	Z dB/dt 0.073 millisecond time channel
SFz[13]:	pV/(A*m ⁴)	Z dB/dt 0.083 millisecond time channel
SFz[14]:	pV/(A*m ⁴)	Z dB/dt 0.096 millisecond time channel

Channel name	Units	Description
SFz[15]:	pV/(A*m ⁴)	Z dB/dt 0.110 millisecond time channel
SFz[16]:	pV/(A*m ⁴)	Z dB/dt 0.126 millisecond time channel
SFz[17]:	pV/(A*m ⁴)	Z dB/dt 0.145 millisecond time channel
SFz[18]:	pV/(A*m ⁴)	Z dB/dt 0.167 millisecond time channel
SFz[19]:	pV/(A*m ⁴)	Z dB/dt 0.192 millisecond time channel
SFz[20]:	pV/(A*m ⁴)	Z dB/dt 0.220 millisecond time channel
SFz[21]:	pV/(A*m ⁴)	Z dB/dt 0.253 millisecond time channel
SFz[22]:	pV/(A*m ⁴)	Z dB/dt 0.290 millisecond time channel
SFz[23]:	pV/(A*m ⁴)	Z dB/dt 0.333 millisecond time channel
SFz[24]:	pV/(A*m ⁴)	Z dB/dt 0.383 millisecond time channel
SFz[25]:	pV/(A*m ⁴)	Z dB/dt 0.440 millisecond time channel
SFz[26]:	pV/(A*m ⁴)	Z dB/dt 0.505 millisecond time channel
SFz[27]:	pV/(A*m ⁴)	Z dB/dt 0.580 millisecond time channel
SFz[28]:	pV/(A*m ⁴)	Z dB/dt 0.667 millisecond time channel
SFz[29]:	pV/(A*m ⁴)	Z dB/dt 0.766 millisecond time channel
SFz[30]:	pV/(A*m ⁴)	Z dB/dt 0.880 millisecond time channel
SFz[31]:	pV/(A*m ⁴)	Z dB/dt 1.010 millisecond time channel
SFz[32]:	pV/(A*m ⁴)	Z dB/dt 1.161 millisecond time channel
SFz[33]:	pV/(A*m ⁴)	Z dB/dt 1.333 millisecond time channel
SFz[34]:	pV/(A*m ⁴)	Z dB/dt 1.531 millisecond time channel
SFz[35]:	pV/(A*m ⁴)	Z dB/dt 1.760 millisecond time channel
SFz[36]:	pV/(A*m ⁴)	Z dB/dt 2.021 millisecond time channel
SFz[37]:	pV/(A*m ⁴)	Z dB/dt 2.323 millisecond time channel
SFz[38]:	pV/(A*m ⁴)	Z dB/dt 2.667 millisecond time channel
SFz[39]:	pV/(A*m ⁴)	Z dB/dt 3.063 millisecond time channel
SFz[40]:	pV/(A*m ⁴)	Z dB/dt 3.521 millisecond time channel
SFz[41]:	pV/(A*m ⁴)	Z dB/dt 4.042 millisecond time channel
SFz[42]:	pV/(A*m ⁴)	Z dB/dt 4.641 millisecond time channel
SFz[43]:	pV/(A*m ⁴)	Z dB/dt 5.333 millisecond time channel
SFz[44]:	pV/(A*m ⁴)	Z dB/dt 6.125 millisecond time channel
SFz[45]:	pV/(A*m ⁴)	Z dB/dt 7.036 millisecond time channel
SFz[46]:	pV/(A*m ⁴)	Z dB/dt 8.083 millisecond time channel
SFx[20]:	pV/(A*m ⁴)	X dB/dt 0.220 millisecond time channel
SFx[21]:	pV/(A*m ⁴)	X dB/dt 0.253 millisecond time channel
SFx[22]:	pV/(A*m ⁴)	X dB/dt 0.290 millisecond time channel
SFx[23]:	pV/(A*m ⁴)	X dB/dt 0.333 millisecond time channel
SFx[24]:	pV/(A*m ⁴)	X dB/dt 0.383 millisecond time channel
SFx[25]:	pV/(A*m ⁴)	X dB/dt 0.440 millisecond time channel
SFx[26]:	pV/(A*m ⁴)	X dB/dt 0.505 millisecond time channel
SFx[27]:	pV/(A*m ⁴)	X dB/dt 0.580 millisecond time channel
SFx[28]:	pV/(A*m ⁴)	X dB/dt 0.667 millisecond time channel
SFx[29]:	pV/(A*m ⁴)	X dB/dt 0.766 millisecond time channel
SFx[30]:	pV/(A*m ⁴)	X dB/dt 0.880 millisecond time channel
SFx[31]:	pV/(A*m ⁴)	X dB/dt 1.010 millisecond time channel
SFx[32]:	pV/(A*m ⁴)	X dB/dt 1.161 millisecond time channel
SFx[33]:	pV/(A*m ⁴)	X dB/dt 1.333 millisecond time channel
SFx[34]:	pV/(A*m ⁴)	X dB/dt 1.531 millisecond time channel
SFx[35]:	pV/(A*m ⁴)	X dB/dt 1.760 millisecond time channel
SFx[36]:	pV/(A*m ⁴)	X dB/dt 2.021 millisecond time channel
SFx[37]:	pV/(A*m ⁴)	X dB/dt 2.323 millisecond time channel

Channel name	Units	Description
SFx[38]:	pV/(A*m ⁴)	X dB/dt 2.667 millisecond time channel
SFx[39]:	pV/(A*m ⁴)	X dB/dt 3.063 millisecond time channel
SFx[40]:	pV/(A*m ⁴)	X dB/dt 3.521 millisecond time channel
SFx[41]:	pV/(A*m ⁴)	X dB/dt 4.042 millisecond time channel
SFx[42]:	pV/(A*m ⁴)	X dB/dt 4.641 millisecond time channel
SFx[43]:	pV/(A*m ⁴)	X dB/dt 5.333 millisecond time channel
SFx[44]:	pV/(A*m ⁴)	X dB/dt 6.125 millisecond time channel
SFx[45]:	pV/(A*m ⁴)	X dB/dt 7.036 millisecond time channel
SFx[46]:	pV/(A*m ⁴)	X dB/dt 8.083 millisecond time channel
SFy[20]:	pV/(A*m ⁴)	Y dB/dt 0.220 millisecond time channel
SFy[21]:	pV/(A*m ⁴)	Y dB/dt 0.253 millisecond time channel
SFy[22]:	pV/(A*m ⁴)	Y dB/dt 0.290 millisecond time channel
SFy[23]:	pV/(A*m ⁴)	Y dB/dt 0.333 millisecond time channel
SFy[24]:	pV/(A*m ⁴)	Y dB/dt 0.383 millisecond time channel
SFy[25]:	pV/(A*m ⁴)	Y dB/dt 0.440 millisecond time channel
SFy[26]:	pV/(A*m ⁴)	Y dB/dt 0.505 millisecond time channel
SFy[27]:	pV/(A*m ⁴)	Y dB/dt 0.580 millisecond time channel
SFy[28]:	pV/(A*m ⁴)	Y dB/dt 0.667 millisecond time channel
SFy[29]:	pV/(A*m ⁴)	Y dB/dt 0.766 millisecond time channel
SFy[30]:	pV/(A*m ⁴)	Y dB/dt 0.880 millisecond time channel
SFy[31]:	pV/(A*m ⁴)	Y dB/dt 1.010 millisecond time channel
SFy[32]:	pV/(A*m ⁴)	Y dB/dt 1.161 millisecond time channel
SFy[33]:	pV/(A*m ⁴)	Y dB/dt 1.333 millisecond time channel
SFy[34]:	pV/(A*m ⁴)	Y dB/dt 1.531 millisecond time channel
SFy[35]:	pV/(A*m ⁴)	Y dB/dt 1.760 millisecond time channel
SFy[36]:	pV/(A*m ⁴)	Y dB/dt 2.021 millisecond time channel
SFy[37]:	pV/(A*m ⁴)	Y dB/dt 2.323 millisecond time channel
SFy[38]:	pV/(A*m ⁴)	Y dB/dt 2.667 millisecond time channel
SFy[39]:	pV/(A*m ⁴)	Y dB/dt 3.063 millisecond time channel
SFy[40]:	pV/(A*m ⁴)	Y dB/dt 3.521 millisecond time channel
SFy[41]:	pV/(A*m ⁴)	Y dB/dt 4.042 millisecond time channel
SFy[42]:	pV/(A*m ⁴)	Y dB/dt 4.641 millisecond time channel
SFy[43]:	pV/(A*m ⁴)	Y dB/dt 5.333 millisecond time channel
SFy[44]:	pV/(A*m ⁴)	Y dB/dt 6.125 millisecond time channel
SFy[45]:	pV/(A*m ⁴)	Y dB/dt 7.036 millisecond time channel
SFy[46]:	pV/(A*m ⁴)	Y dB/dt 8.083 millisecond time channel
BFz	(pV*ms)/(A*m ⁴)	Z B-Field data for time channels 4 to 46
BFx	(pV*ms)/(A*m ⁴)	X B-Field data for time channels 20 to 46
BFy:	(pV*ms)/(A*m ⁴)	Y B-Field data for time channels 20 to 46
SFxFF:	pV/(A*m ⁴)	Fraser Filtered X dB/dt
NchanBF:		Latest time channels of TAU calculation
TauBF:	ms	Time constant B-Field
NchanSF:		Latest time channels of TAU calculation
TauSF:	ms	Time constant dB/dt
PLM:		60 Hz power line monitor

Electromagnetic B-field and dB/dt Z component data is found in array channel format between indexes 4 – 46, and X and Y component data from 20 – 46, as described above.

- Database of the Resistivity Depth Images in Geosoft GDB format, containing the following channels:

Table 6: Geosoft Resistivity Depth Image GDB Data Format

Channel name	Units	Description
Xg:	metres	UTM Easting NAD83 Zone 9 North
Yg:	metres	UTM Northing NAD83 Zone 9 North
Dist:	meters	Distance from the beginning of the line
Depth:	meters	array channel, depth from the surface
Z:	meters	array channel, depth from sea level
AppRes:	Ohm-m	array channel, Apparent Resistivity
TR:	meters	EM system height from sea level
Topo:	meters	digital elevation model
Radarb:	metres	Calculated EM transmitter-receiver loop terrain clearance from radar altimeter
SF:	$\text{pV}/(\text{A} \cdot \text{m}^4)$	array channel, dB/dT
MAG:	nT	TMI data
CVG:	nT/m	CVG data
DOI:	metres	Depth of Investigation: a measure of VTEM depth effectiveness
PLM:		60Hz Power Line Monitor

- Database of the VTEM Waveform “GL160037_waveform_final.gdb” in Geosoft GDB format, containing the following channels:

Table 7: Geosoft database for the VTEM waveform

Channel name	Units	Description
Time:	milliseconds	Sampling rate interval, 5.2083 microseconds
Tx_Current:	amps	Output current of the transmitter

- Grids in Geosoft GRD and GeoTIFF format, as follows:

<i>bb_BFz36:</i>	B-Field Z Component Channel 36 (Time Gate 2.021 ms)
<i>bb_CVG:</i>	Calculated Vertical Derivative (nT/m)
<i>bb_DEM:</i>	Digital Elevation Model (metres)
<i>bb_Hgcxline:</i>	Measured Cross-Line Gradient (nT/m)
<i>bb_Hginline:</i>	Measured In-Line Gradient (nT/m)
<i>bb_PLM:</i>	Power Line Monitor (60Hz)
<i>bb_SFxFF20:</i>	Fraser Filtered dB/dt X Component Channel 20 (Time Gate 0.220ms)
<i>bb_SFz15:</i>	dB/dt Z Component Channel 15 (Time Gate 0.110 ms)
<i>bb_SFz30:</i>	dB/dt Z Component Channel 30 (Time Gate 0.880 ms)
<i>bb_SFz45:</i>	dB/dt Z Component Channel 45 (Time Gate 7.036 ms)
<i>bb_TauBF:</i>	B-Field Z Component, Calculated Time Constant (ms)
<i>bb_TauSF:</i>	dB/dt Z Component, Calculated Time Constant (ms)
<i>bb_TiltDerivative:</i>	Magnetic Tilt derivative (radians)
<i>bb_TMI:</i>	Total Magnetic Intensity (nT)
<i>bb_TotalHorgrad:</i>	Magnetic Total Horizontal Gradient (nT/m)

where *bb* represents the block name

A Geosoft .GRD file has a .GI metadata file associated with it, containing grid projection information. A grid cell size of 37.5 metres was used.

6. CONCLUSIONS AND RECOMMENDATIONS

A helicopter-borne versatile time domain electromagnetic (VTEMplus) and horizontal magnetic gradiometer geophysical survey has been completed over Kudz Ze Kayah, Pelly and Wolf situated near Wolverine Lake, Yukon.

The total area coverage is 241 km². Total survey line coverage 1589 line kilometres. The principal sensors included a Time Domain EM system and a horizontal magnetic gradiometer using two caesium magnetometers. Results have been presented as stacked profiles, and contour colour images at a scale of 1:20,000 (Kudz Ze Kayah and Pelly) and 1:10,000 (Wolf). A formal Interpretation has not been included or requested.

Based on the geophysical results obtained, a number of TEM anomalous zones are identified across the blocks. All of these anomalies are considered to be induced by low to moderate conductive targets. They can be seen overlapping the TAU decay parameter image presented with the calculated vertical magnetic gradient (CVG) contours in the Appendix C.

The main conductive zones in the Kudz Ze Kayah blocks are oriented NE-SW in the western part to NW-SE in the centre part having strong association with the magnetic anomalies. The conductive zone in the southern part of L3252-L3370 oriented NE-SW exhibits AIIP phenomenon and follows the magnetic trend. Most of the conductors can be approximated as “thick” subvertical plates and some as “thin” plates with the inherent double-peak response. Some of the zones being on the edge of the survey boundary are not well defined. Detailed resistivity depth sections were created for all the survey lines. According to the detailed resistivity depth imaging, the top of the EM response sources varies in depth from about 50-80m deep).

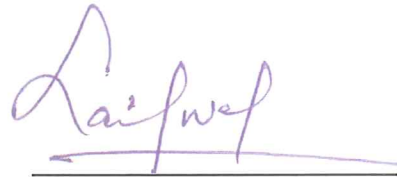
The main conductive zones in the Pelly and Wolf blocks are oriented NE-SW and are associated with the magnetic anomalies. Most of the conductors can be approximated as “thick” subvertical plates and some as “thin” plates with the inherent double-peak response. Some of the zones being on the edge of the survey boundary are not well defined. Detailed resistivity depth sections were created for all the survey lines. According to the detailed resistivity depth imaging, the top of the EM response sources varies in depth from about 50-80m deep).

If the conductors correspond to an exploration model, it is recommended picking anomalies with conductance grading and center localization of the targets, detail resistivity depth imaging and Maxwell plate modelling prior to ground follow up and drill testing. Since the EM conductors have close associations with the magnetic anomalies, 3D inversions and detailed structural interpretation for magnetic data are also suggested.

Respectfully submitted²,



Nick Venter
Geotech Ltd.



Gaurav Nailwal
Geotech Ltd.



Geoffrey Plastow, P. Geo.
Data Processing Manager
Geotech Ltd.

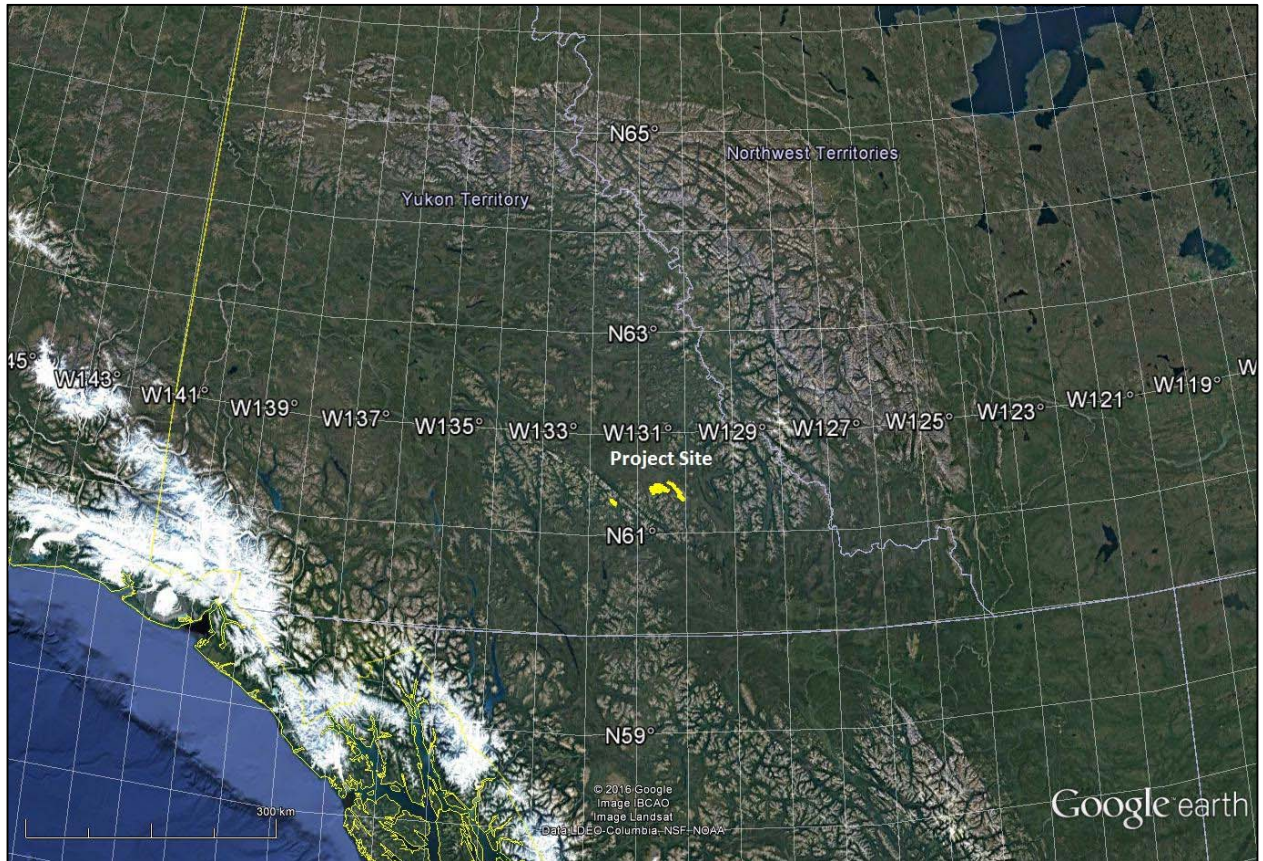


October, 2016

² Final data processing of the EM and magnetic data were carried out by Gaurav Nailwal, from the office of Geotech Ltd. in Aurora, Ontario, under the supervision of Geoffrey Plastow, P. Geo. Data Processing Manager.

APPENDIX A

SURVEY AREA LOCATION MAP



Overview of the Survey Area

APPENDIX B

SURVEY AREA COORDINATES

(WGS 84, UTM Zone 9 North)

Kudz Ze Kayah

X	Y
412005	6816377
411085	6813001
412018	6812815
411005	6809041
410084	6809227
410135	6809405
409300	6809419
409351	6811643
409717	6813012
407553	6813037
407608	6815024
406881	6815278
407894	6819052
408586	6818811
411027	6818759
411277	6819654
411542	6819646
412042	6821440
412810	6821429
412954	6821854
413832	6821826
413873	6822014
418263	6821917
418108	6821307
419619	6821248
419610	6820829
419959	6820821
420088	6821230
420984	6821215
420967	6820356
420720	6819511
421420	6819495
421411	6818924
422192	6819644
421920	6818615
422803	6818606
422796	6818201
424555	6818157
424540	6817946

X	Y
424595	6817942
424592	6817798
424908	6817791
424888	6816652
426229	6816114
427312	6816090
427314	6815756
427981	6815528
426968	6811754
426301	6811982
426225	6811981
425854	6812109
425857	6812241
425392	6812268
425202	6812337
423875	6812878
422249	6813577
422250	6813676
421994	6813681
421820	6813755
421818	6813673
421361	6813681
420907	6813830
420568	6813519
421195	6815893
419970	6814803
419805	6814773
412005	6816377

Wolf

X	Y
364237	6806799
362839	6806136
362839	6802966
362839	6802966
367270	6799467
369510	6799467
369522	6802462
369247	6802459
369187	6802527
364237	6806799

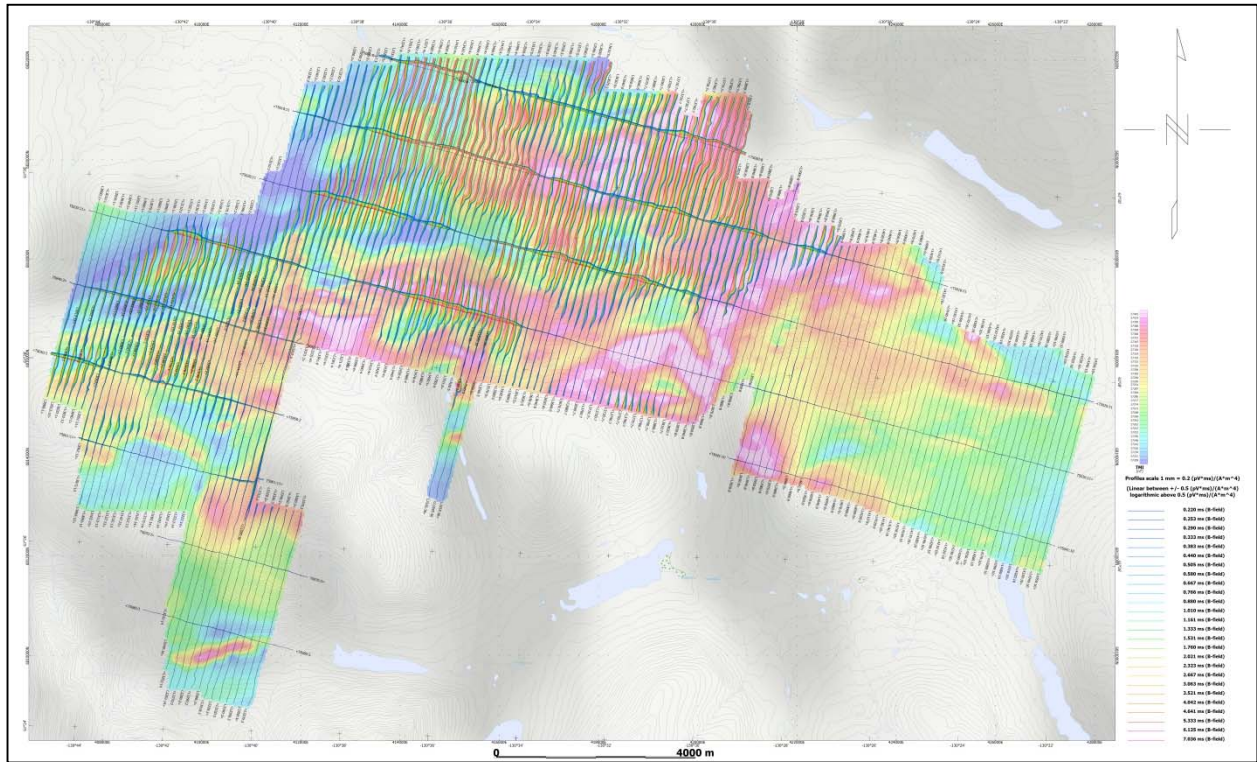
Pelly

X	Y
435126	6814679
437356	6816687
439476	6814734
438973	6814291
439488	6813548
439798	6813298
441018	6812431
441631	6812018
441611	6811991
441705	6811918
441722	6811933
442175	6811564
442440	6811361
442497	6811434
442712	6811256
442320	6810986
442440	6810812
442386	6810743
441065	6809551
441171	6809418
441339	6809288
441315	6809236
441525	6808965
441587	6809012
442719	6807596
443001	6807246
442159	6806577
443015	6805829
443895	6805661
445285	6804164
443055	6802156
441666	6803654
440786	6803821
439926	6804567
439329	6804578
438315	6805839
438033	6806190
437785	6806498
438466	6807113

X	Y
437929	6807783
437474	6808348
437468	6808564
437348	6809053
437438	6809123
437339	6809247
437326	6809424
437402	6809489
437424	6809541
437407	6809597
437427	6809658
437445	6809717
437499	6809764
437474	6809798
437501	6809904
437468	6809978
438112	6810557
438078	6810592
437739	6810834
437548	6810985
437660	6811098
437652	6811217
437567	6811281
437497	6811293
437480	6811331
437258	6811541
437225	6811581
436743	6812284
437246	6812727

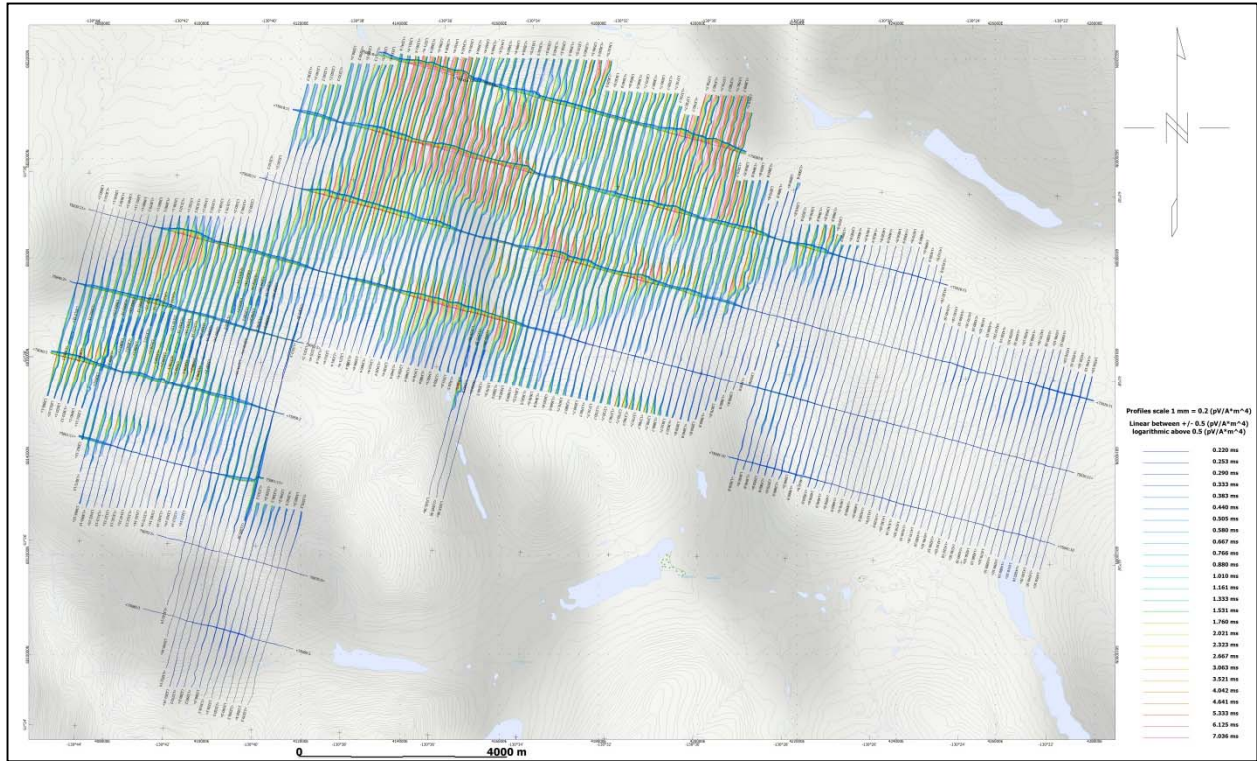
APPENDIX C

GEOPHYSICAL MAPS¹

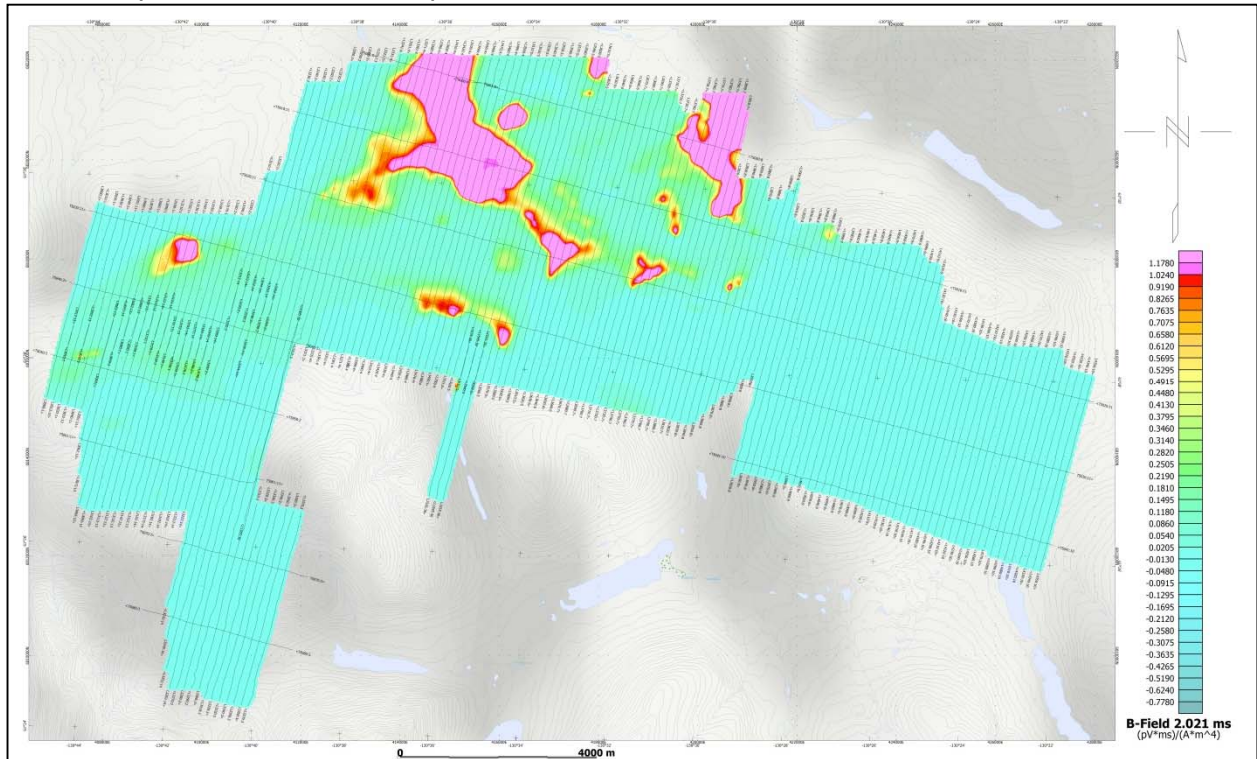


Kudz Ze Kayah - VTEM B-Field Z Component Profiles, Time Gates 0.220 to 7.036 ms

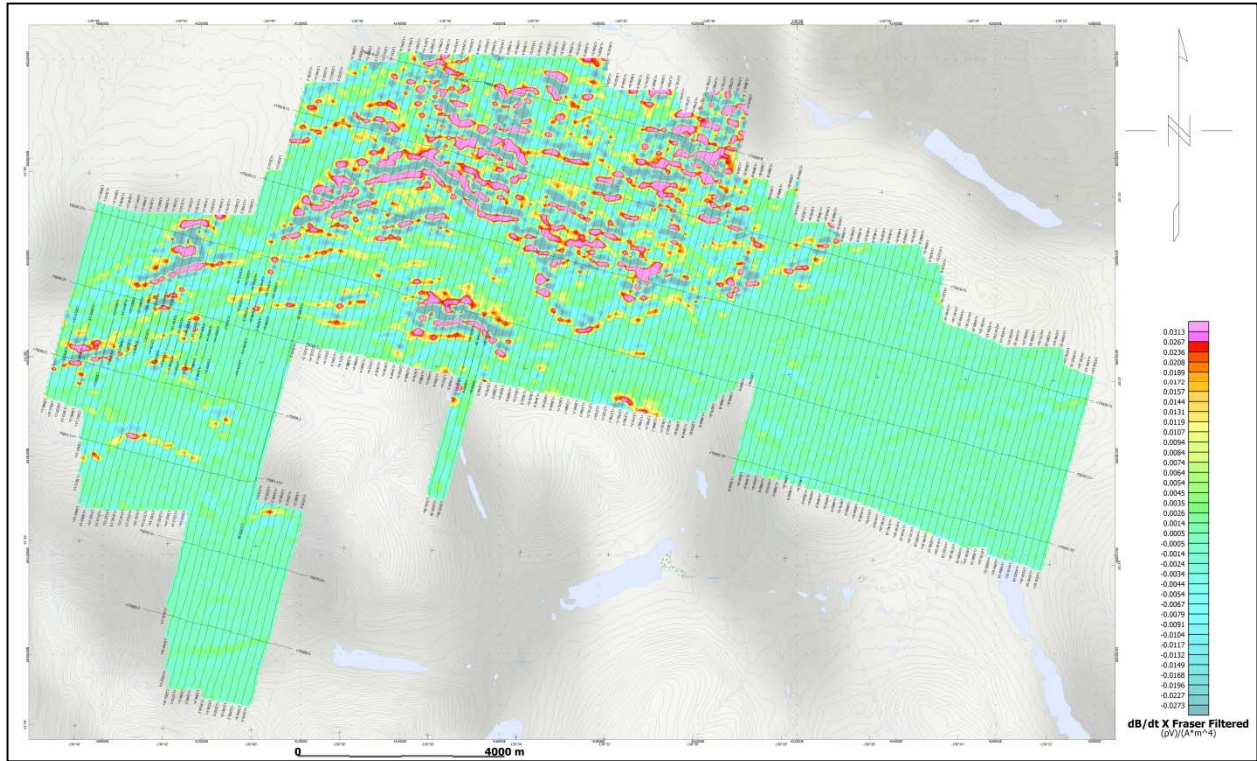
¹ Full size geophysical maps are also available in PDF format on the final DVD



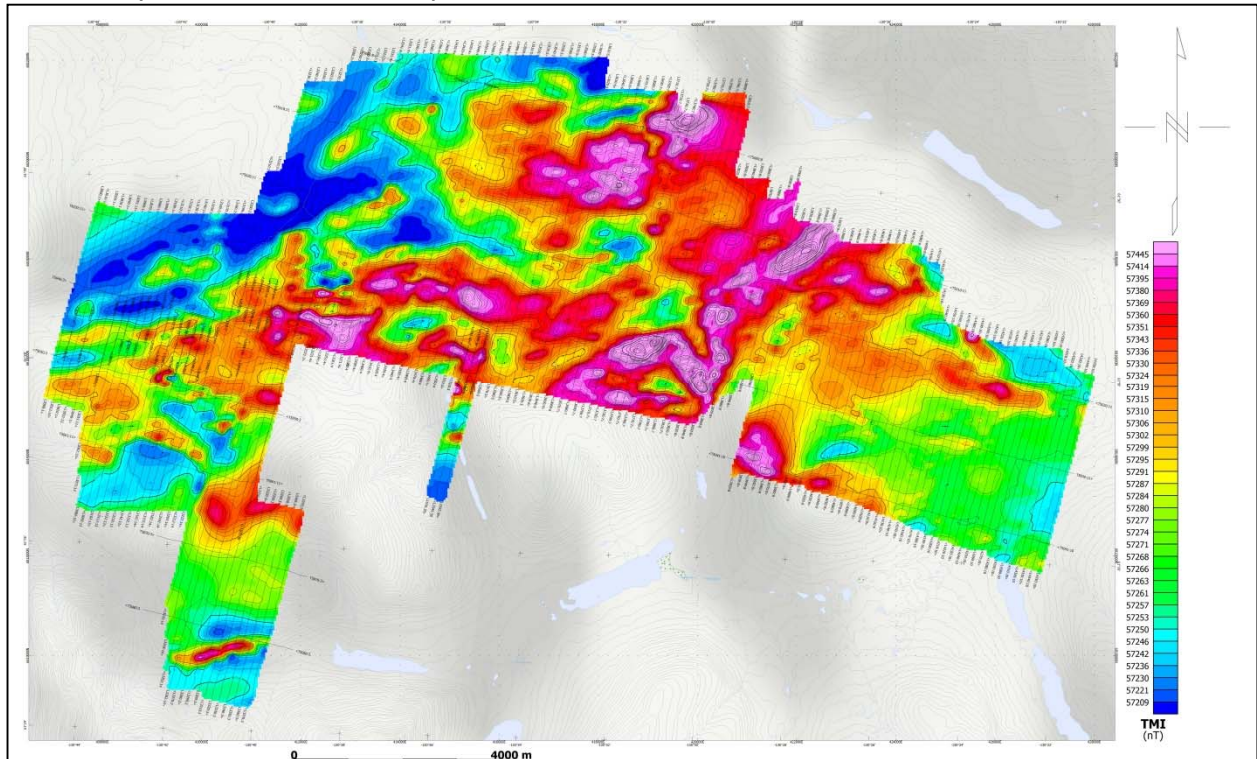
Kudz Ze Kayah - VTEM dB/dt Z Component Profiles, Time Gates 0.220 to 7.036 ms



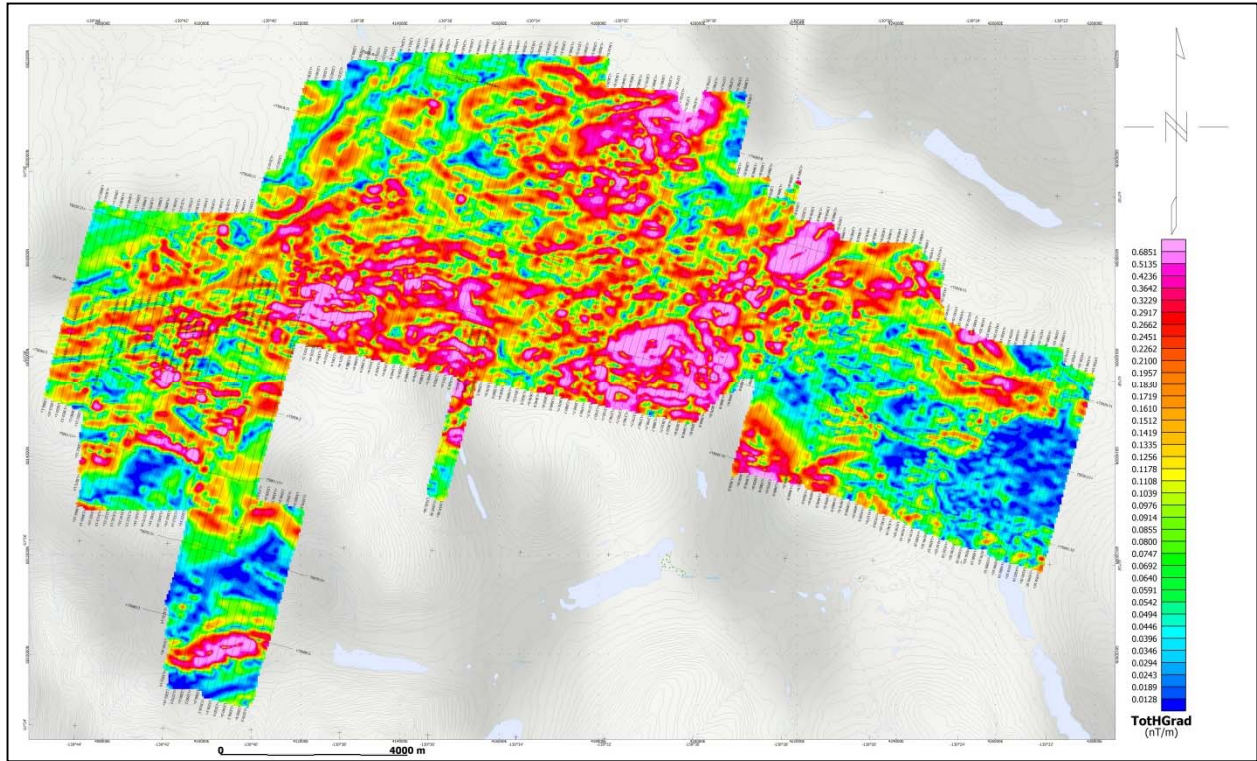
Kudz Ze Kayah - VTEM B-Field Z Component Channel 36, Time Gate 2.021 ms



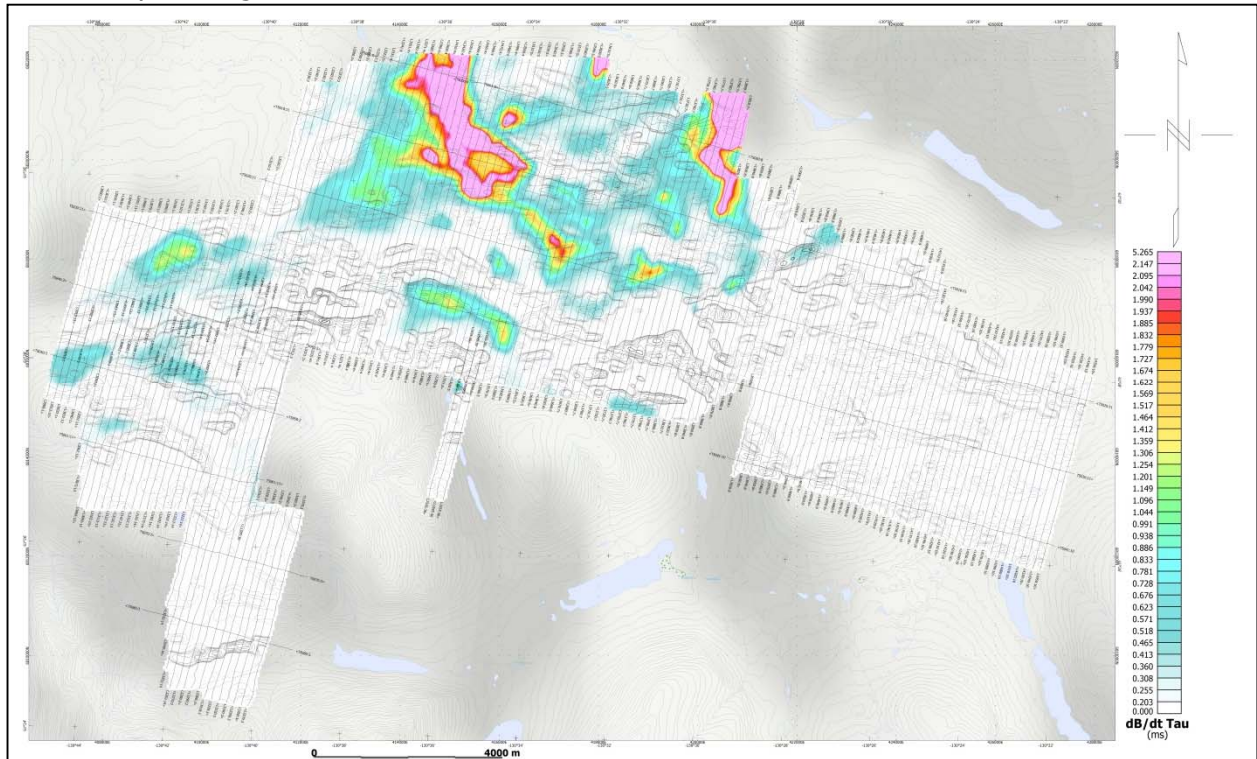
Kudz Ze Kayah - VTEM dB/dt X Component Fraser Filtered Channel 20, Time Gate 0.220 ms



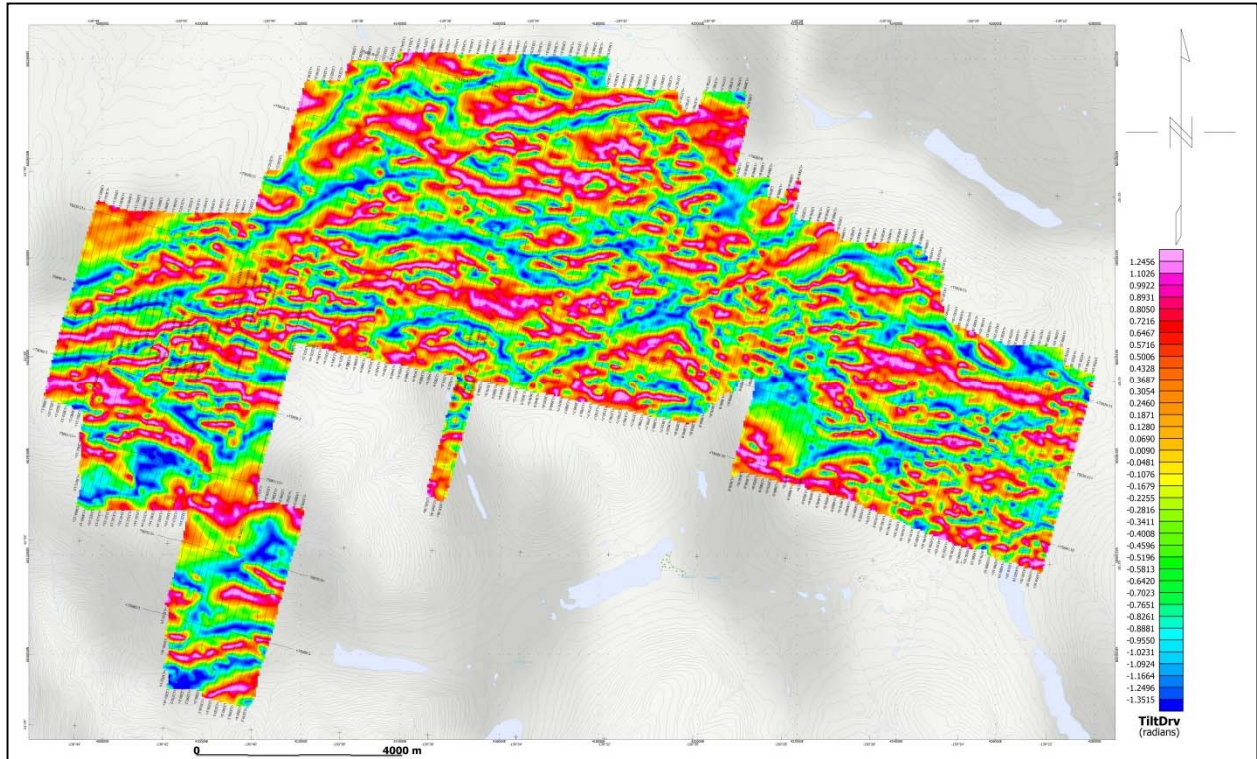
Kudz Ze Kayah - Total Magnetic Intensity (TMI)



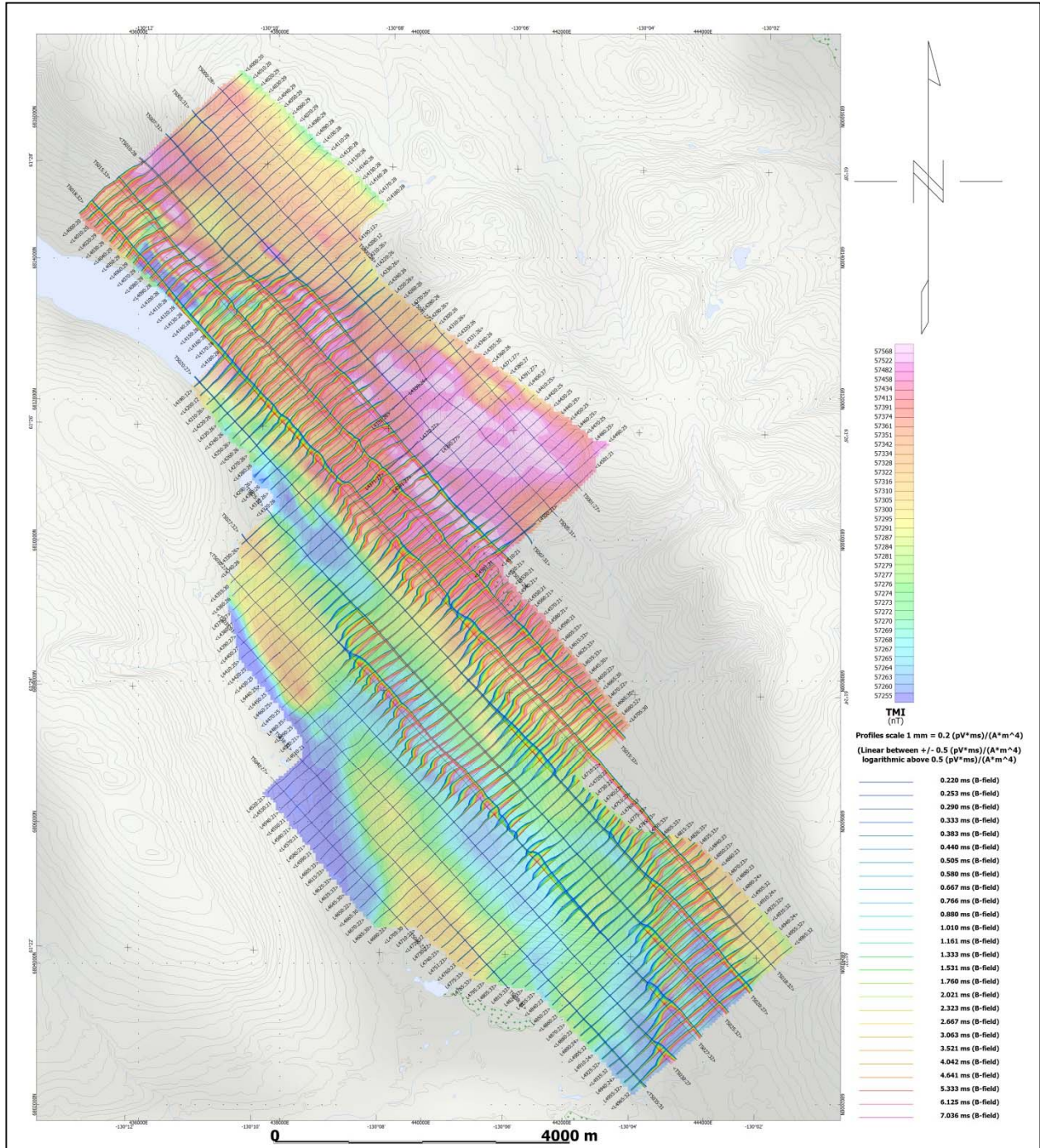
Kudz Ze Kayah - Magnetic Total Horizontal Gradient



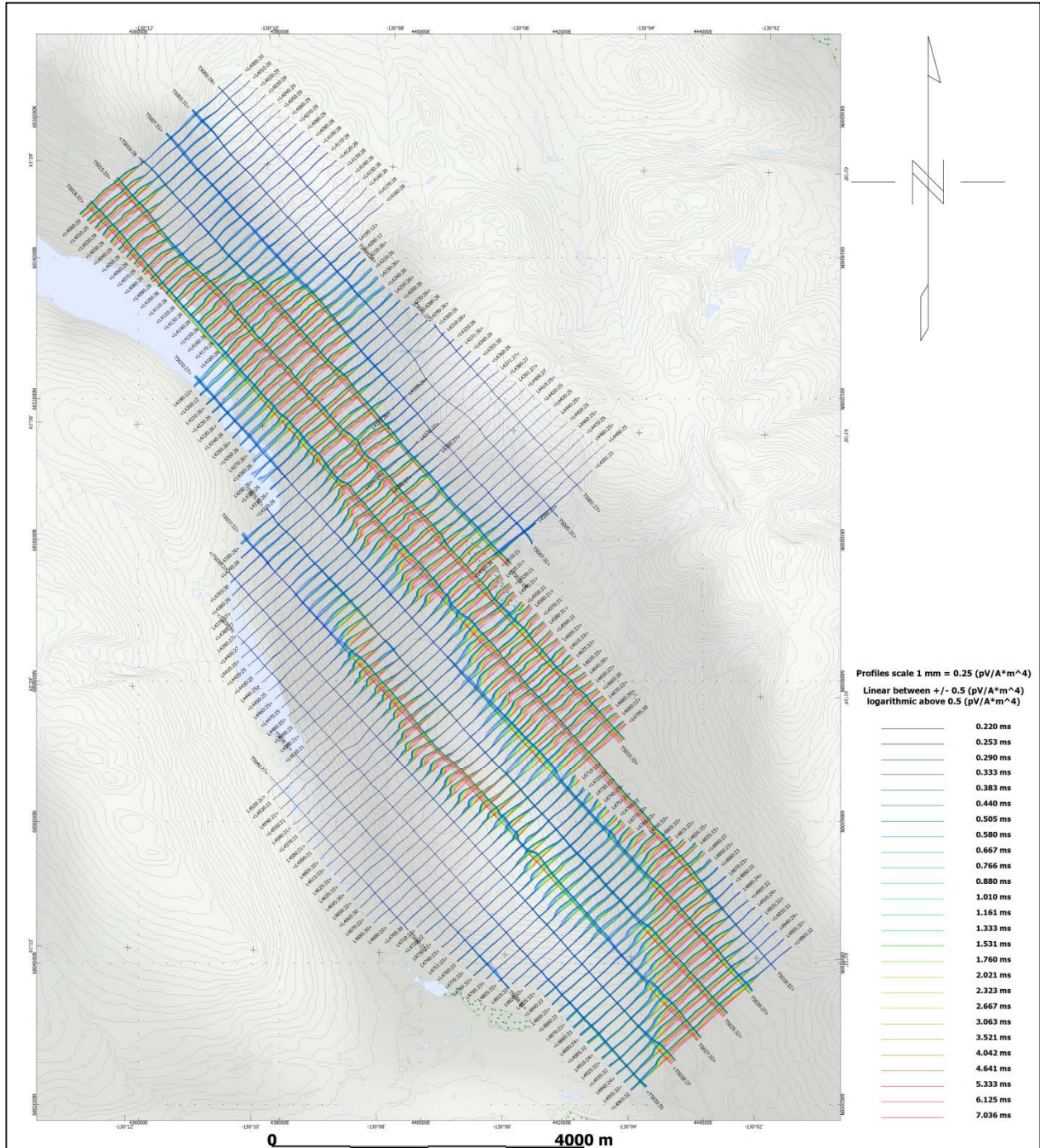
Kudz Ze Kayah - dB/dt Calculated Time Constant (Tau) with Calculated Vertical Derivative contours



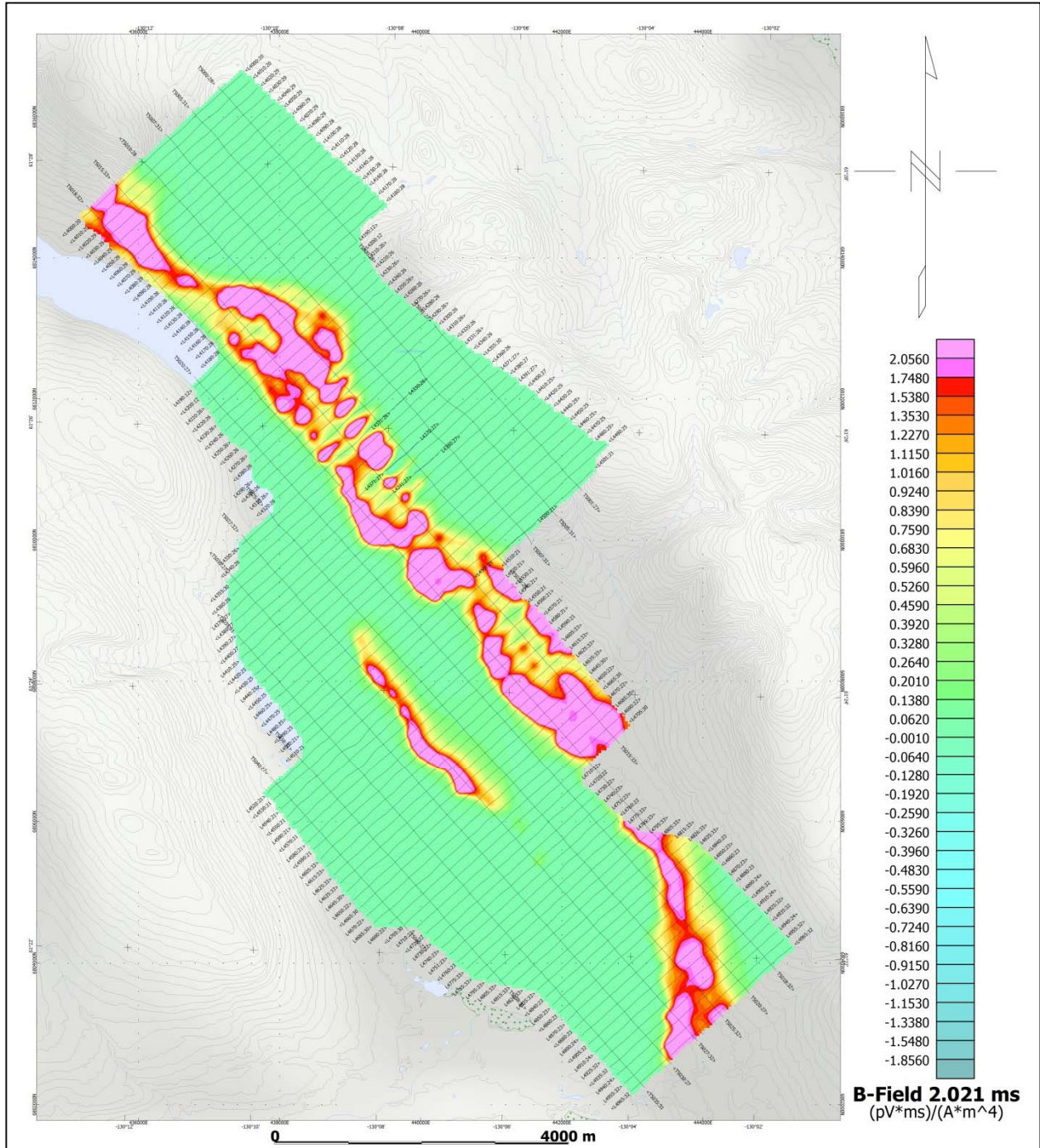
Kudz Ze Kayah - Magnetic Tilt - Angle Derivative



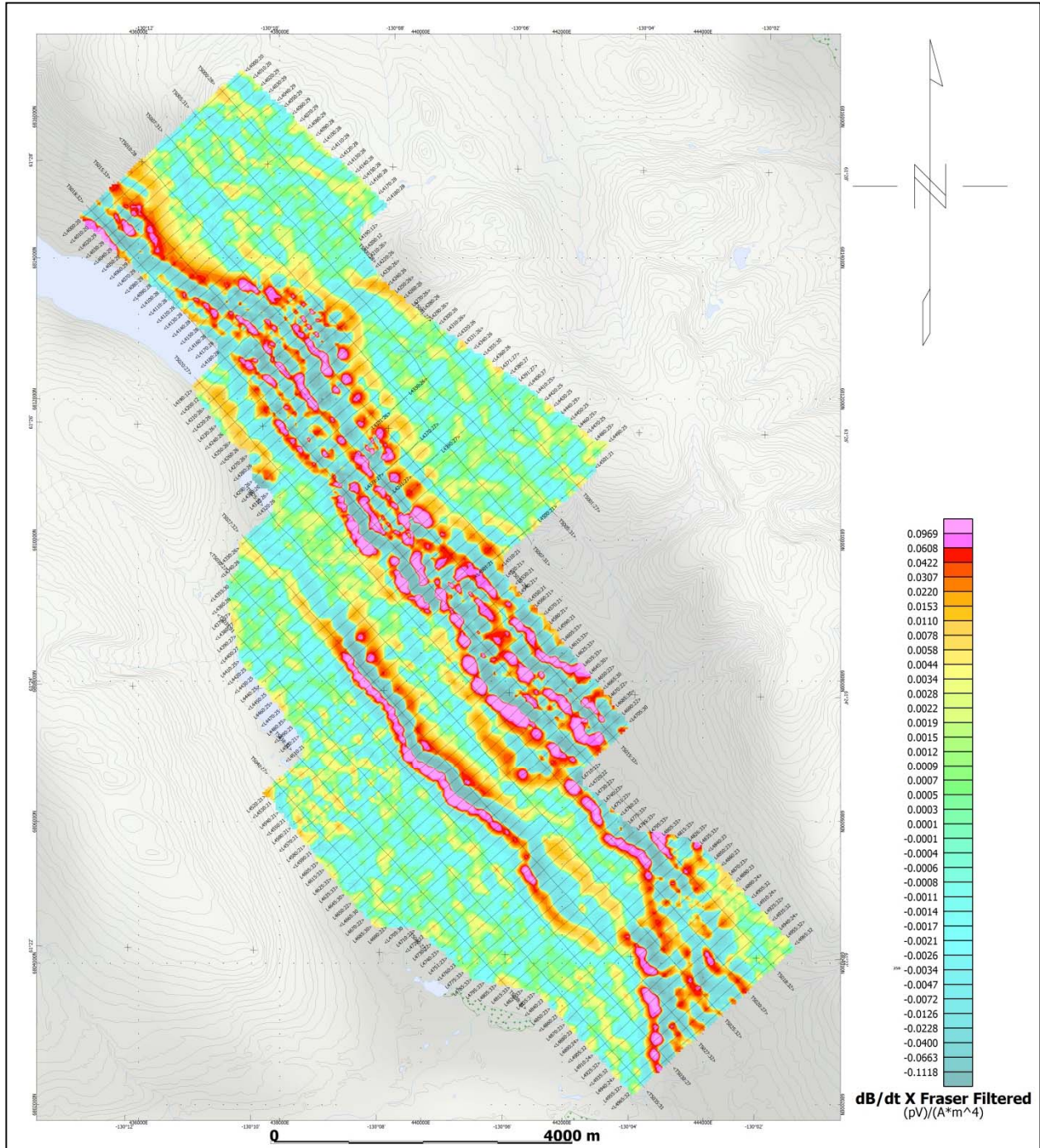
Pelly - VTEM B-Field Z Component Profiles, Time Gates 0.220 to 7.036 ms



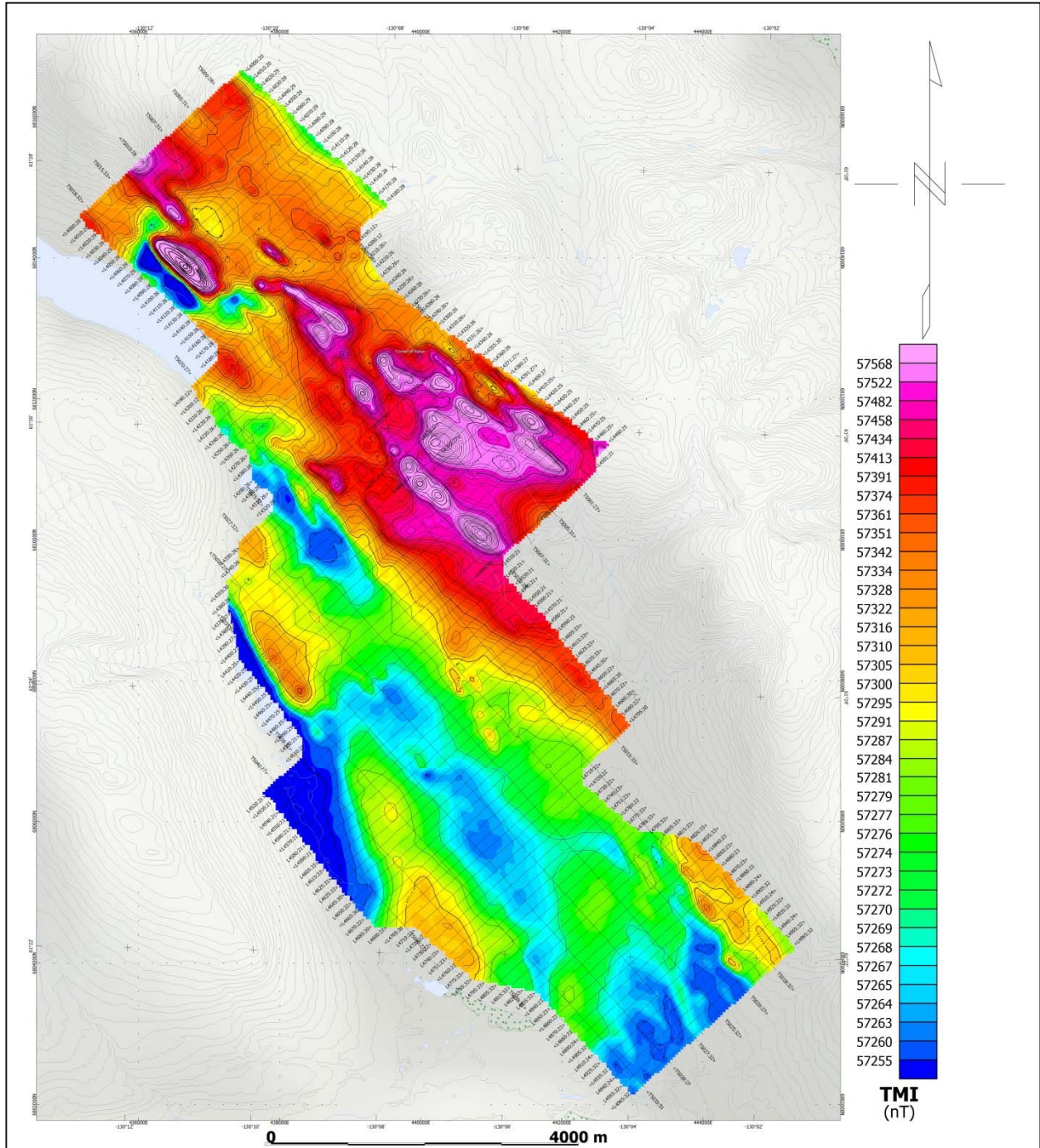
Pelly - VTEM dB/dt Z Component Profiles, Time Gates 0.220 to 7.036 ms



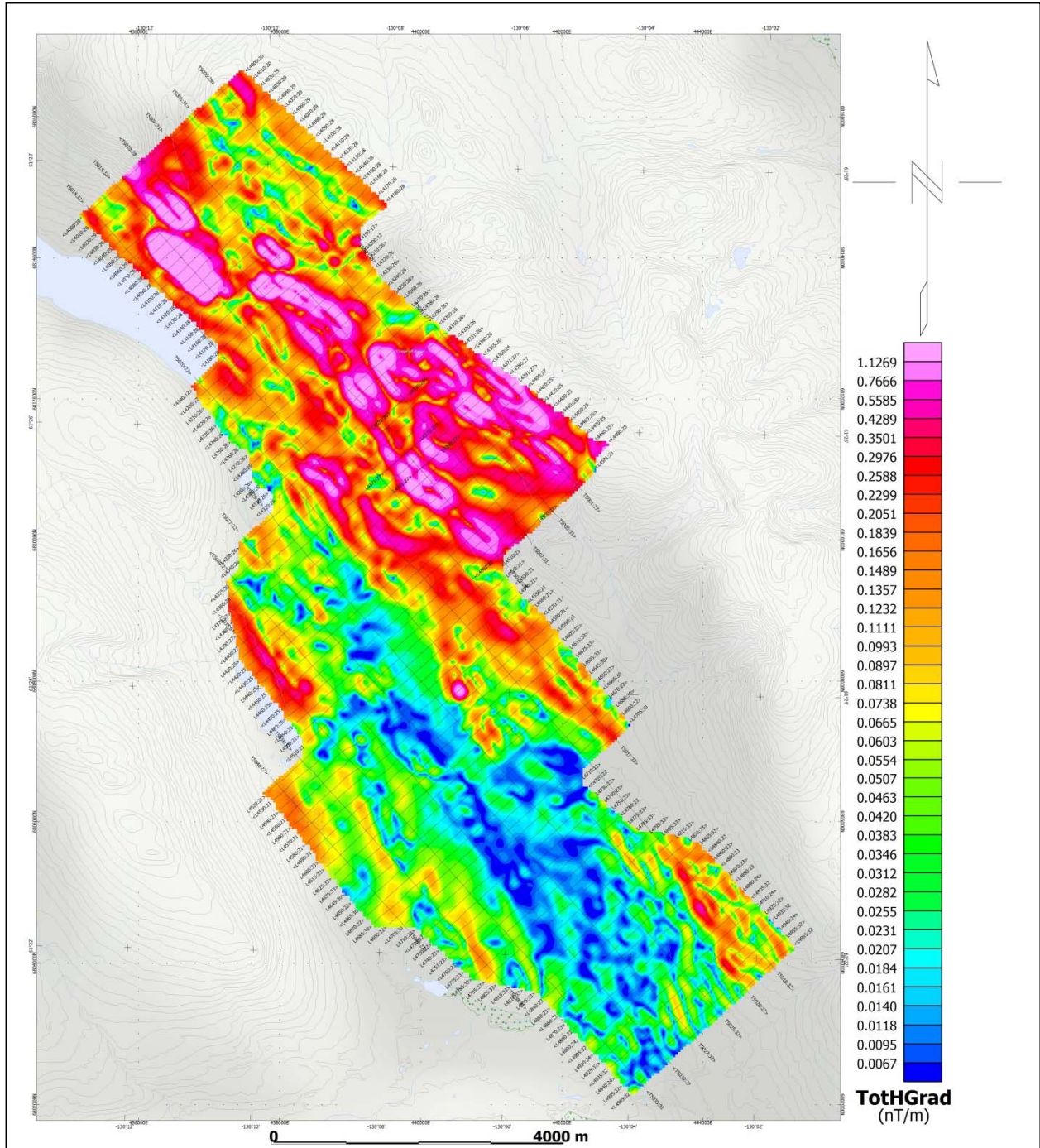
Pelly - VTEM B-Field Z Component Channel 36, Time Gate 2.021 ms



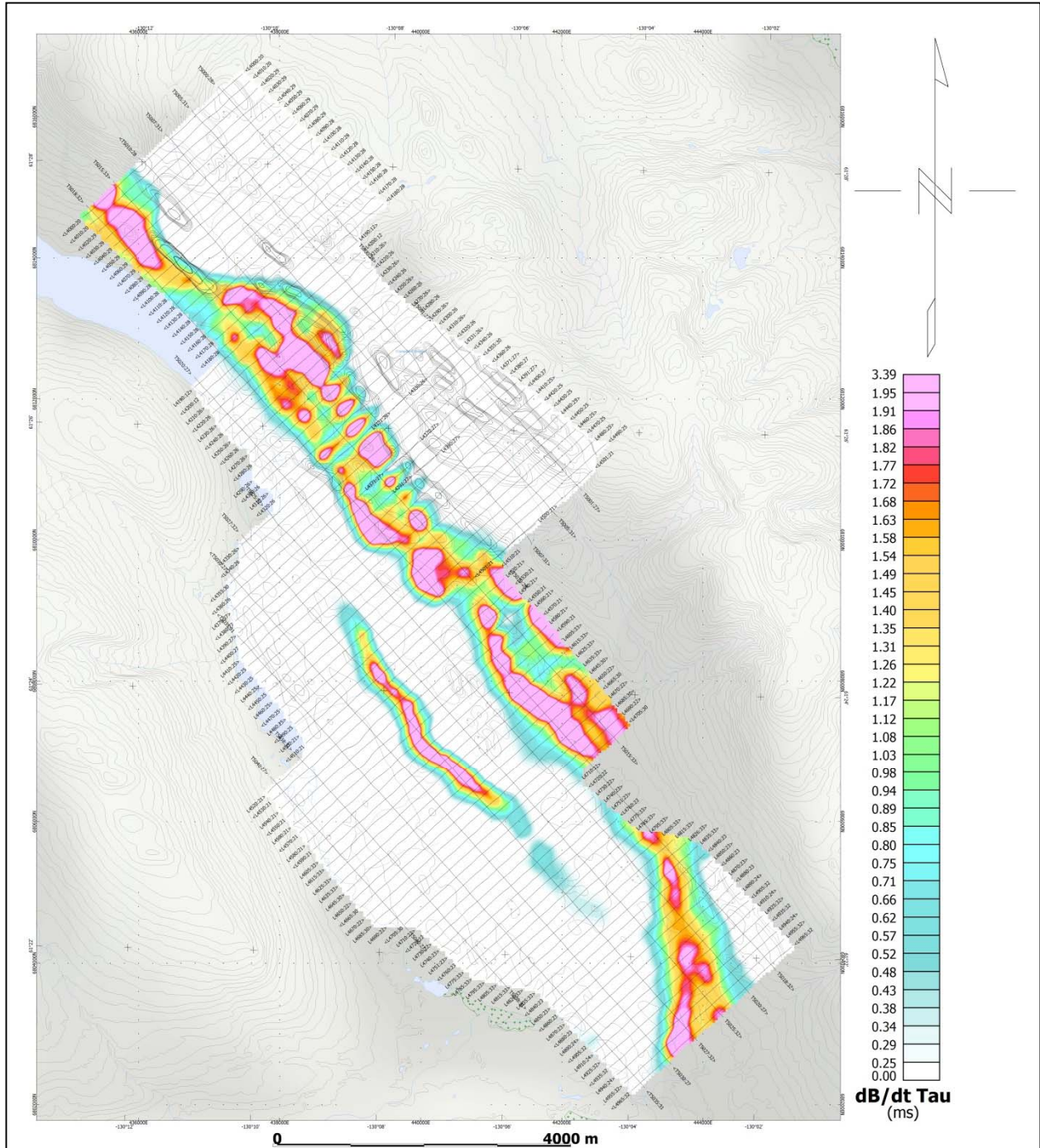
Pelly - VTEM dB/dt X Component Fraser Filtered Channel 20, Time Gate 0.220 ms



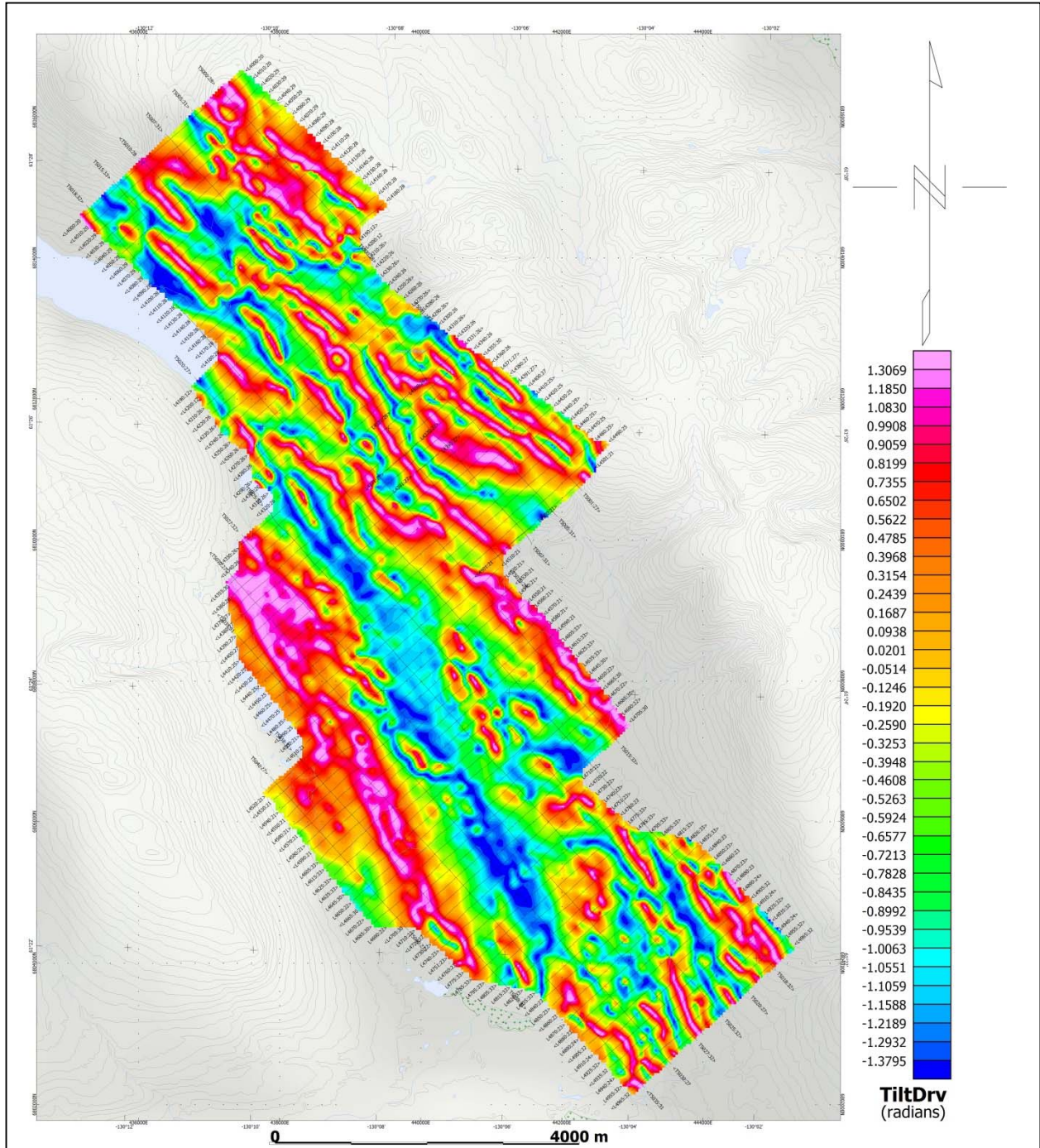
Pelly - Total Magnetic Intensity (TMI)



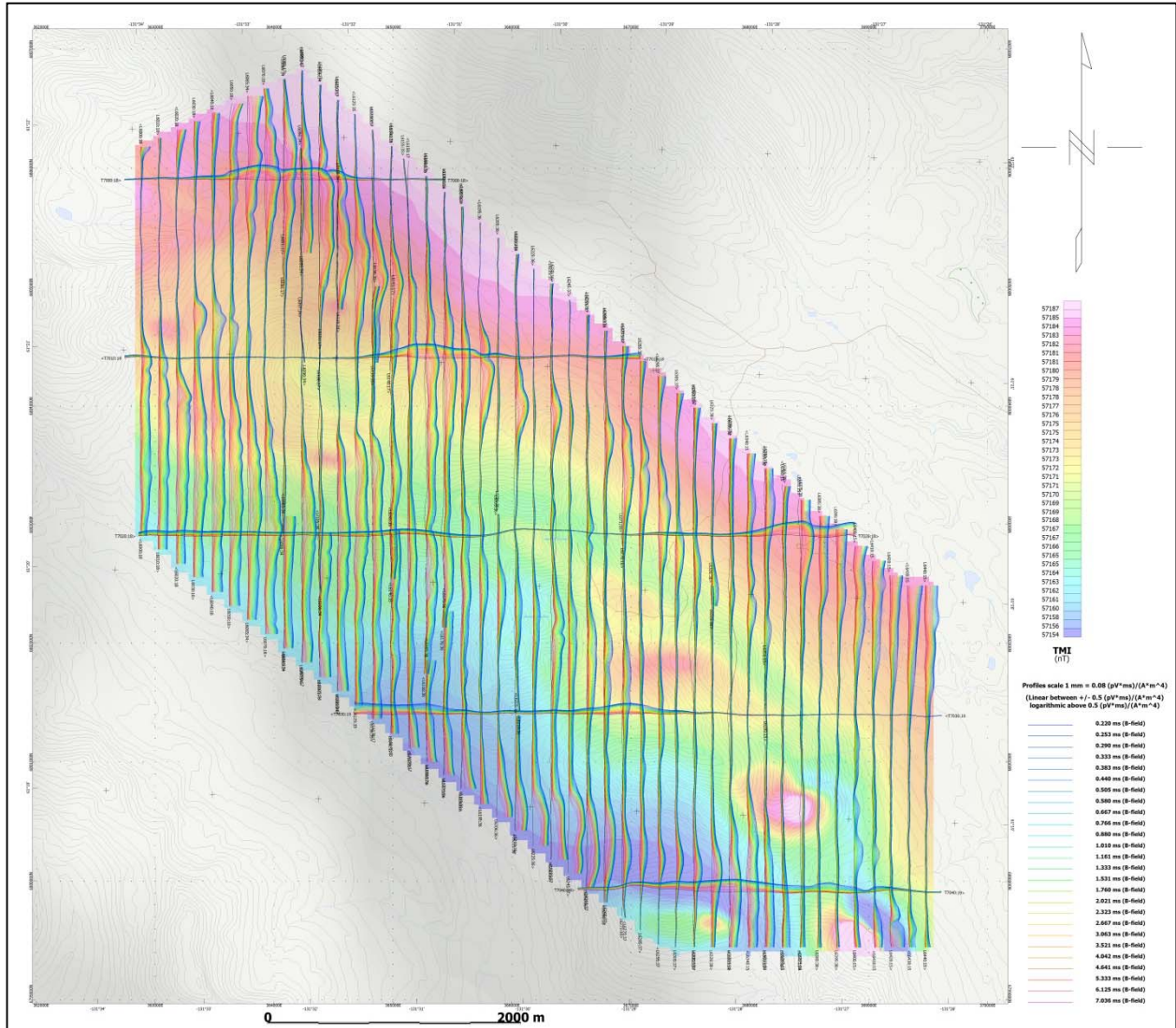
Pelly - Magnetic Total Horizontal Gradient



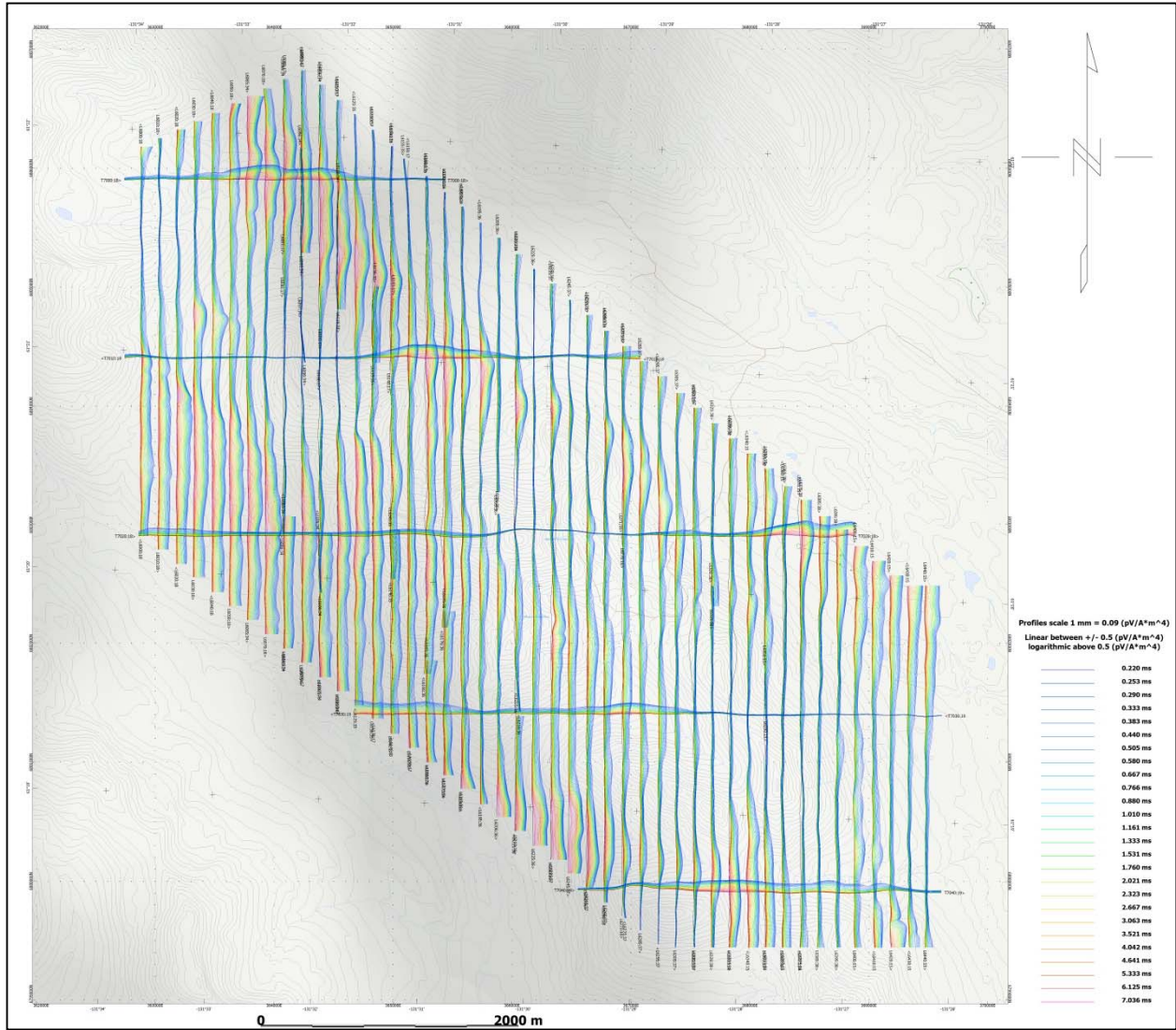
Pelly - dB/dt Calculated Time Constant (Tau) with Calculated Vertical Derivative contours



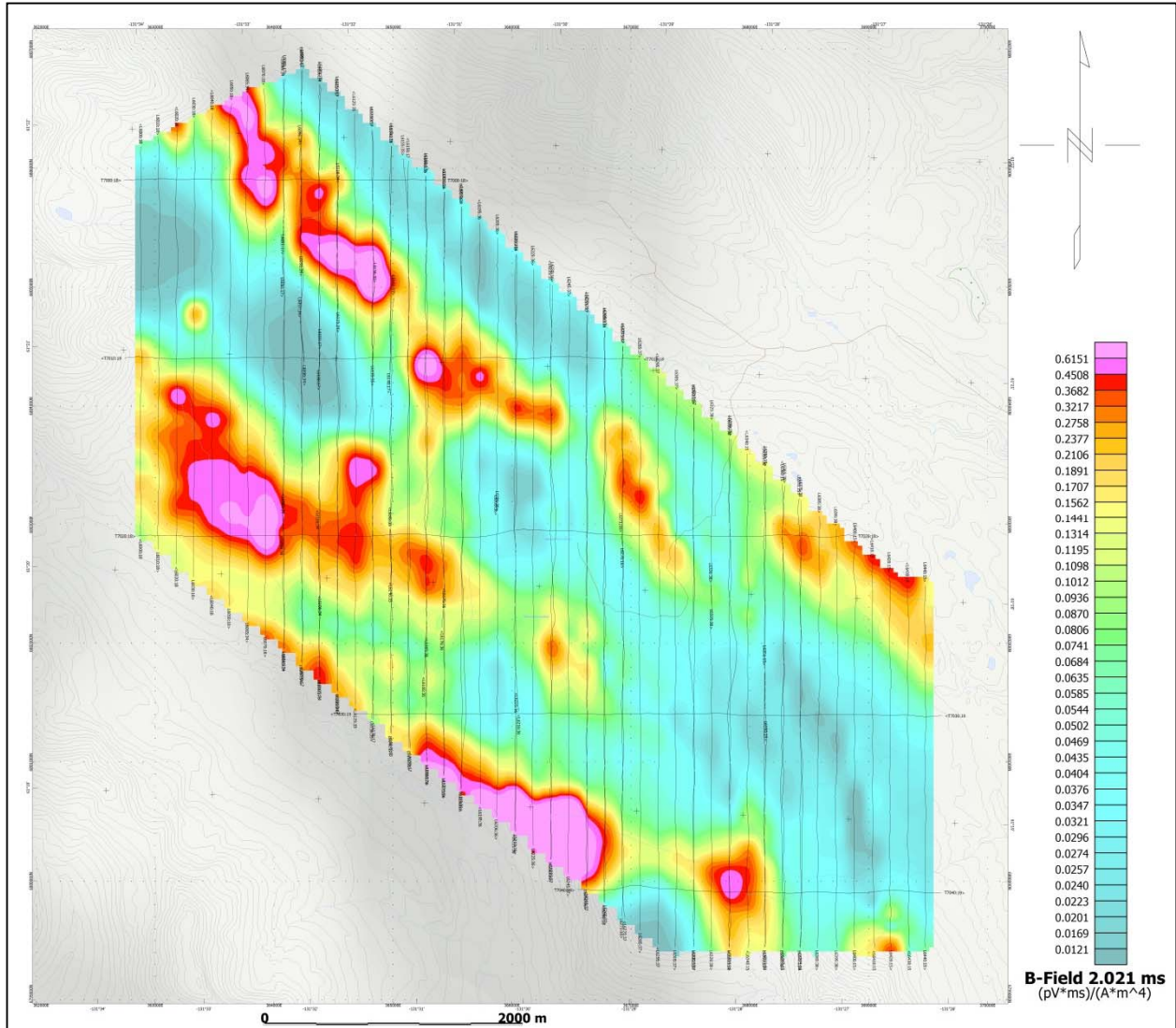
Pelly - Magnetic Tilt - Angle Derivative



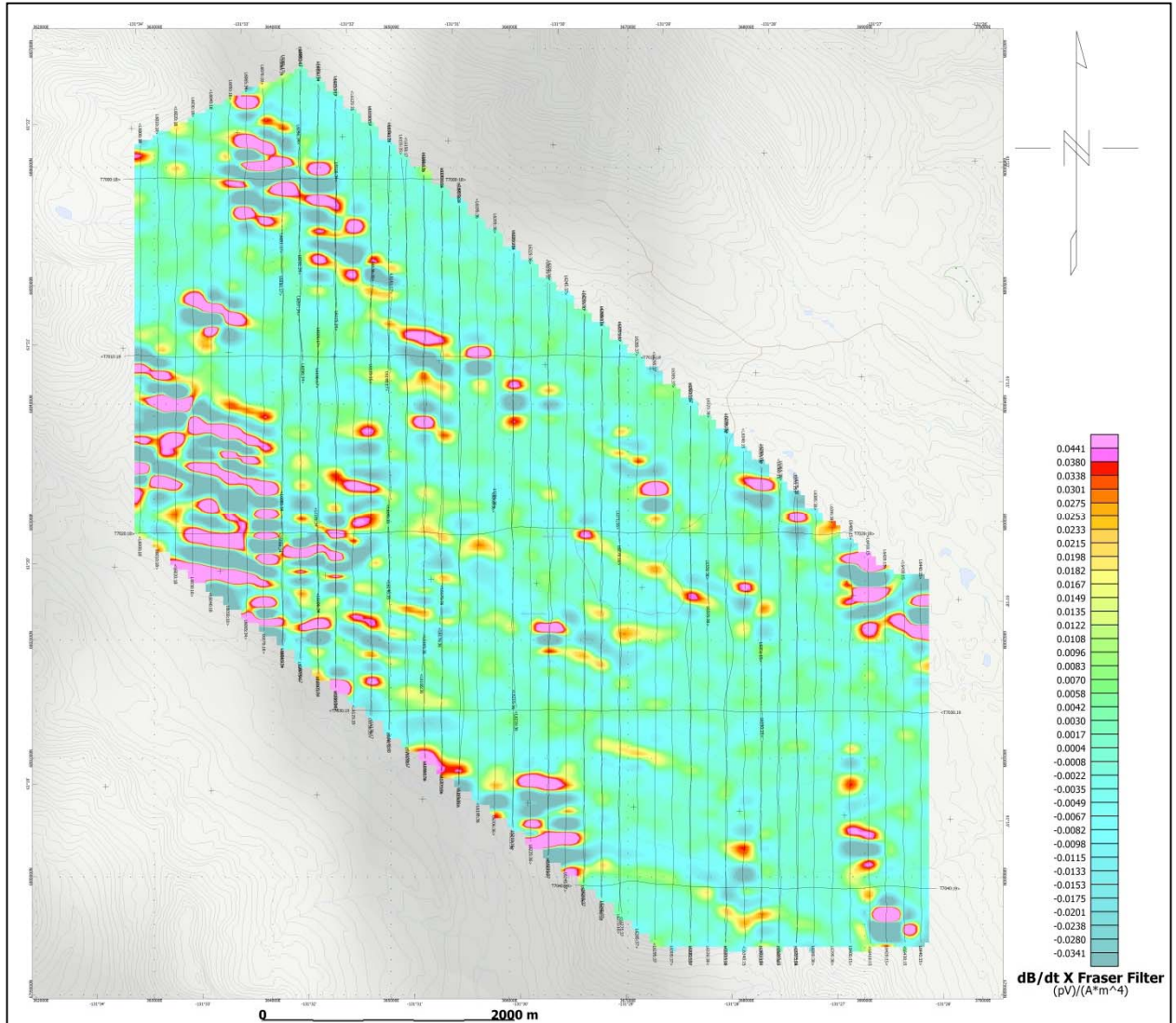
Wolf - VTEM B-Field Z Component Profiles, Time Gates 0.220 to 7.036 ms



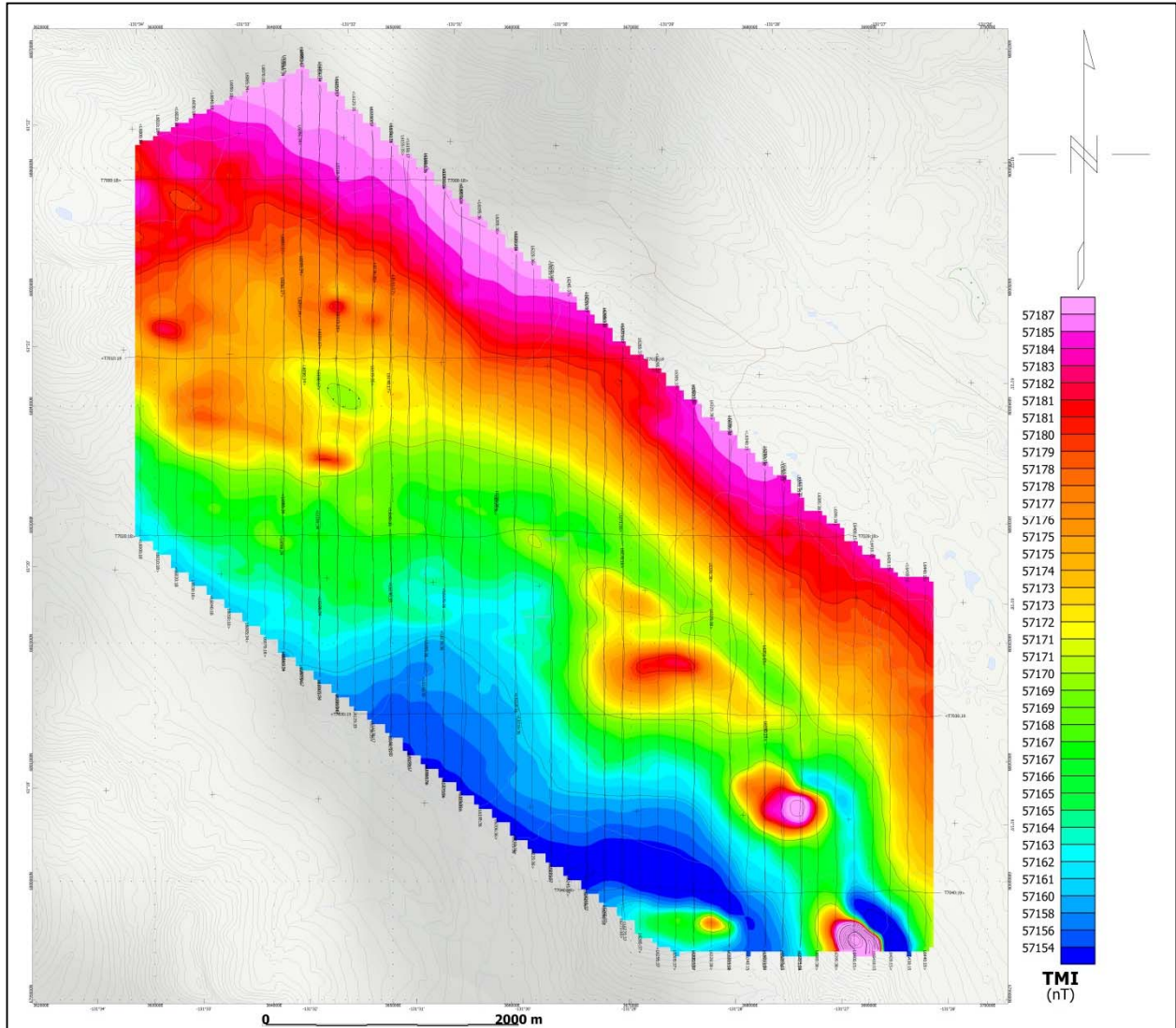
Wolf - VTEM dB/dt Z Component Profiles, Time Gates 0.220 to 7.036 ms



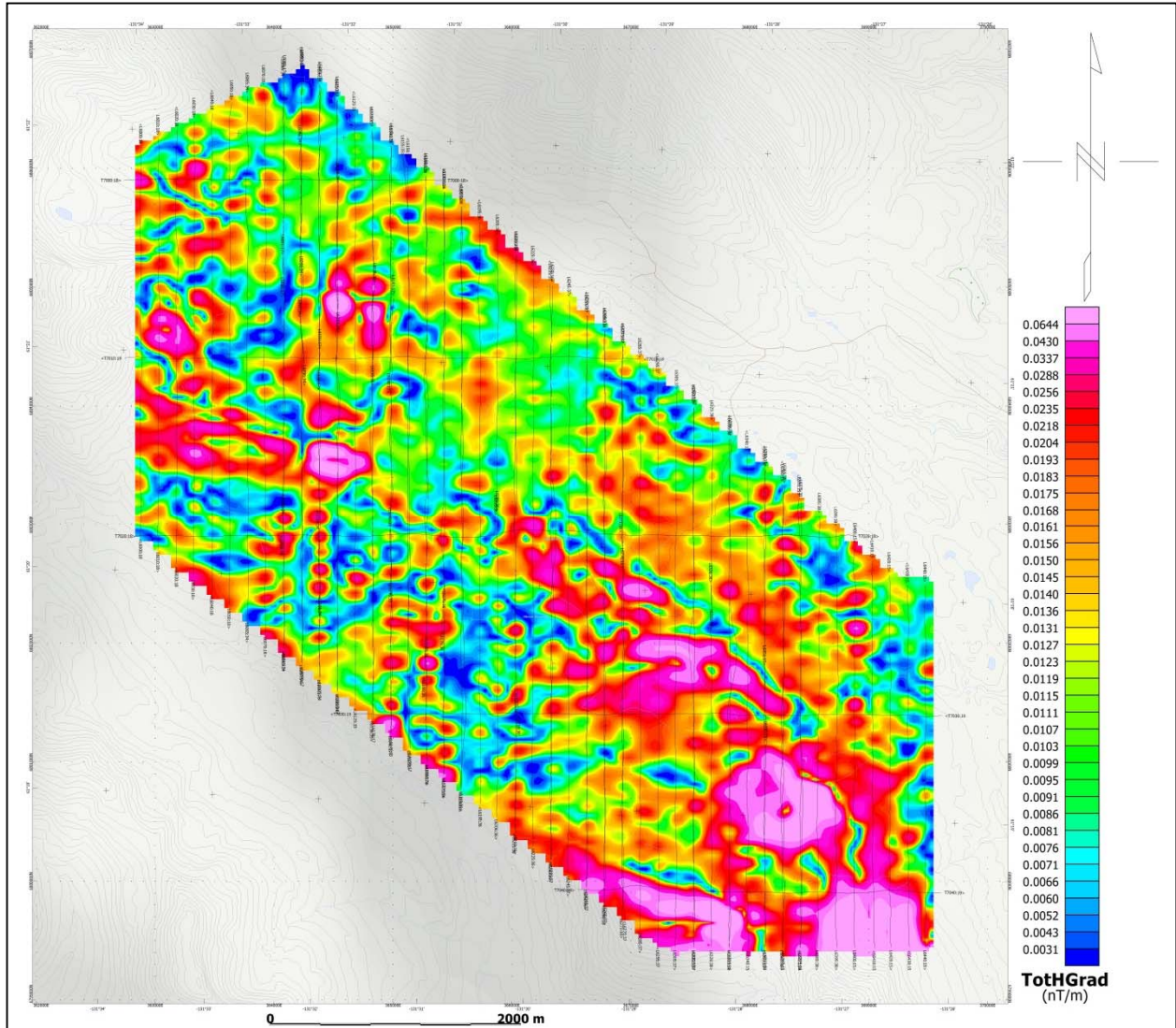
Wolf - VTEM B-Field Z Component Channel 36, Time Gate 2.021 ms



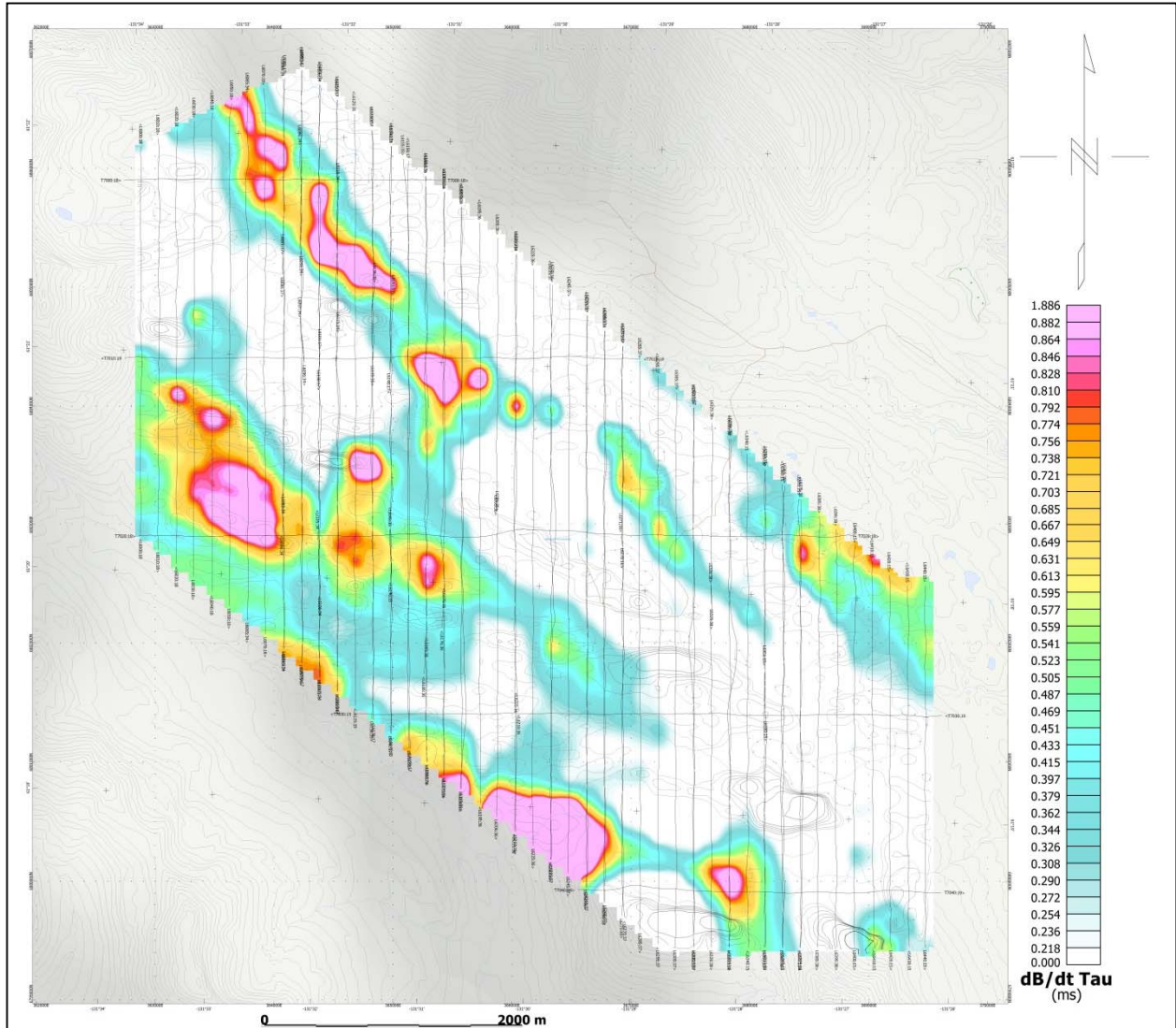
Wolf - VTEM dB/dt X Component Fraser Filtered Channel 20, Time Gate 0.220 ms



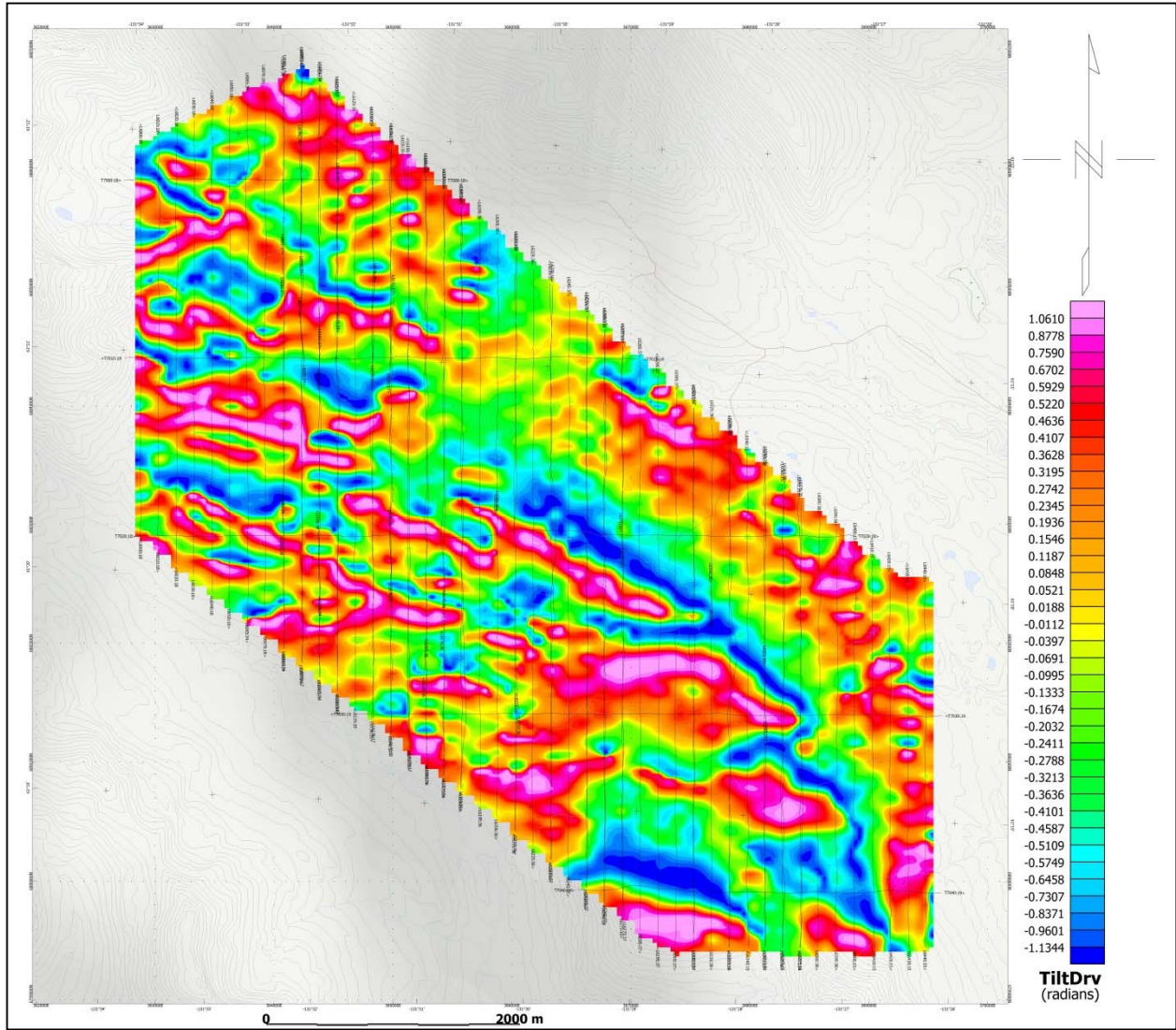
Wolf - Total Magnetic Intensity (TMI)



Wolf - Magnetic Total Horizontal Gradient



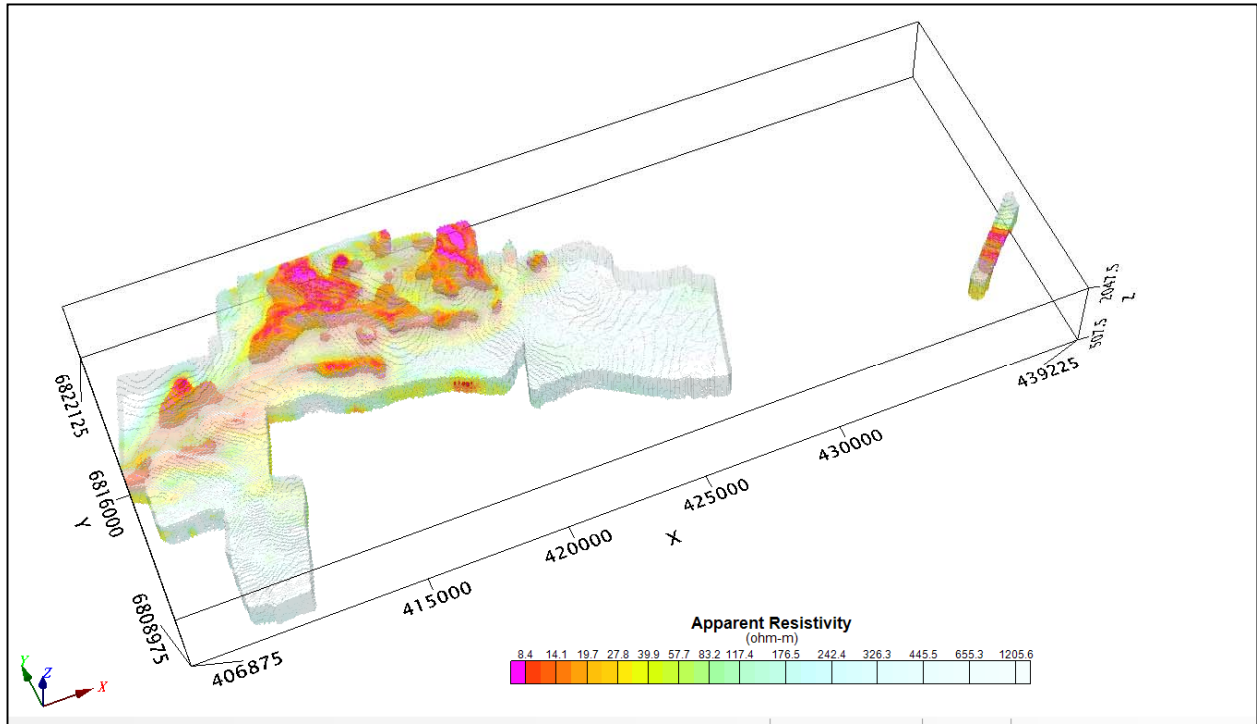
Wolf - dB/dt Calculated Time Constant (Tau) with Calculated Vertical Derivative contours



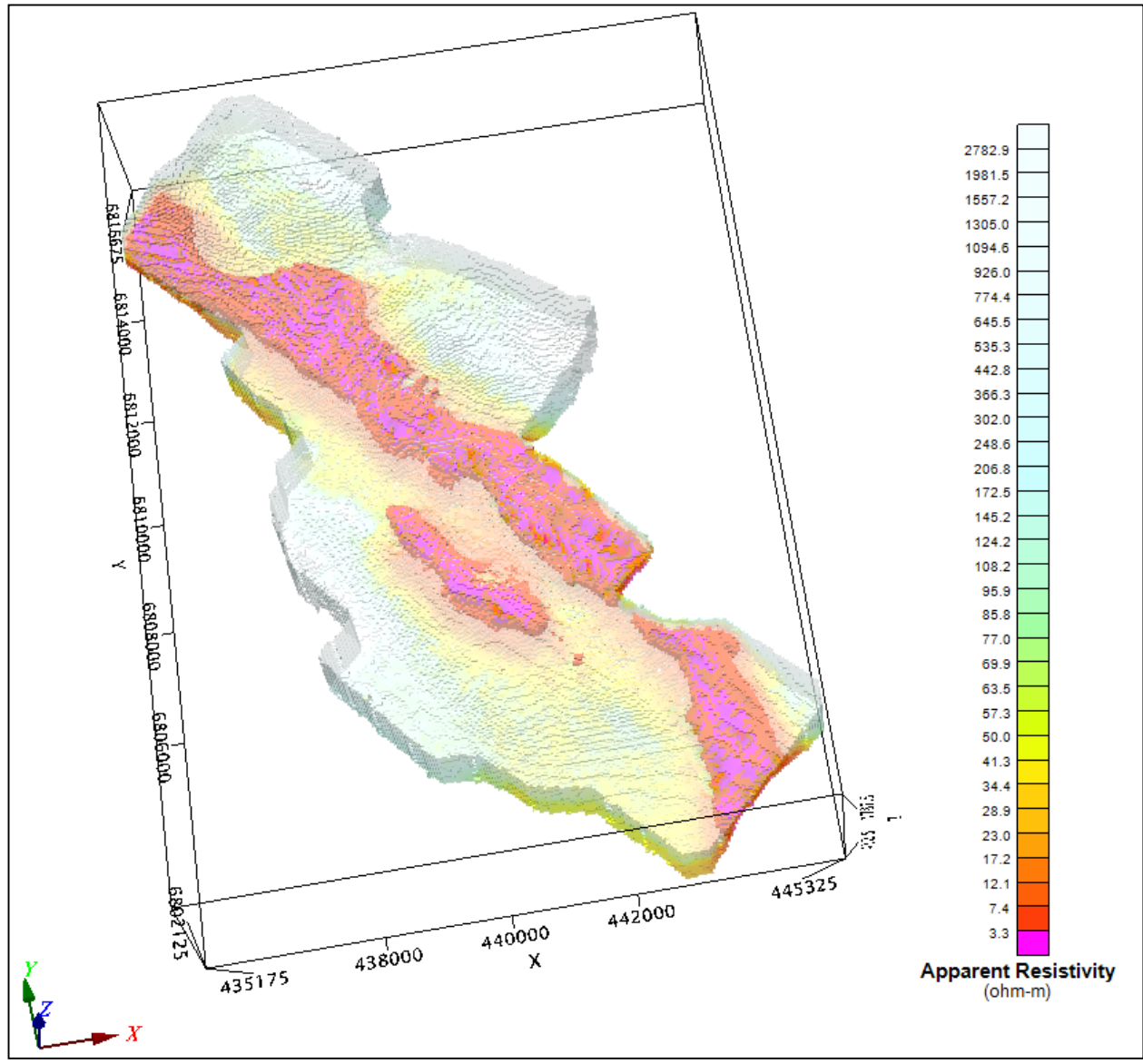
Wolf - Magnetic Tilt - Angle Derivative

RESISTIVITY DEPTH IMAGE (RDI) MAPS

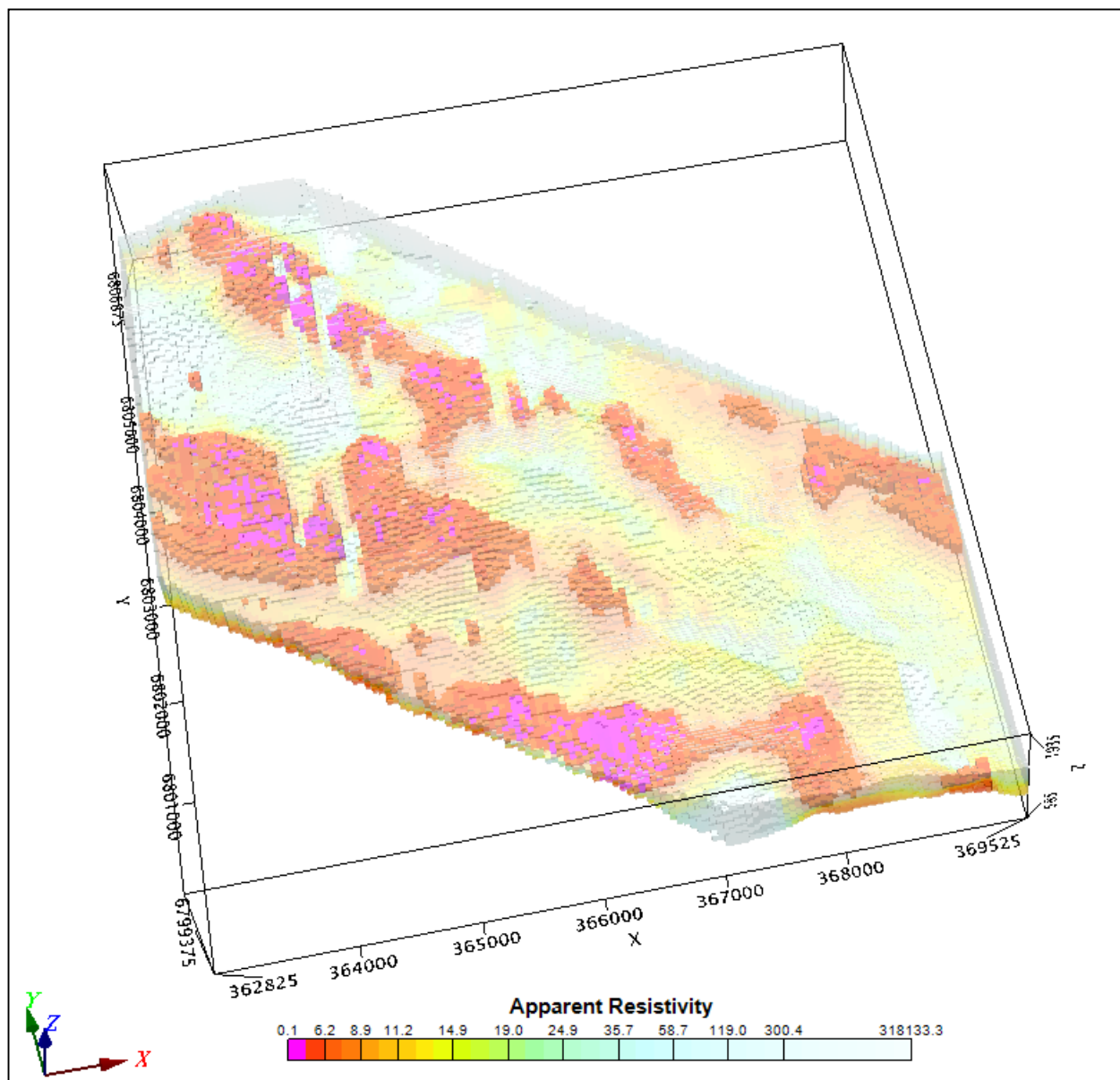
3D Resistivity-Depth Image (RDI)



Kudz Ze Kayah



Pelly



Wolf

APPENDIX D

GENERALIZED MODELING RESULTS OF THE VTEM SYSTEM INTRODUCTION

The VTEM system is based on a concentric or central loop design, whereby, the receiver is positioned at the centre of a transmitter loop that produces a primary field. The wave form is a bi-polar, modified square wave with a turn-on and turn-off at each end.

During turn-on and turn-off, a time varying field is produced (dB/dt) and an electro-motive force (emf) is created as a finite impulse response. A current ring around the transmitter loop moves outward and downward as time progresses. When conductive rocks and mineralization are encountered, a secondary field is created by mutual induction and measured by the receiver at the centre of the transmitter loop.

Efficient modeling of the results can be carried out on regularly shaped geometries, thus yielding close approximations to the parameters of the measured targets. The following is a description of a series of common models made for the purpose of promoting a general understanding of the measured results.

A set of models has been produced for the Geotech VTEM® system dB/dT Z and X components (see models D1 to D15). The Maxwell™ modeling program (EMIT Technology Pty. Ltd. Midland, WA, AU) used to generate the following responses assumes a resistive half-space. The reader is encouraged to review these models, so as to get a general understanding of the responses as they apply to survey results. While these models do not begin to cover all possibilities, they give a general perspective on the simple and most commonly encountered anomalies.

As the plate dips and departs from the vertical position, the peaks become asymmetrical.

As the dip increases, the aspect ratio (Min/Max) decreases and this aspect ratio can be used as an empirical guide to dip angles from near 90° to about 30°. The method is not sensitive enough where dips are less than about 30°.

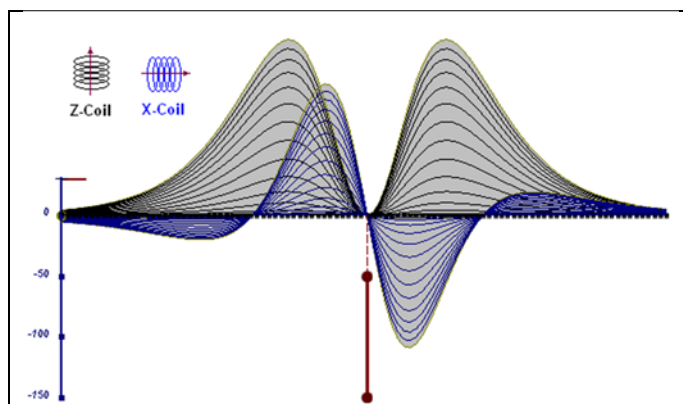


Figure D-1: vertical thin plate

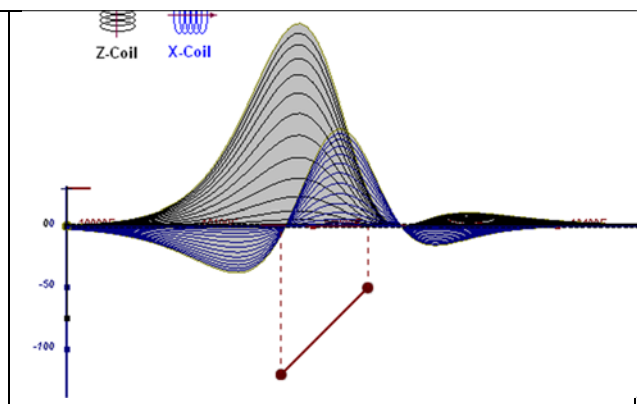


Figure D-2: inclined thin plate

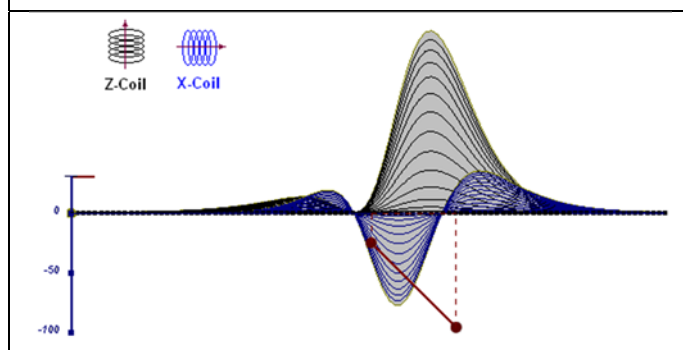


Figure D-3: inclined thin plate

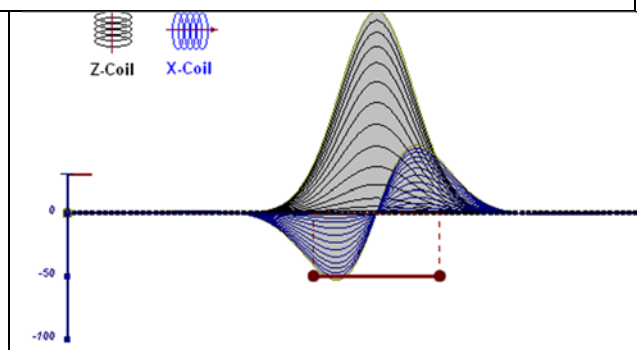


Figure D-4: horizontal thin plate

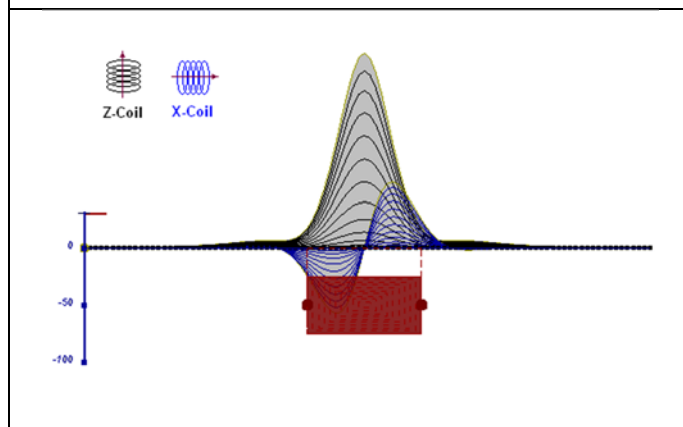


Figure D-5: horizontal thick plate (linear scale of the response)

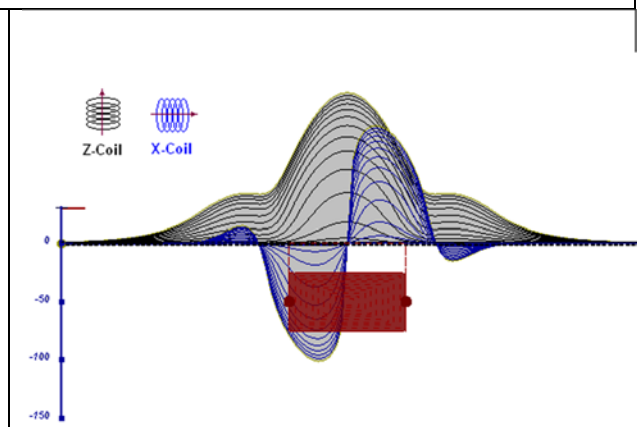


Figure D-6: horizontal thick plate (log scale of the response)

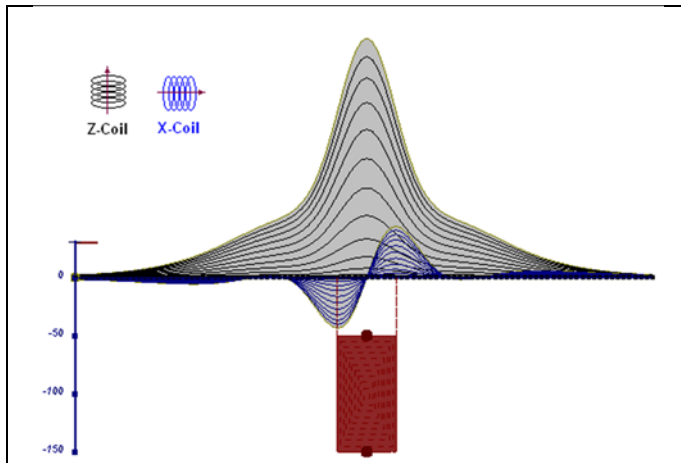


Figure D-7: vertical thick plate (linear scale of the response). 50 m depth

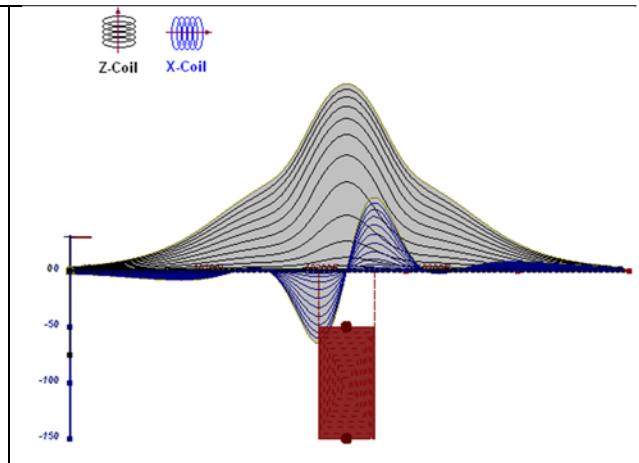


Figure D-8: vertical thick plate (log scale of the response). 50 m depth

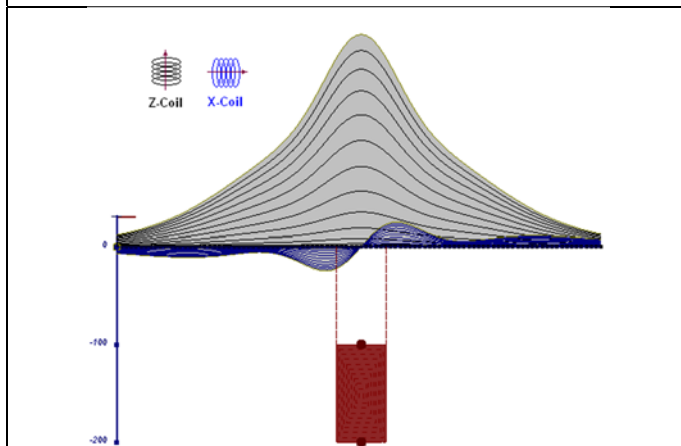


Figure D-9: vertical thick plate (linear scale of the response). 100 m depth

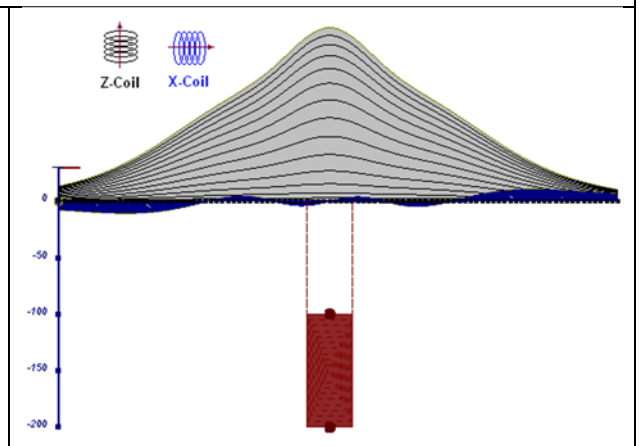


Figure D-10: vertical thick plate (linear scale of the response). Depth / horizontal thickness=2.5

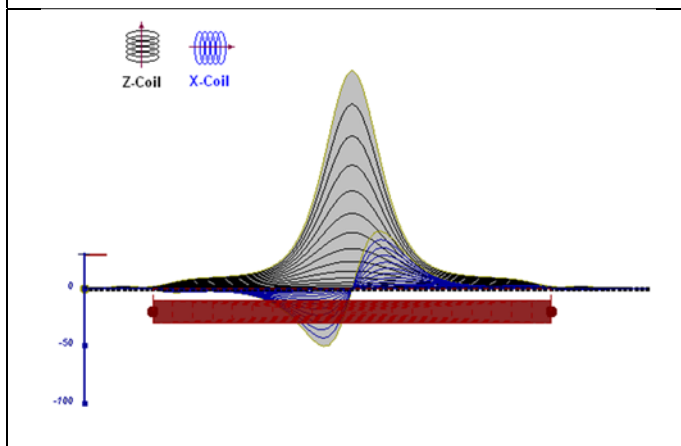


Figure D-11: horizontal thick plate (linear scale of the response)

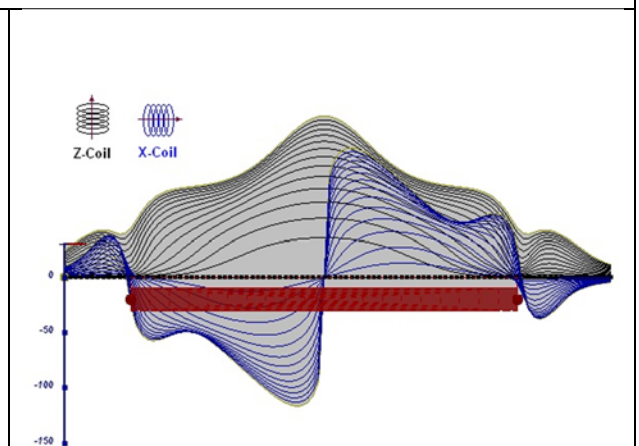


Figure D-12: horizontal thick plate (log scale of the response)

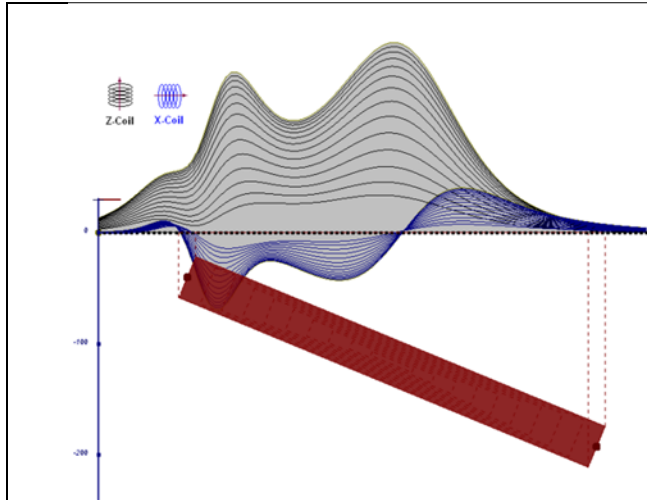


Figure D-13: inclined long thick plate

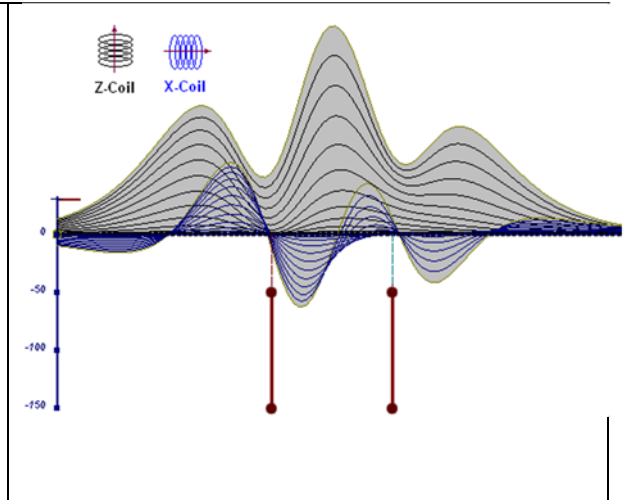


Figure D-14: two vertical thin plates

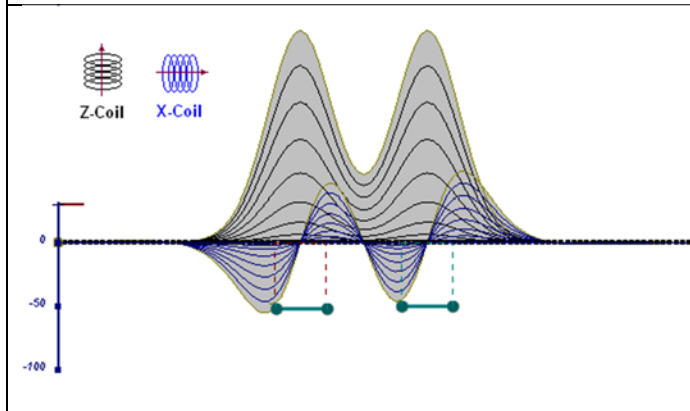


Figure D-15: two horizontal thin plates

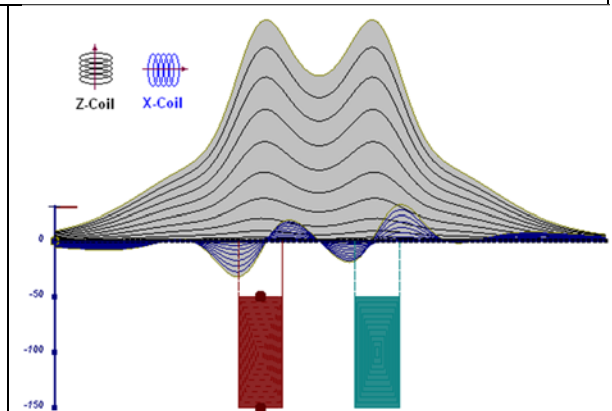


Figure D-16: two vertical thick plates

The same type of target but with different thickness, for example, creates different form of the response:

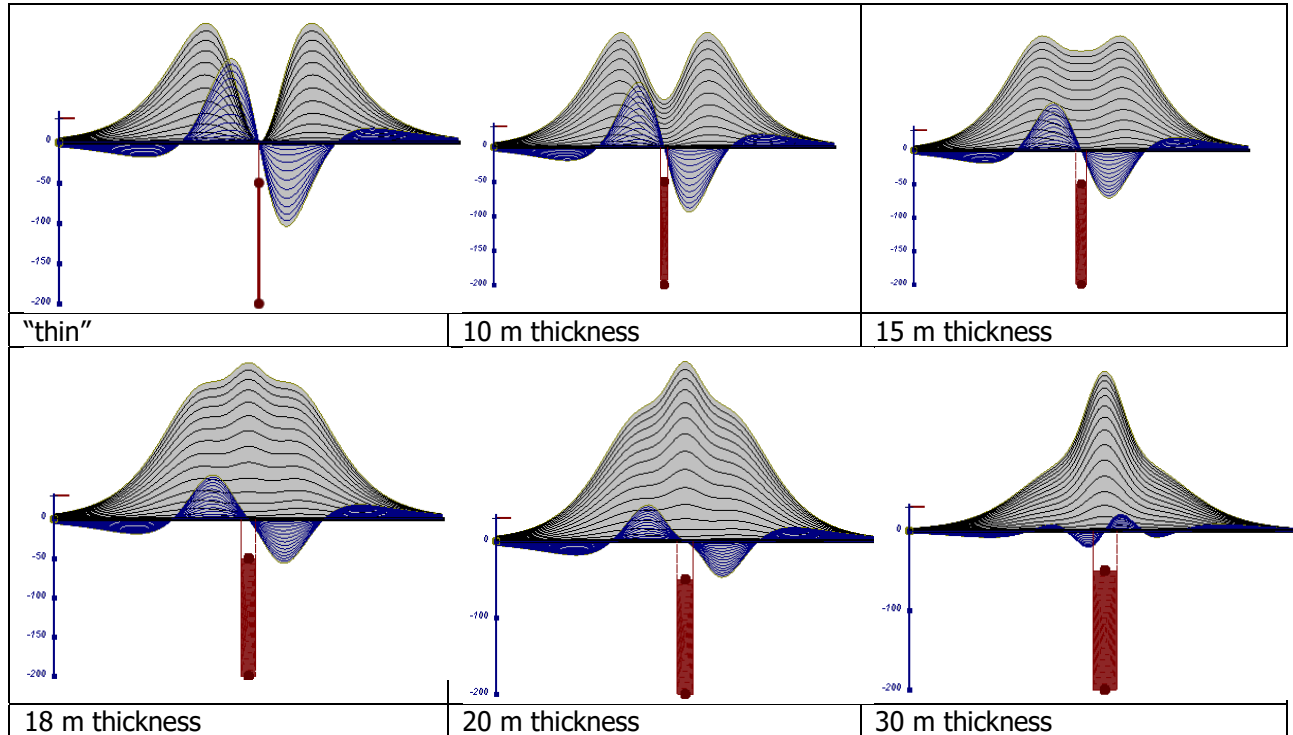


Figure D-17: Conductive vertical plate, depth 50 m, strike length 200 m, depth extends 150 m.

Alexander Prikhodko, PhD, P.Ge
Geotech Ltd.

September 2010

APPENDIX E

EM TIME CONSTANT (TAU) ANALYSIS

Estimation of time constant parameter¹ in transient electromagnetic method is one of the steps toward the extraction of the information about conductances beneath the surface from TEM measurements.

The most reliable method to discriminate or rank conductors from overburden, background or one and other is by calculating the EM field decay time constant (TAU parameter), which directly depends on conductance despite their depth and accordingly amplitude of the response.

THEORY

As established in electromagnetic theory, the magnitude of the electro-motive force (emf) induced is proportional to the time rate of change of primary magnetic field at the conductor. This emf causes eddy currents to flow in the conductor with a characteristic transient decay, whose Time Constant (Tau) is a function of the conductance of the survey target or conductivity and geometry (including dimensions) of the target. The decaying currents generate a proportional secondary magnetic field, the time rate of change of which is measured by the receiver coil as induced voltage during the Off time.

The receiver coil output voltage (e_0) is proportional to the time rate of change of the secondary magnetic field and has the form,

$$e_0 \propto (1 / \tau) e^{-(t/\tau)}$$

Where,

$\tau = L/R$ is the characteristic time constant of the target (TAU)

R = resistance

L = inductance

From the expression, conductive targets that have small value of resistance and hence large value of τ yield signals with small initial amplitude that decays relatively slowly with progress of time. Conversely, signals from poorly conducting targets that have large resistance value and small τ , have high initial amplitude but decay rapidly with time¹ (Fig. E1).

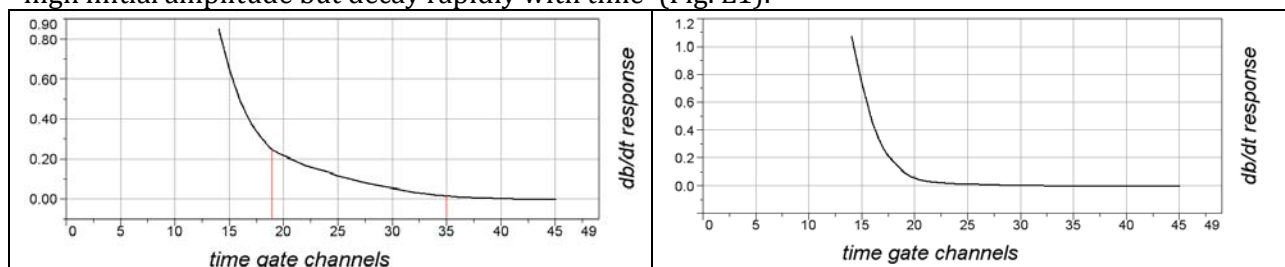


Figure E-1: Left – presence of good conductor, right – poor conductor.

¹ McNeill, JD, 1980, "Applications of Transient Electromagnetic Techniques", Technical Note TN-7 page 5, Geonics Limited, Mississauga, Ontario.

EM Time Constant (Tau) Calculation

The EM Time-Constant (TAU) is a general measure of the speed of decay of the electromagnetic response and indicates the presence of eddy currents in conductive sources as well as reflecting the “conductance quality” of a source. Although TAU can be calculated using either the measured dB/dt decay or the calculated B-field decay, dB/dt is commonly preferred due to better stability (S/N) relating to signal noise. Generally, TAU calculated on base of early time response reflects both near surface overburden and poor conductors whereas, in the late ranges of time, deep and more conductive sources, respectively. For example early time TAU distribution in an area that indicates conductive overburden is shown in Figure 2.

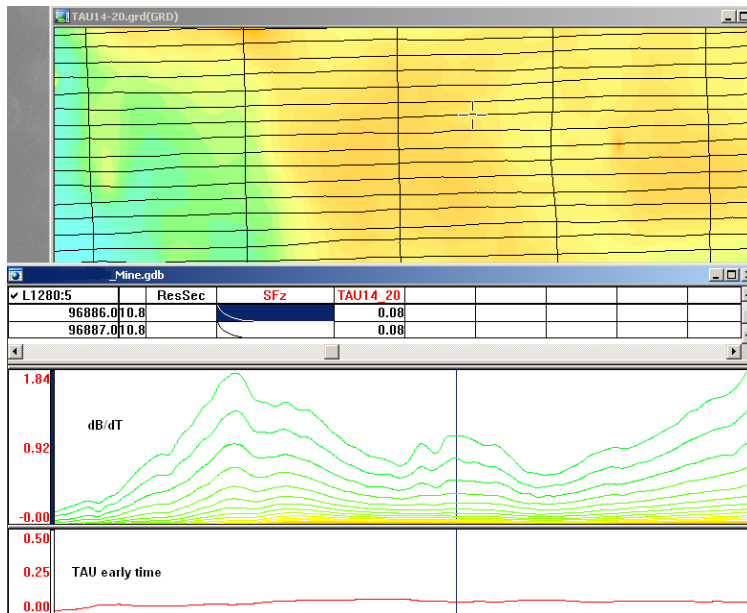


Figure E-2: Map of early time TAU. Area with overburden conductive layer and local sources.

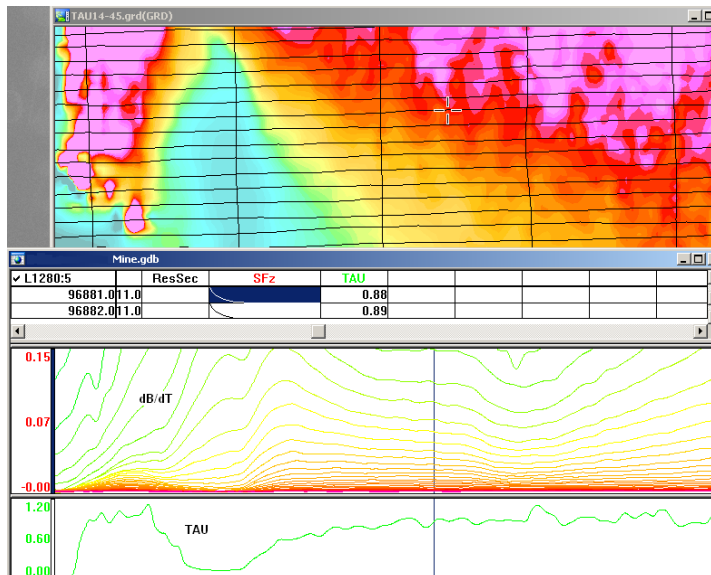


Figure E-3: Map of full time range TAU with EM anomaly due to deep highly conductive target.

There are many advantages of TAU maps:

- TAU depends only on one parameter (conductance) in contrast to response magnitude;
- TAU is integral parameter, which covers time range and all conductive zones and targets are displayed independently of their depth and conductivity on a single map.
- Very good differential resolution in complex conductive places with many sources with different conductivity.
- Signs of the presence of good conductive targets are amplified and emphasized independently of their depth and level of response accordingly.

In the example shown in Figure 4 and 5, three local targets are defined, each of them with a different depth of burial, as indicated on the resistivity depth image (RDI). All are very good conductors but the deeper target (number 2) has a relatively weak dB/dt signal yet also features the strongest total TAU (Figure 4). This example highlights the benefit of TAU analysis in terms of an additional target discrimination tool.

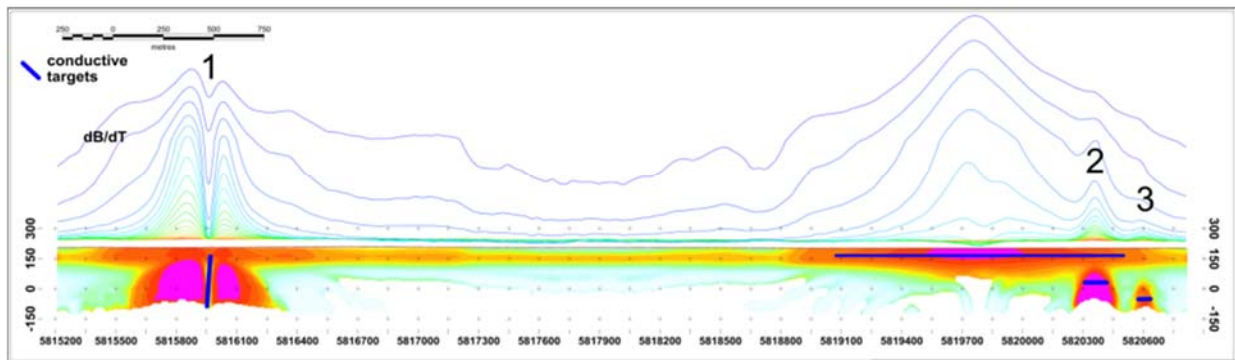


Figure E-4: dB/dt profile and RDI with different depths of targets.

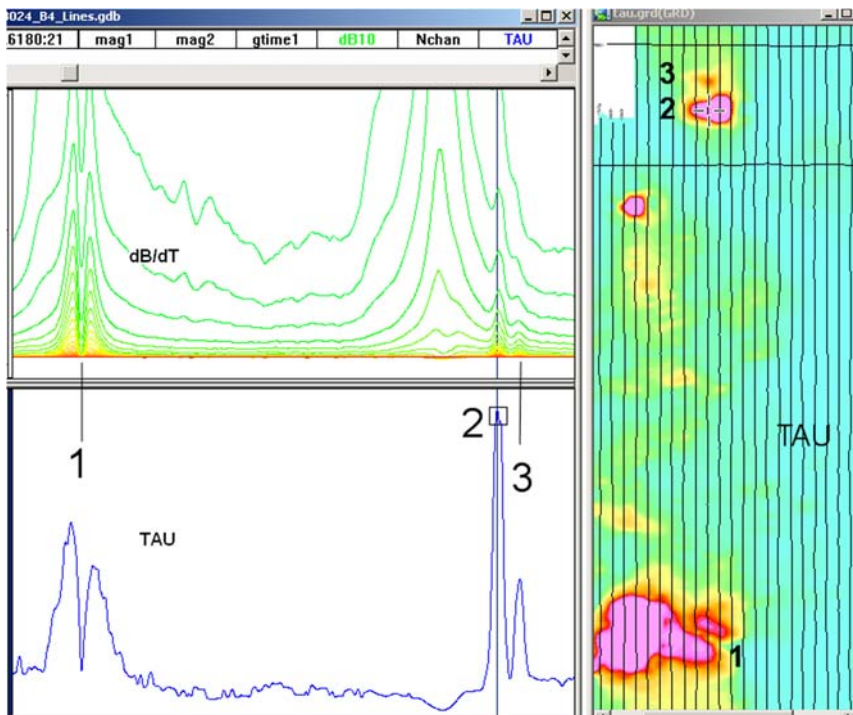


Figure E-5: Map of total TAU and dB/dt profile.

The EM Time Constants for dB/dt and B-field were calculated using the “sliding Tau” in-house program developed at Geotech2. The principle of the calculation is based on using of time window (4 time channels) which is sliding along the curve decay and looking for latest time channels which have a response above the level of noise and decay. The EM decays are obtained from all available decay channels, starting at the latest channel. Time constants are taken from a least square fit of a straight-line (log/linear space) over the last 4 gates above a pre-set signal threshold level (Figure F6). Threshold settings are pointed in the “label” property of TAU database channels. The sliding Tau method determines that, as the amplitudes increase, the time-constant is taken at progressively later times in the EM decay. Conversely, as the amplitudes decrease, Tau is taken at progressively earlier times in the decay. If the maximum signal amplitude falls below the threshold, or becomes negative for any of the 4 time gates, then Tau is not calculated and is assigned a value of “dummy” by default.

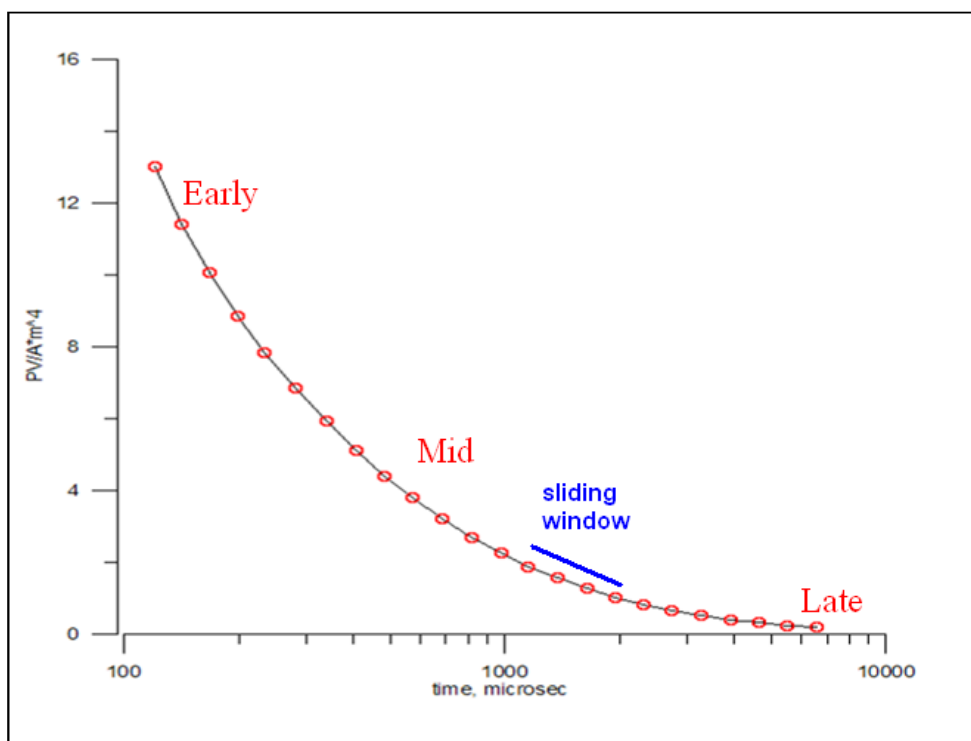


Figure E-6: Typical dB/dt decays of Vtem data

Alexander Prikhodko, PhD, P.Ge
Geotech Ltd.

September 2010

² by A.Prikhodko

APPENDIX F

TEM RESISTIVITY DEPTH IMAGING (RDI)

Resistivity depth imaging (RDI) is technique used to rapidly convert EM profile decay data into an equivalent resistivity versus depth cross-section, by deconvolving the measured TEM data. The used RDI algorithm of Resistivity-Depth transformation is based on scheme of the apparent resistivity transform of Maxwell A.Meju (1998)¹ and TEM response from conductive half-space. The program is developed by Alexander Prikhodko and depth calibrated based on forward plate modeling for VTEM system configuration (Fig. 1-10).

RDIs provide reasonable indications of conductor relative depth and vertical extent, as well as accurate 1D layered-earth apparent conductivity/resistivity structure across VTEM flight lines. Approximate depth of investigation of a TEM system, image of secondary field distribution in half space, effective resistivity, initial geometry and position of conductive targets is the information obtained on base of the RDIs.

Maxwell forward modeling with RDI sections from the synthetic responses (VTEM system).

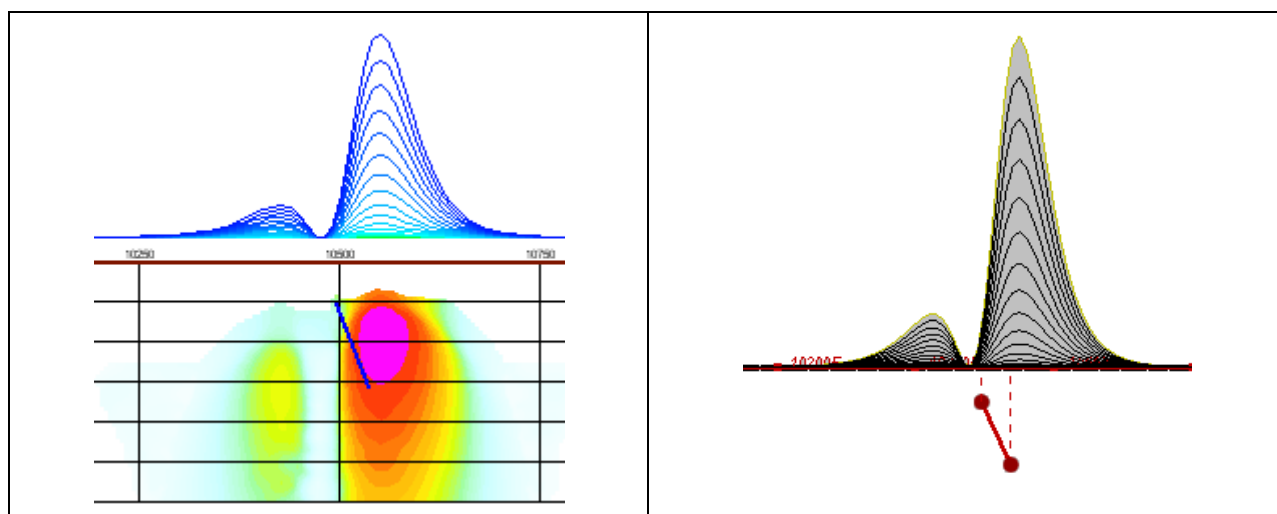


Figure F-1: Maxwell plate model and RDI from the calculated response for conductive "thin" plate (depth 50 m, dip 65 degree, depth extend 100 m).

¹ Maxwell A.Meju, 1998, Short Note: A simple method of transient electromagnetic data analysis, *Geophysics*, **63**, 405–410.

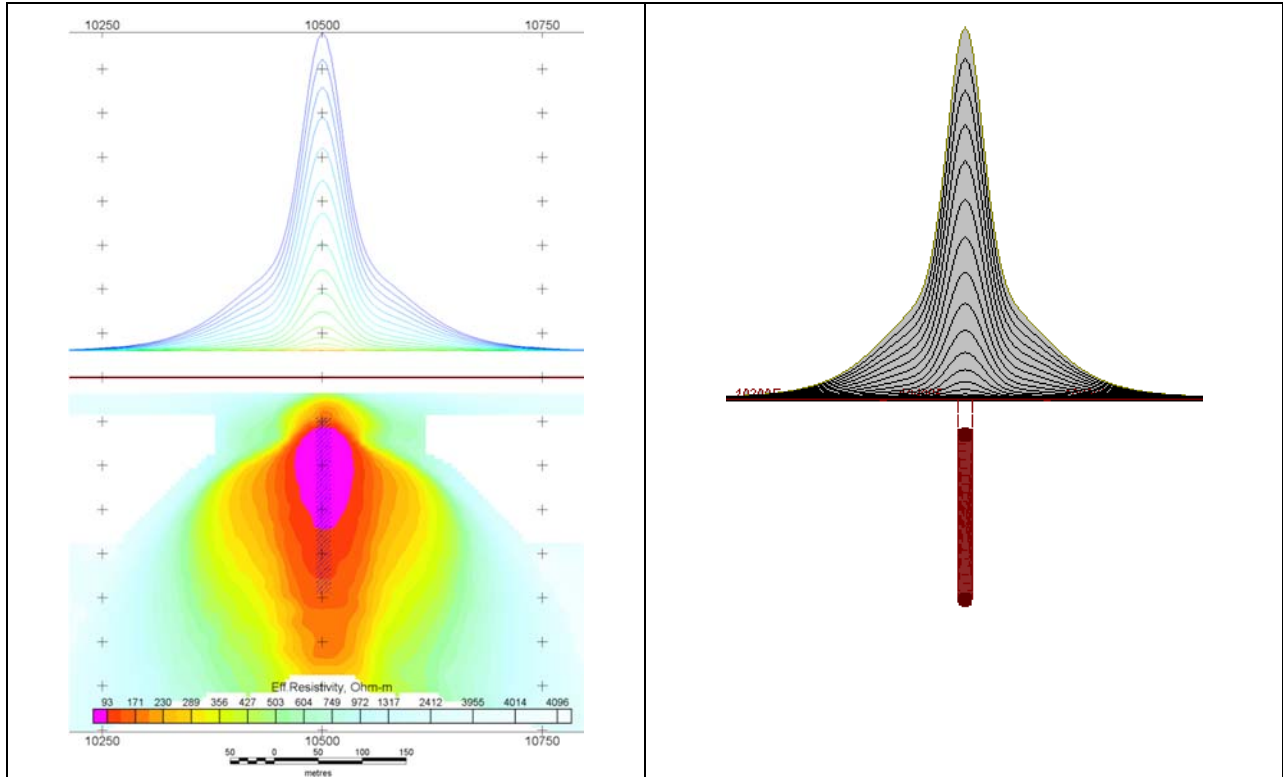


Figure F-2: Maxwell plate model and RDI from the calculated response for "thick" plate 18 m thickness, depth 50 m, depth extend 200 m).

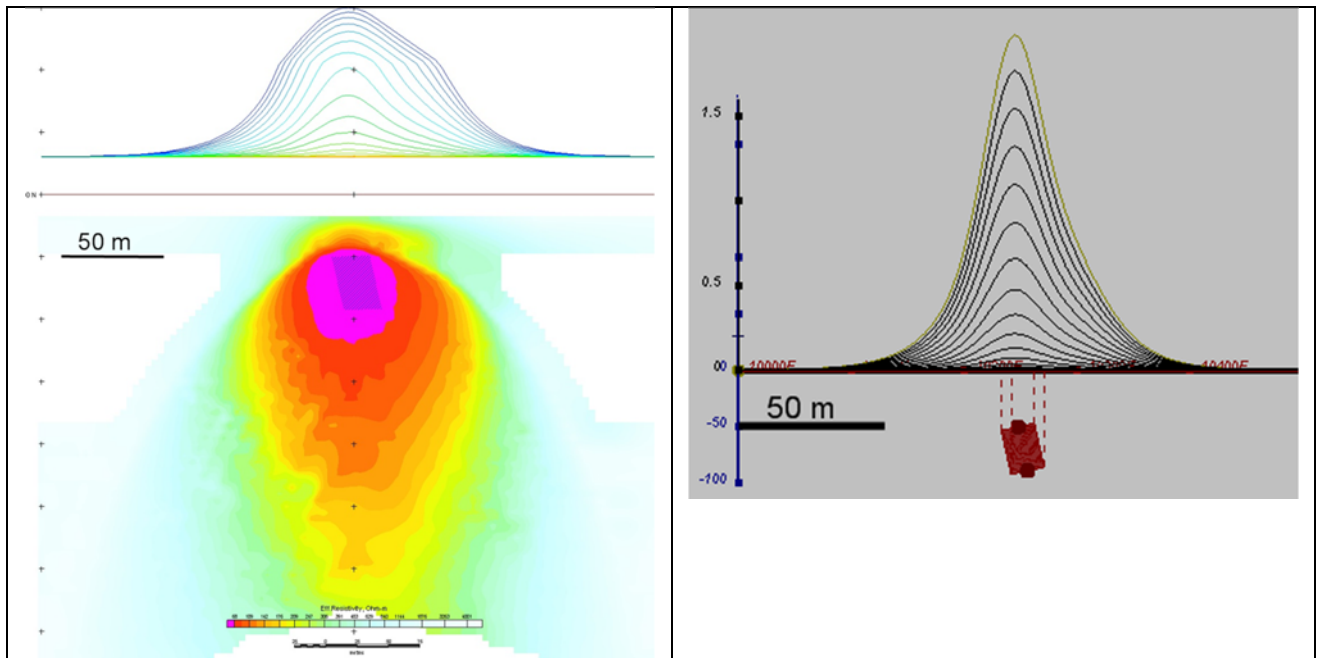


Figure F-3: Maxwell plate model and RDI from the calculated response for bulk ("thick") 100 m length, 40 m depth extend, 30 m thickness

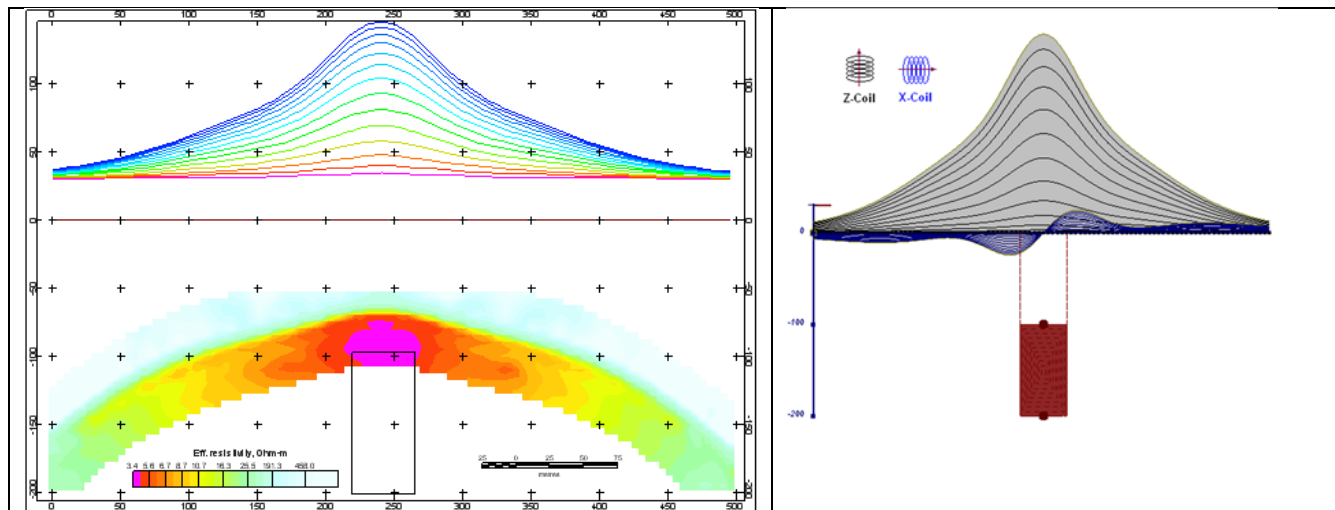


Figure F-4: Maxwell plate model and RDI from the calculated response for "thick" vertical target (depth 100 m, depth extend 100 m). 19-44 chan.

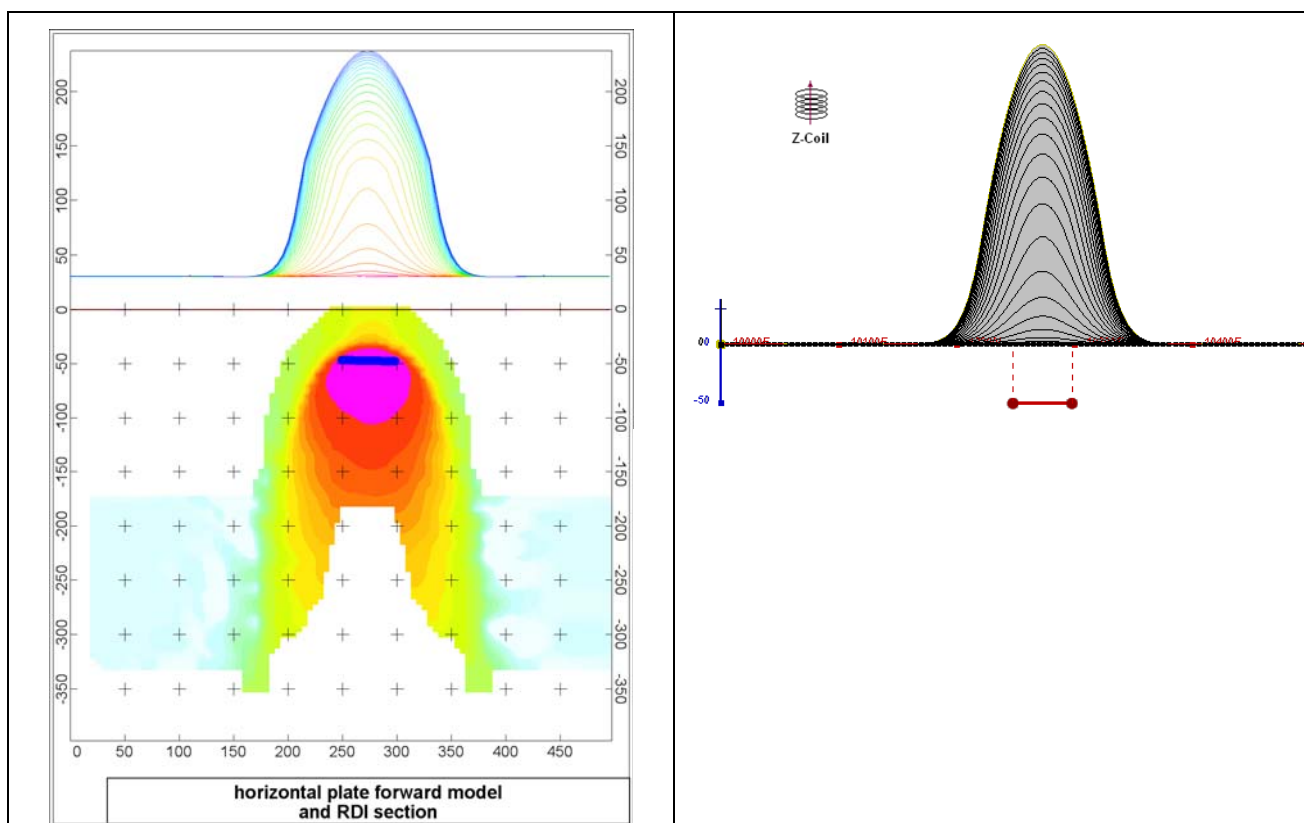


Figure F-5: Maxwell plate model and RDI from the calculated response for horizontal thin plate (depth 50 m, dim 50x100 m). 15-44 chan.

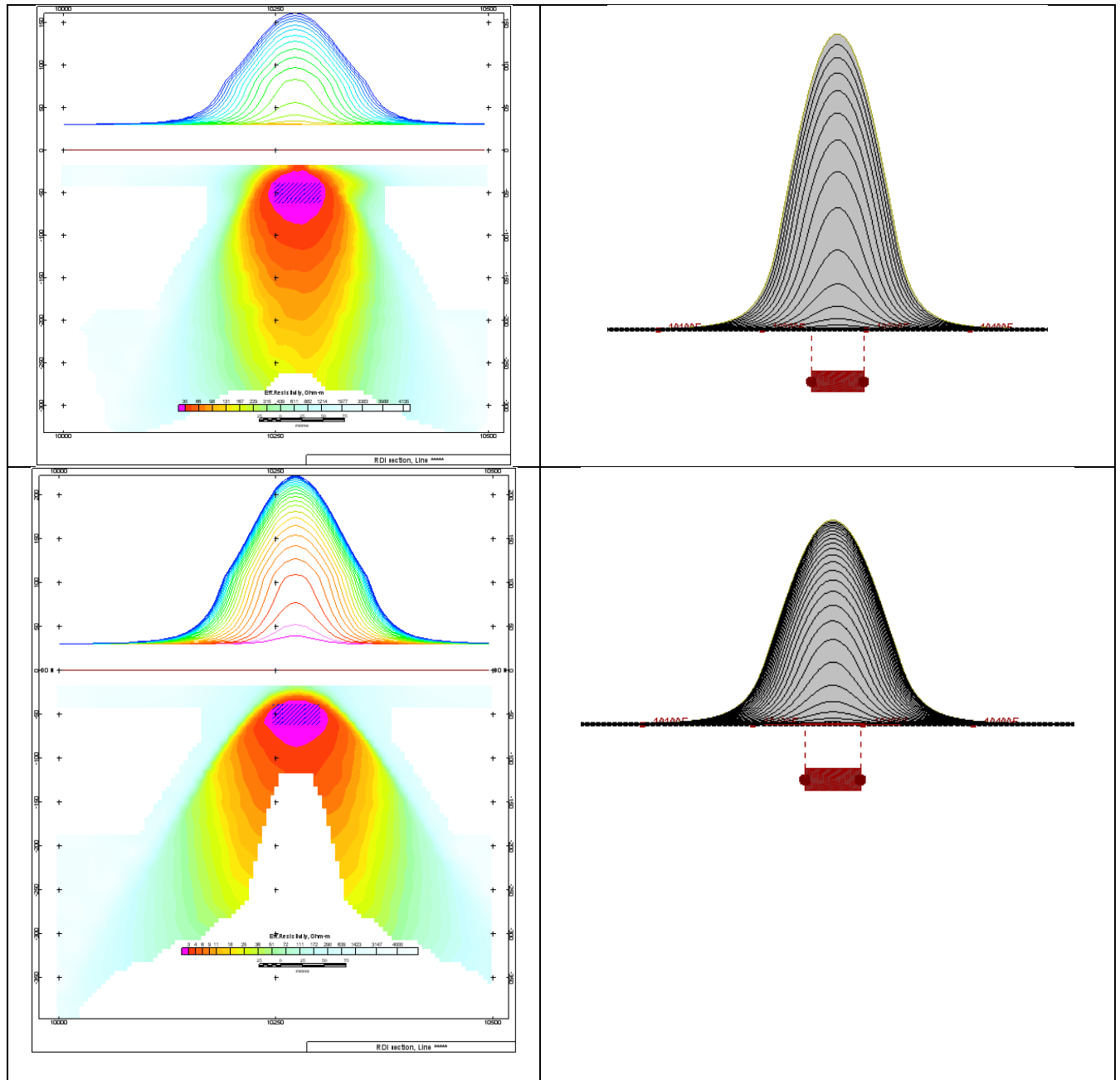


Figure F-6: Maxwell plate model and RDI from the calculated response for horizontal thick (20m) plate – less conductive (on the top), more conductive (below).

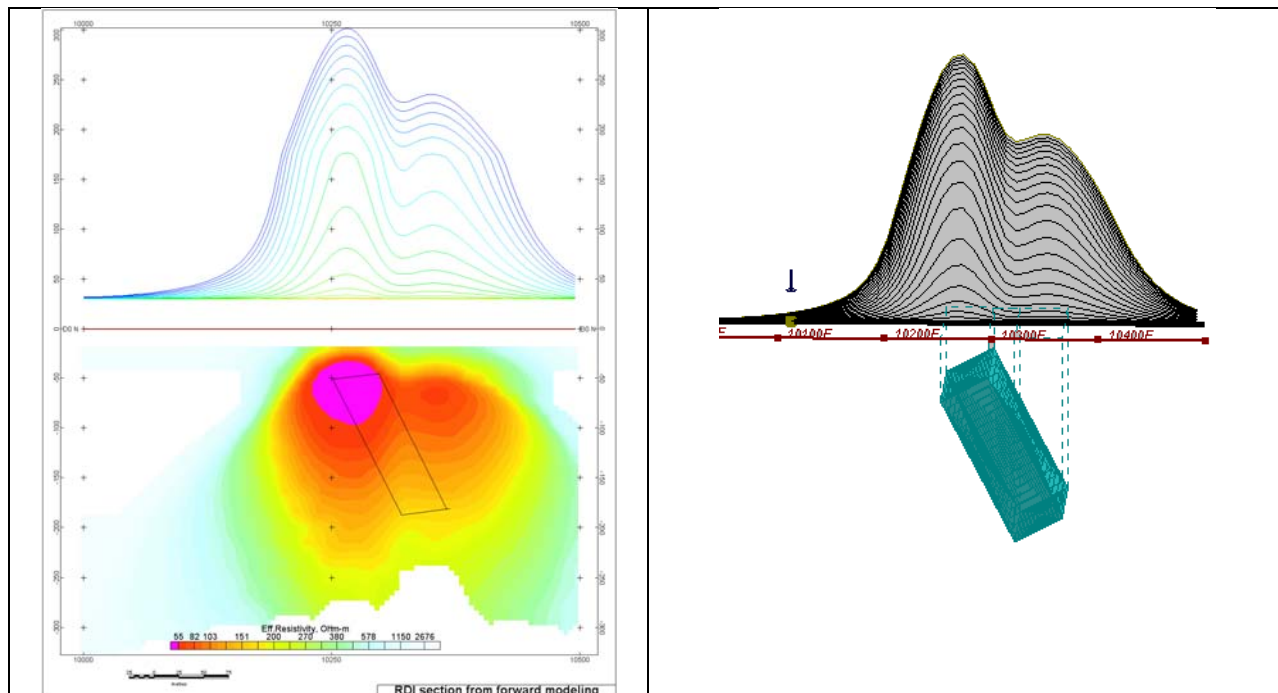


Figure F-7: Maxwell plate model and RDI from the calculated response for inclined thick (50m) plate. Depth extends 150 m, depth to the target 50 m.

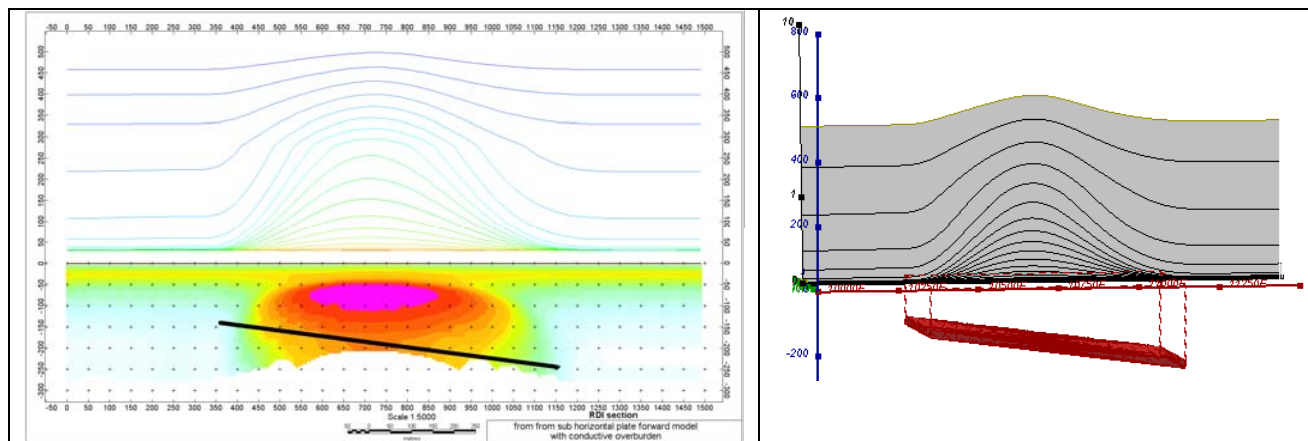


Figure F-8: Maxwell plate model and RDI from the calculated response for the long, wide and deep subhorizontal plate (depth 140 m, dim 25x500x800 m) with conductive overburden.

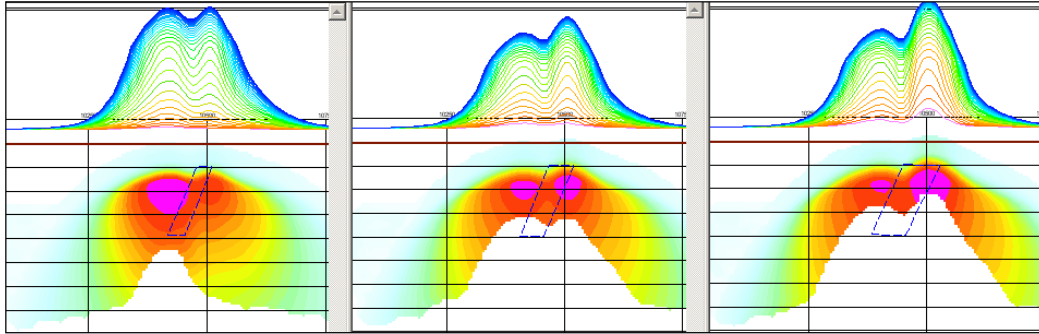


Figure F-9: Maxwell plate models and RDIs from the calculated response for "thick" dipping plates (35, 50, 75 m thickness), depth 50 m, conductivity 2.5 S/m.

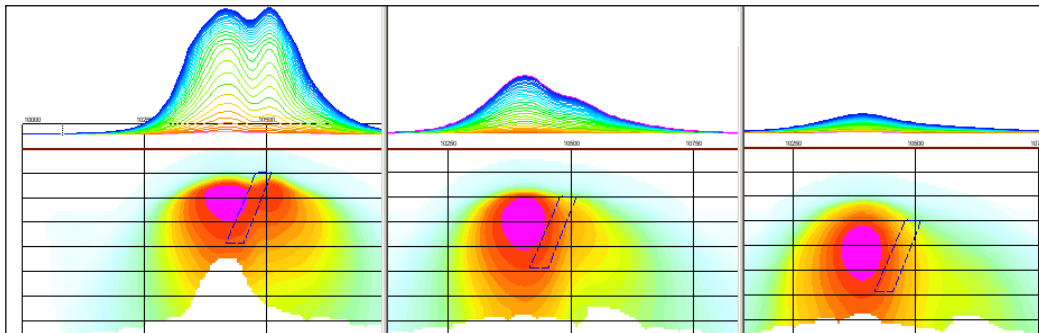


Figure F-10: Maxwell plate models and RDIs from the calculated response for "thick" (35 m thickness) dipping plate on different depth (50, 100, 150 m), conductivity 2.5 S/m.

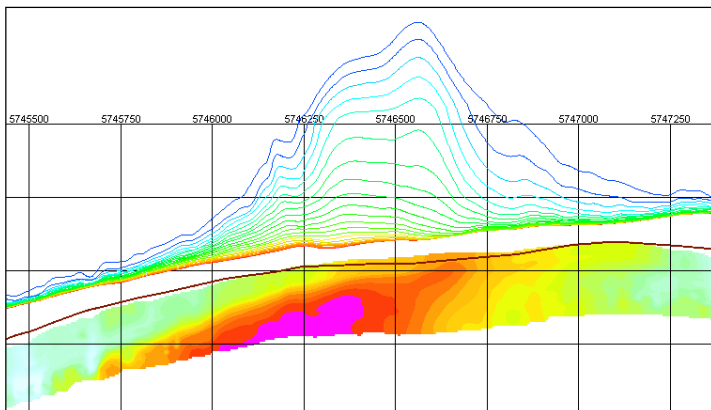
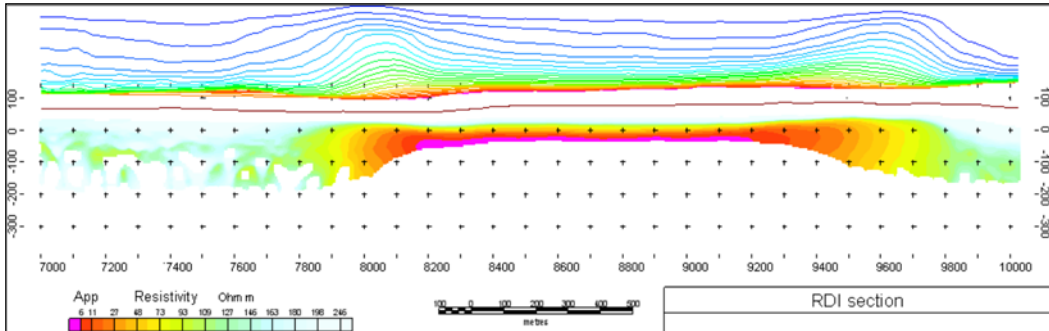
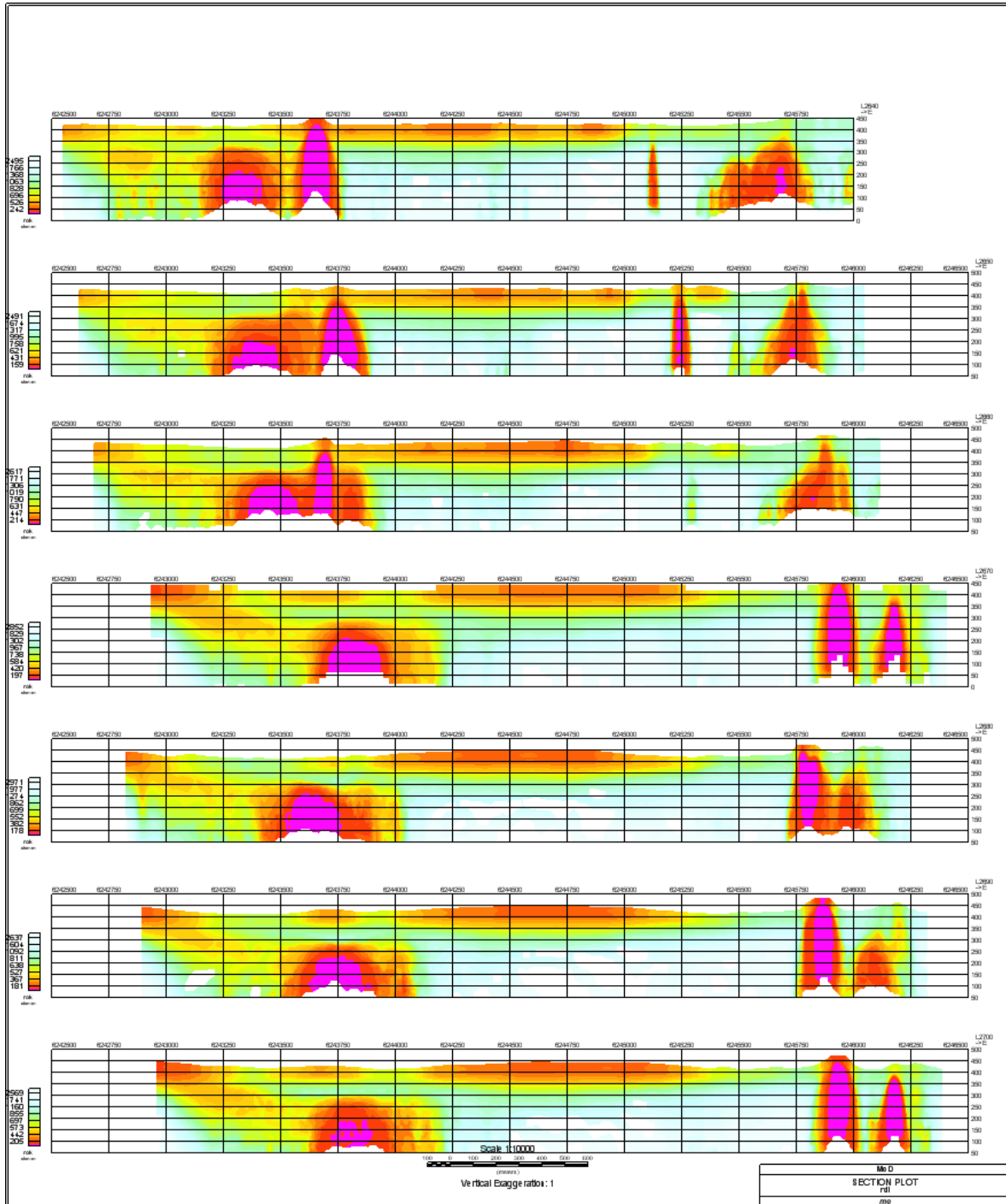


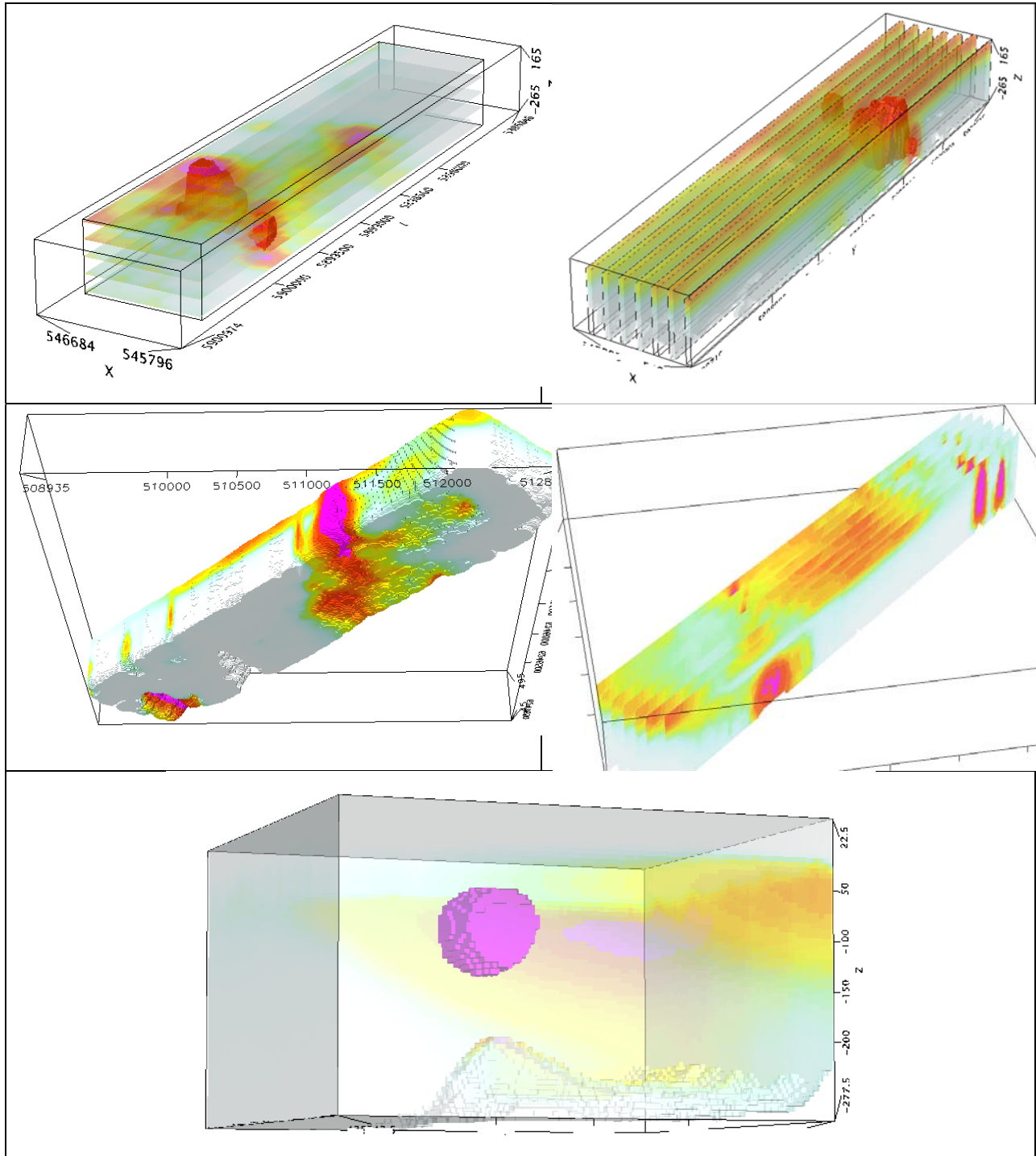
Figure F-11: RDI section for the real horizontal and slightly dipping conductive layers

FORMS OF RDI PRESENTATION

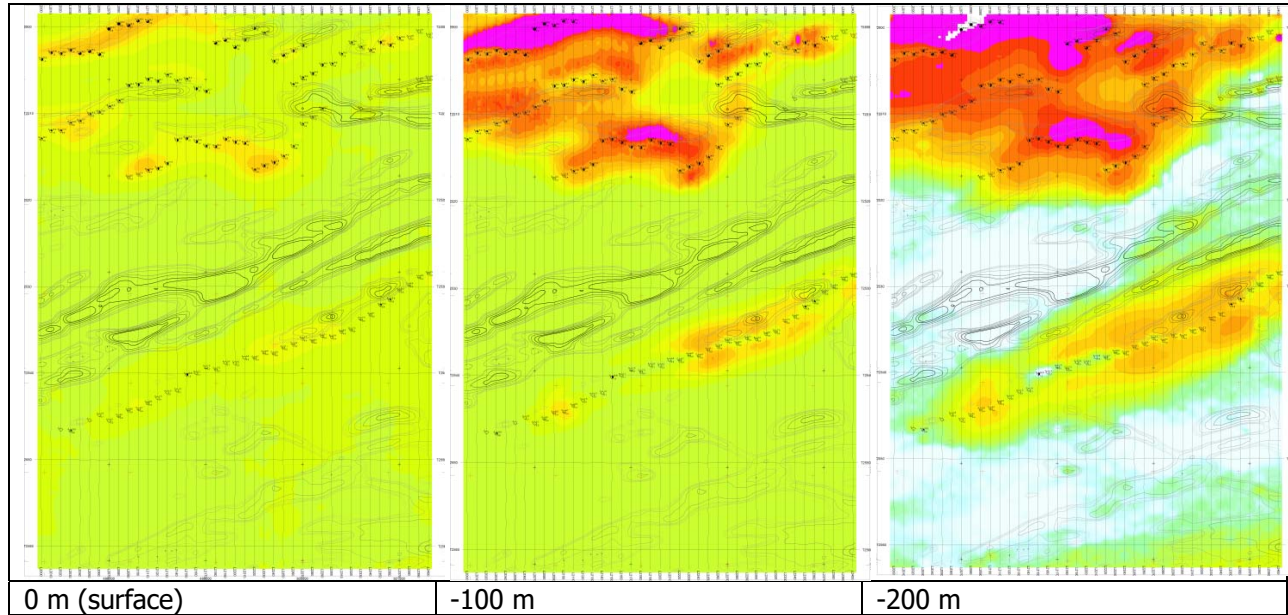
PRESENTATION OF SERIES OF LINES



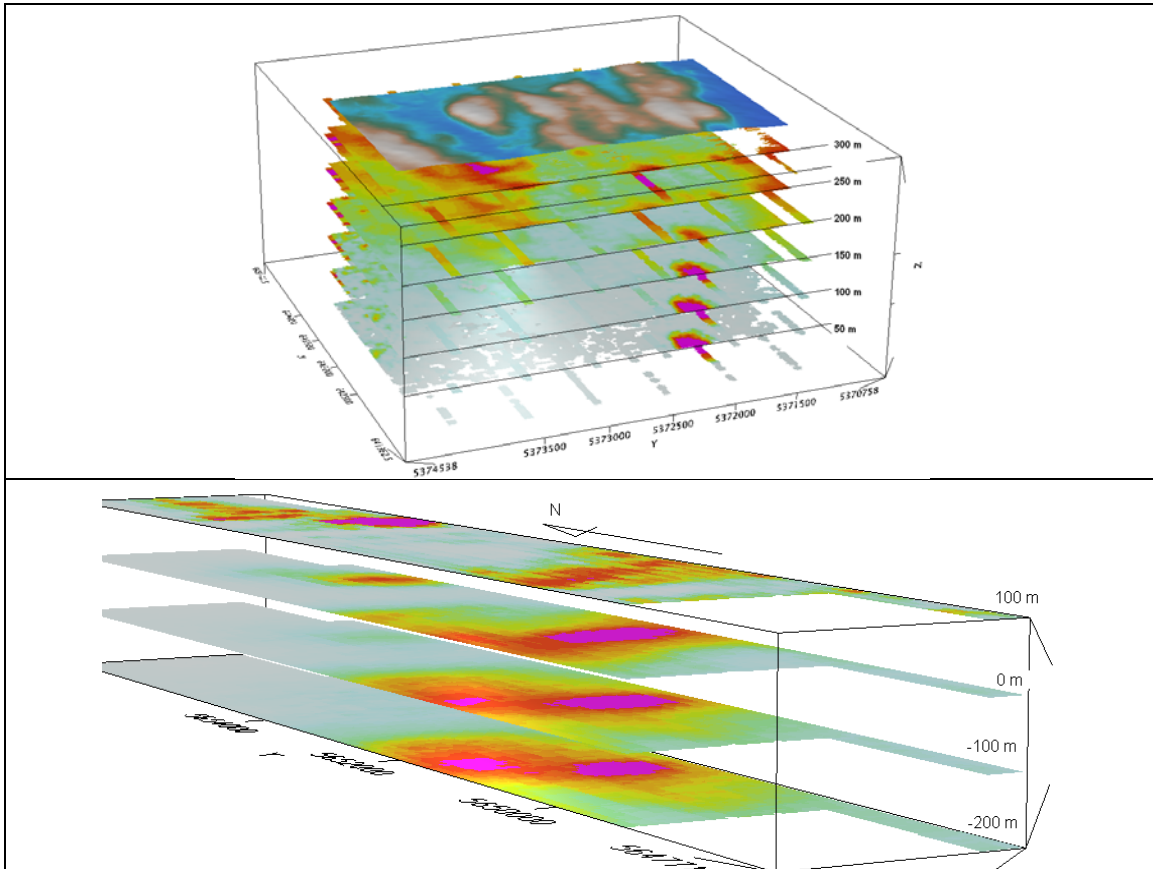
3D PRESENTATION OF RDIS



APPARENT RESISTIVITY DEPTH SLICES PLANS:

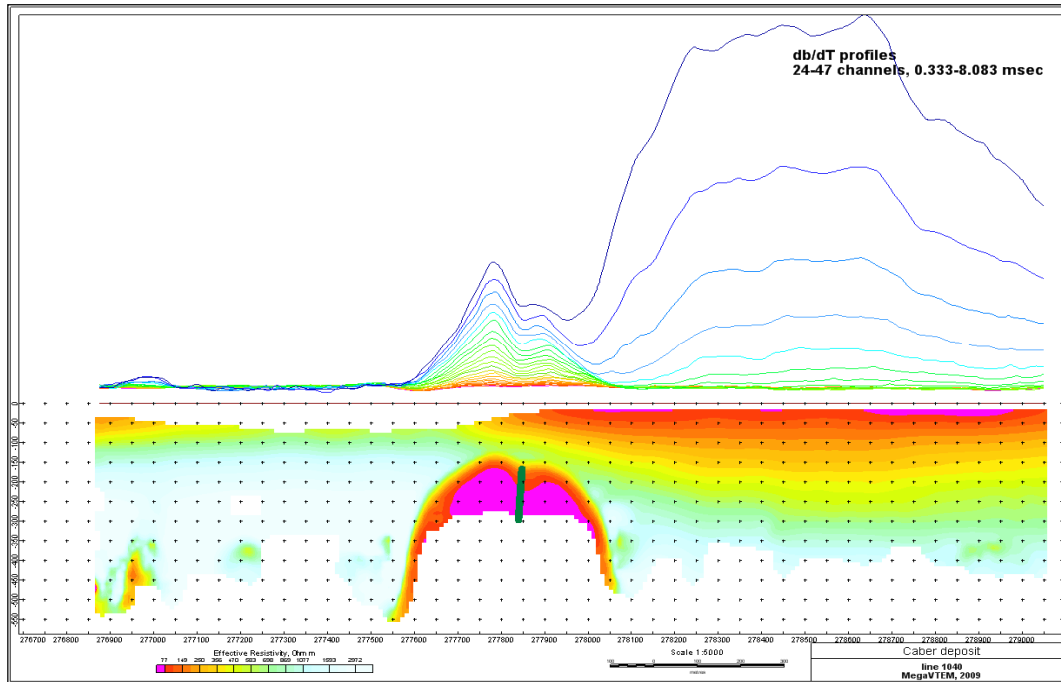


3D VIEWS OF APPARENT RESISTIVITY DEPTH SLICES:

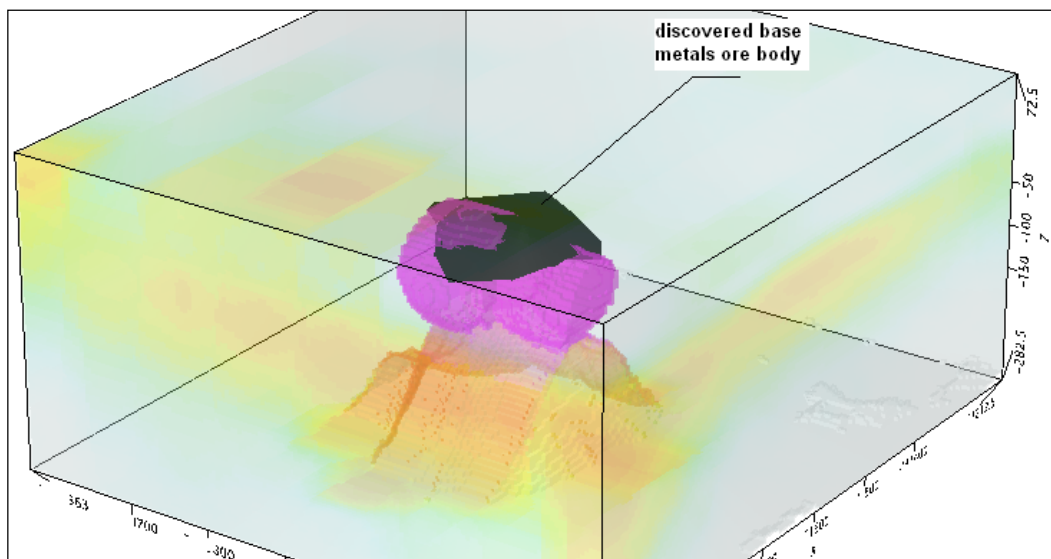


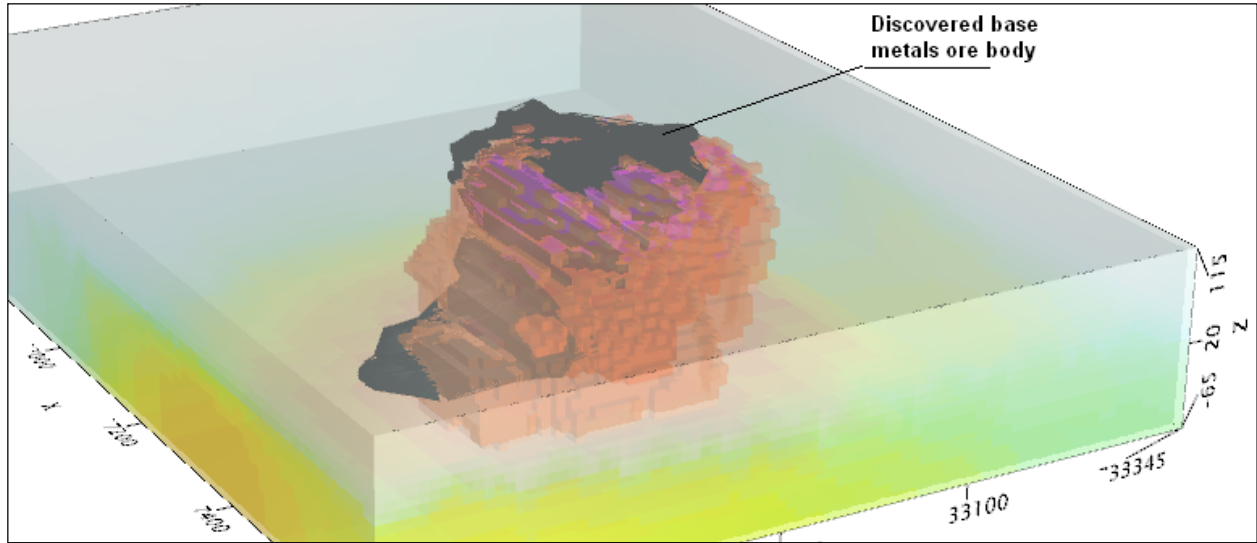
REAL BASE METAL TARGETS IN COMPARISON WITH RDIS:

RDI section of the line over Caber deposit ("thin" subvertical plate target and conductive overburden).



3D RDI VOXELS WITH BASE METALS ORE BODIES (MIDDLE EAST):





Alexander Prikhodko, PhD, P.Ge
Geotech Ltd.
April 2011

APPENDIX G
RESISTIVITY DEPTH IMAGES (RDI)
Please see attached DVD for the PDF.